CHEMICAL OPTIMIZATION OF *IN SITU* EMPLACEMENT OF NANO-PARTICULATE IRON SULFIDE IN POROUS MEDIA

by

Jun Hee Lee

A dissertation submitted in partial fulfillment
of the requirements for the degree of
Doctor of Philosophy
(Environmental Engineering)
in The University of Michigan
2009

Doctoral Committee:

Associate Professor Terese M. Olson, Chair
Professor Kim F. Hayes
Associate Professor Udo Becker
Associate Professor Avery H. Demond

To my parents,

Kyung Sue,

Jaewon and Jenna

Acknowledgement

I am greatly thankful to my God for preparing my way and being with me all the times.

Financial support for this research was provided by funds from Department of Defense, Strategic Environmental Research and Development Project (SERDP) Project CU-1375 and Rackham Graduate School Research Grant.

I would like to thank all my dissertation committee members: Dr. Hayes, Dr. Demond, and Dr. Becker for their times and assistance and especially to Dr. Olson who always inspired me and taught me so much. I would like to thank to Tom Yavaraski for help in performing in iron analysis and other support in the experiments. I would also like to thank my colleagues, Dr. Sung Pil Hyun, Dr. Hoon Young Jeong, Dr. Tanya Gallegos, Monica Higgins, and Young Soo Han for discussions on this work.

Finally, thanks to my family; to my mother who keeps on praying for me, to my father whom I completely rely on, to my Jae Won and Jenna who are the source of my pleasure, and my Kyung Sue, without you I would not be here.

Table of Contents

List of Figures

List of Tables

ABSTRACT

CHEMICAL OPTIMIZATION OF *IN SITU* EMPLACEMENT OF NANO-PARTICULATE IRON SULFIDE IN POROUS MEDIA

by

Jun Hee Lee

Chair: Terese M. Olson

Chemical optimization of an alternative construction method for permeable reactive barriers (PRBs) was investigated. Conventional trench-and-fill construction methods of PRBs are limited to shallow and thin aquifers, and hindered by the presence of a highly consolidated aquitard, subsurface utilities, or aboveground structures. *In situ* emplacement of reactive materials by direct injection technique offers a potential cost effective method to overcome these obstacles. The feasibility is largely expected to depend on whether sufficient coverage of the sand by FeS can be obtained without plugging the inlet region. Optimal deposition rates of FeS nanoparticle were established by modulating the chemistry of influent FeS suspensions. Such optimal conditions can be obtained when electrostatic interactions between FeS particles are sufficiently unfavorable while interaction between FeS particles and the quartz sand are sufficiently

favorable. These optimum conditions were obtained at neutral pH, pH 6.5 to 8.3, and relatively low ionic strength, 0.025 M. At these conditions 3.4×10^{-6} mole FeS on average was deposited per gram of sand.

To better understand the surface charge characteristics of FeS, aggregation rates studies were performed as a function of solution chemistry. The stability of FeS suspension gradually increased as pH increased in the neutral pH region, suggesting that the FeS surface becomes more negatively charged as pH increases. The stability sharply increased between pH 8.3 and 9.0, which can be explained by the hypothesis that FeS has multiple surface functional groups.

Loss rates of FeS coating were investigated to evaluate the longevity of FeS-type PRBs as a function of solution chemistry. Over the pH range tested, pH 5.5 to 10.0, particulate iron detachment due to repulsive interactions was not observed on FeS pre-coated sands. When FeS was deposited by direct injection, however, detachment by repulsion appeared to explain greater FeS loss at more alkaline pH. In the range of pH 5.5 to 7.5, the dissolution rates of FeS increased as pH decreases, achieving steady-state effluent concentrations of 6.1 mg L^{-1} as Fe at pH 5.5. Excessive iron loss rates at relatively acidic pH might significantly shorten the long term operation of FeS-type PRBs.

Chapter 1

Introduction

Contamination of subsurface aquifers threatens many groundwater supplies in the United States and remediation of these sites often proves to be a costly long term project. Among the many remediation approaches that have been tried, permeable reactive barriers (PRBs) are one of the most promising techniques (Gavaskar, 1999; Day et al., 1999). A PRB is *in situ* remediation technique in which a zone of reactive material is placed in the flow path of the contaminant plume. The contaminants are subsequently treated or sequestered as they flow through the reactive material. PRBs are generally considered to be cost effective due to low operation and maintenance costs resulting from the *in situ* and passive nature of the remedial system, although there are uncertainties regarding the design life of reactive materials (Interstate Technology & Regulatory Council (ITRC), 2005; United States Environmental Protection Agency (USEPA), 2002). In comparison to pump-and-treat systems that have well documented cost information, PRB systems are cost effective if PRB functions for more than 10 years before replacement or rejuvenation of reactive materials is necessary (ITRC, 2005). The longer a PRB functions, the more cost effective it is. PRB systems, however, typically require

higher construction costs than conventional pump-and-treat methods. Construction costs are the largest cost factor including reactive media, emplacement, waste disposal, health and safety, and site restoration (ITRC, 2005). The emplacement method, therefore, can significantly impact the cost-effectiveness of a PRB.

Conventional methods of constructing reactive barriers employ relatively costly trench-and-fill methods, which involve soil excavation and then backfilling with the reactive material. Trench-and-fill methods also have significant limitations. Excavation of the trench can be relatively costly and applications are limited to depths of approximately 20 m or less (Cantrell and Kaplan, 1997). The presence of highly consolidated aquitards, subsurface utilities, or aboveground structures can also be obstacles to a trench-and-fill installation approach. To overcome these obstacles, an alternative emplacement method was tested in this research. This method involves injecting a colloidal suspension of the reactive material into the aquifer and allowing the particles to deposit on existing granular media.

The feasibility of direct injection of reactive materials into the subsurface to remediate contaminated aquifers has recently been demonstrated by several researchers. Various reactive materials i.e. zero valent iron, bimetallic nanoparticles, and functionalized titanium oxides, were examined using either emulsification or particle surface modification approaches in laboratory and small scale field experiments (Cantrell et al., 1997; Elliot and Zhang, 2001; Schrick et al., 2004; Saleh et al., 2007). These successful attempts of direct injection technique into subsurface environments drive us to

study further for a promising alternative installation method of PRBs that can be applied at greater depths, less affected by the geological obstacles and structures.

Particles injection methods, however, introduce the risk of plugging the injection zone if particle deposition rates are too high. For successful emplacement the injection conditions must achieve sufficient but relatively uniform coating, to minimize the loss of permeability. For colloidal suspensions with ionized surface groups, filtration rates depend in part on the electrostatic forces between colloids and packed bed media, which are a function of the solution and surface chemistry of the colloids and bed media. Suspension stability with respect to aggregation, another necessary condition to avoid plugging in the injection zone, also depends on particle interaction forces. In this research, nanosized iron sulfide particles were investigated as a potential reactive media and experiments were conducted to determine the optimal solution conditions for particle deposition. The effect of geochemical conditions on the loss of iron sulfide coatings was also examined.

Iron sulfide minerals have been recognized as an effective reagent in terms of their reactivity with a wide variety of common contaminants and high adsorptive capacity due to its high reactive surface and large surface area. A number of laboratory scale studies have shown that the mineral mackinawite, a ferrous monosulfide FeS, can be used to treat a variety of contaminants, including redox metals, non-redox metals, and chlorinated organic compounds. For example, FeS can remove non-redox metals by precipitation of highly insoluble metal sulfide phases (Cole el al., 2000). Mackinawite is also an effective reductant so that oxidized forms of metals, i.e. hexavalent chromium,

are reduced and subsequently removed by adsorption or formation of mixed-metal sulfide phases (Patterson et al., 1997; Chung, 1989). FeS has demonstrated abiotic reducing potential for the dechlorination of chlorinated organic contaminants, for example, tetrachloroethylene (PCE) and trichloroethylene (TCE) transform to acetylene and *cis*-1,2-dichloroethylene (*cis*-DCE) by abiotic reductive dechlorination (Butler and Hayes, 1997, 1998; Jeong and Hayes, 2003). An attractive property of this mineral for remediation purposes, is its large surface area. Freshly synthesized FeS particles in the literature are typically a few nanometers in size and have a large surface area and highly reactive surfaces (Wolthers et al., 2003; Jeong et al., 2008; Ohfugi and Rickard, 2006). The mean specific surface area (SSA) has been reported range between ~220 and ~424 $m^2\ L^{-1}$ with average diameters of 2 to 10.8 nm.

The surface charge characteristics of FeS particles are important for a mechanistic understanding of FeS deposition on porous media. However, estimates of the point of zero charge (pH_{pzc}) and surface potential pH dependence of FeS (nanoparticulate mackinawite) are inconsistent in the literature (Bebie et al., 1998; Wolthers et al. 2005; Gallegos, 2007). It was hypothesized that the dissolution of FeS may interfere with conventional electrokinetic-based estimates of its surface potential and an alternative indirect approach to examining FeS surface charge was undertaken instead. In this dissertation a qualitative understanding of the pH dependence of FeS surface charge was obtained by quantitatively measuring the initial aggregation rates of FeS suspensions as a function of pH.

The feasibility of FeS as a reactive PRB material will depend, in part, on its longevity once it is emplaced. FeS particles deposited on the surface of subsurface grain may detach and remobilize, for example, during the operation of a PRB. FeS dissolution may also lead to loss of the reactive media. In this research the loss rates and mechanisms of previously deposited FeS were examined as a function of solution chemistry.

1.1 Objectives of Research

This research focused on the chemical optimization of iron sulfide nanoparticles deposition in porous media to meet the goals of constructing PRBs. The optimal deposition rates can be controlled by changing surface chemistry of iron sulfide by modulating suspension chemistry. Thus the primary objectives of this research are as follows;

FeS suspension stability characterization

Indirect characterizations of the surface charge of FeS were obtained by examining the stability of suspensions as a function of solution chemistry. Initial aggregation rates were quantitatively measured as a function of pH, ionic strength, and buffer concentrations.

Chemical optimization for emplacement of nano-sized FeS particles in porous media

The feasibility of *in situ* colloid injection methods to generate an iron sulfide-type PRB was investigated by establishing the chemical conditions necessary to generate an

FeS-coated quartz sand media. Model bed materials and synthetic nano-sized FeS were used to obtain a mechanistic understanding of the optimal conditions for FeS deposition.

FeS release tests from FeS-coated sand

Deposited FeS particles on sand surfaces can be released by dissolution or detachment under varying chemical conditions. In order to examine the longevity of a FeS-type barrier, iron and particle release rates as a function of pore water chemistry were examined. Model packed beds of FeS-coated sand were used to evaluate the mechanisms of iron release as a function of solution chemistry. Separation steps were conducted to distinguish the particulate or dissolved states of iron in the column effluent.

1.2 Dissertation Organization

Chapter 1 of the dissertation provides a brief description of this research. Chapter 2 contains a review of relevant literature, including the characteristics of iron sulfide as a reactive material, background regarding PRBs and emplacement techniques, surface properties of colloids affecting deposition and release rates, i.e., electrostatic properties of colloids, and models of colloid filtration in granular media. Chapter 3 discusses the methodologies and materials commonly used in this research, i.e., synthesis of mackinawite and iron analysis. Methodologies for specific experimental tasks are discussed in their own chapters. Chapter 4 presents the experimental findings of the stability of iron sulfide nanoparticles as a function of solution chemistry. Chapter 5 discusses the results of column tests that were designed to ascertain optimal chemical

conditions for colloidal FeS deposition on granular quartz bed media. Chemical control of colloid deposition rates were exerted by varying the solution pH and ionic strength, and thus the resulting electrostatic forces between the FeS particles and sand surfaces. Chapter 6 contains the results of iron release experiments, in which columns of FeS-coated sand were eluted with particle-free solution at varying pH, ionic strength and buffer content, while particulate and dissolved concentrations in the column effluent were monitored. Mechanistic interpretations of the observed rates of FeS dissolution and detachment of deposited FeS particles are provided. Chapter 7 provides a summary of the conclusions and implications of this research and suggested future research to advance PRB technologies.

Chapter 2

Background

2.1 Permeable Reactive Barriers (PRBs)

Permeable Reactive Barrier (PRB) technologies are increasingly being applied to remediate contaminated groundwater. A PRB typically consists of a zone of reactive media placed perpendicular to groundwater flow as shown in Figure 2.1. As groundwater flows through the zone, targeted contaminants are either sequestered or degraded by the barrier. A number of reactive materials are used to treat various targeted contaminants; zero valent iron, ferric oxides, granular activated carbon, apatite, bone char, zeolites, peat, humate, limestone, calcium polysulfide, compost, and others. Among these, zero valent iron is the most frequently used reactive media since it can treat a variety of contaminants; chlorinated organic compounds, metals, chlorinated solvent, and radionuclides. There have been as many as 200 PRB applications worldwide since their initial use in the mid 1990s (ITRC, 2005). Among those, about 60% are iron based. In the United States, there have been 67 full scale iron based PRB sites. Although some of the applications have had significant problems with permeability and hydraulics, these problems have typically resulted from the construction techniques or inadequate site

characterization rather than chemical precipitation and clogging of reactive media (ITRC 2005; Henderson and Demond, 2007).

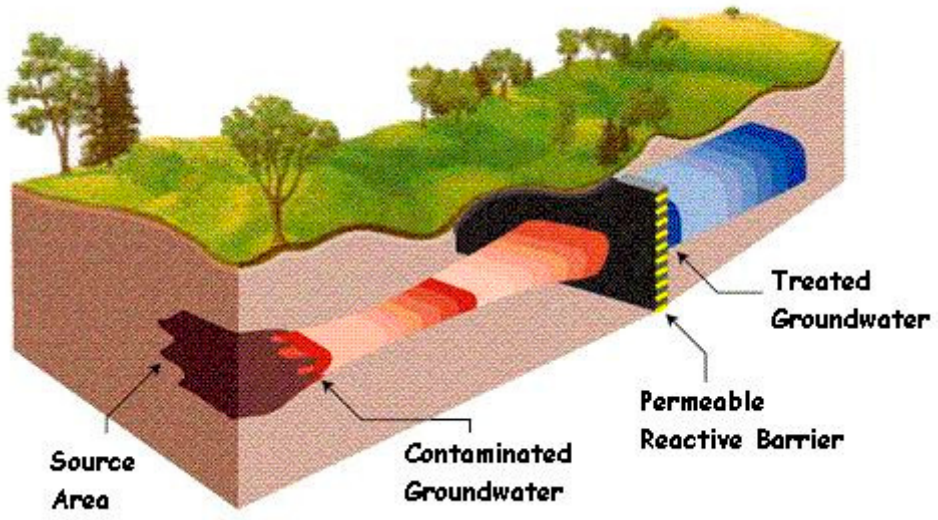

Figure 2.1 Schematic of a permeable reactive barrier (USEPA, www.epa.gov)

As a passive, *in situ* approach to treatment, PRBs represent a less energy intensive alternative to conventional *ex situ* methods, such as pump-and-treat or excavate-and-treat. This is particularly the case of sites contaminated with residual or pools of dense non-aqueous phase liquids (DNAPLs), given the long term nature of cleanup projects at such sites. Remediation by pump-and-treat is often projected to require hundreds of years. The National Research Council (1994) extensively investigated 77 sites within the US where full scale pump-and-treat was being used. 67 of the 77 reviewed sites have not reached cleanup goals. Compared to other *in situ* remediation strategies, such as natural

attenuation, PRBs offer the advantage of plume containment and can be applied to address more refractory contaminants.

2.1.1 Trench-and-Fill Excavation Limitations

Despite the advantages offered by PRBs, limitations exist in terms of the current configurations and materials that are used to employ them. Most PRB installations are constructed by 'trench-and-fill' methods, in which the subsurface zone is excavated and then backfilled with the reactive media (Day et al., 1999, Gavaskar, 1999). Although trench-and-fill methods are effective, the method is limited to shallow aquifers less than 20 meters in depth and thin aquifers (Cantrell and Kaplan, 1997a). USEPA (2002) reported a cost analysis of PRB implementation based on 22 field installations. The construction cost is accounted for 75.9 % of the total cost on average. The deeper and wider the contaminated aquifer was, the more costly is the PRB was to construct. The presence of a highly consolidated aquitard, subsurface utilities or aboveground structures can also be an obstacle to install a trench-and-fill barrier. Some exploratory research has begun to develop alternate construction methods that could extend PRB applications. One such method is *in situ* emplacement, in which the reactive media is injected as a colloidal suspension into a target zone and deposited on aquifer grain surfaces. These methods are reviewed herein and the feasibility of colloidal injection is investigated in this research.

2.1.2 Limitations of Zero Valent Iron Media

The development of alternate reactive materials could also help to extend PRB use and longevity. Zero valent iron, the most commonly used reactive media, is versatile

in terms of the wide range of contaminants it can remove. Upon corrosion of ZVI, however, increases in pH occur, often with the simultaneous precipitation of a variety of metal oxides and carbonates. These phases can eventually lead to excessive reductions in hydraulic conductivity (plugging) and reduced reactivity. An alternate medium that has been considered by various researchers because of its versatile reactivity with many contaminants is mackinawite, FeS (Butler and Hayes, 1998, 1999; Jeong and Hayes 2003; Liu et al., 2008). Preliminary thermodynamic modeling of the amount of precipitate formation in a FeS barrier has also suggested that slower losses of hydraulic conductivity may be obtained with FeS media relative to ZVI (Henderson and Demond, unpublished data). FeS is also produced as a corrosion product in some ZVI barriers (Hansson et al., 2006) and so its behavior is of interest. In this research, FeS particles are examined for their potential use in PRBs constructed by *in situ* emplacement methods.

2.1.3 *In Situ* Emplacement of Colloids in Porous Media by Injection

The feasibility of direct emplacement of nanoparticulate FeS as a potential PRB construction technique was investigated in this research. Several researchers have studied direct injection techniques to emplace a variety of reactive materials into a subsurface aquifer (Cantrell 1997 a,b; Mattigod, 2005; Zhang 2003; Elliott and Zhang, 2001; Schrick et al., 2004). These studies include a mixture of laboratory and field-scale investigations.

Cantrell et al. (1997 a,b) showed successful injection of a suspension containing 1 to 3 μm ZVI particles in coarse sand column tests with the addition of a shear-thinning fluid to increase the fluid viscosity in porous media. The colloidal particles with shear-

thinning fluid resulted in more even deposition through the column length at relatively higher injection rates and lower colloidal suspension concentration of zerovalent iron minerals. The shear-thinning fluids served to reduce the significant sedimentation velocity of these relatively large and dense colloids.

Elliott and Zhang (2001) performed a field demonstration application of bimetallic (Fe/Pd) nanoparticles (100-200 nm in diameter) to treat chlorinated compounds, i.e. trichloroethene (TCE), at a well characterized contaminated site. *In situ* injections of 0.75 – 1.5 g L^{-1} of bimetallic nanoparticle suspension were performed by gravitational feeding at an injection well. Iron and TCE concentrations were monitored at an injection well and three down gradient monitoring wells spaced 1.5 m apart for 4 weeks. Approximately 45 to 96% reductions in TCE concentration were observed between the injection well and the furthest monitoring well (4.5 m distance). Iron concentrations in the wells after 3 weeks of injection were 32 and 10 mg L^{-1} at the injection well and monitoring wells, respectively, while background iron concentrations were less than 1 mg L^{-1}. There were no significant changes in hydraulic conductivity after 6 weeks of injection.

Researchers have also studied direct injection methods to remediate contaminated subsurface aquifers using other materials such as vegetable oils and functionalized titanium oxide nanoparticles. Mattigod et al. (2005) injected functionalized TiO_2 nanoparticles into lab scale sand columns to evaluate their injectability into a porous medium. TiO_2 particles with diameters between 40 – 60 nm, were coated with an organosilane monolayer possessing terminal ethylenediamine (EDA) ligands, and then

treated with Cu(II) to bind a cationic Cu-EDA complex to the nanoparticle surface. A 60 wt % suspension of this sorbent with 2% of ammonium carboxylate dispersant was injected into the silica sand column. The sorbents were uniformly deposited through the column without a significant increase in inlet pressure.

Coulibaly and Bordon (2004) investigated the injection of edible soybean oil to construct a PRB reactive zone using laboratory column tests. The edible oil served as an organic substrate to stimulate anaerobic biodegradation. They found that properly prepared oil emulsions could be distributed through sand columns without excessive loss of permeability. Key factors in generating the desired droplet were the oil-water interfacial tension and the mixing energy input. It was necessary that the oil droplets (1) be sufficiently stable, (2) be significantly smaller than the pore size of the sediment to avoid clogging pore path, and (3) have a low to moderate tendency to stick to each other and the aquifer sediments. It was also found that greater differences in zeta potential between the droplets and sand/clay grains reduced the potential for droplets to stick to the grain surfaces.

In this research the feasibility and the chemical optimization of direct injection of iron sulfide nanoparticles was investigated using model quartz sand columns without the addition of additives, i.e., surfactants or shear thinning fluids. Chemical optimization was investigated by manipulating the pH and ionic strength of pore water to achieve uniform and maximum deposition through the column media.

2.2 Characteristics of FeS

2.2.1 Reactivity of FeS

A number of materials have been proposed for reactive media of PRBs: iron minerals, modified zeolites, peat moss, chitosan, titanium oxide, apatite, limestone, coal, activated carbon, and etc (Scherer et al., 2000). Among these, iron minerals are common reactive materials for PRBs. Zerovalent iron (ZVI) have been widely studied and used from laboratory scale to full scale field installment (Blowes et al. 2000; Arnold and Roberts, 2000; Matheson and Tratnyek, 1994). Iron sulfide minerals such as mackinawite are also known for their ability to scavenge trace metals (Coles et al., 2000; Patterson and Fendorf, 1997) and to reductively dechlorinate chlorinated organic compounds (Butler and Hayes, 1998 and 1999, Jeong and Hayes, 2003) in anaerobic environments.

In this research, nanosized iron monosulfide (FeS, Mackinawite) particles are examined as a reactive material for permeable reactive barriers. Although zerovalent iron (ZVI) has been intensively studied for the last decade as a reactive material for PRB application, iron sulfide minerals are a potentially effective alternative of reactive material in terms of their (1) reactivity with a wide variety of common contaminants (Butler and Hayes, 1998 and 1999; Jeong and Hayes, 2003; Coles, 2000; Patterson, 1997), (2) high adsorptive capacity due to its high reactive surface and large surface area (Wolthers et al., 2005; Jeong and Hayes, 2003), and (3) potential for microbially mediated regeneration under sulfide reducing environment (Hansson et al., 2006).

Iron monosulfide (FeS) has been recognized as an effective reactive material for the removal of various forms of contaminants such as chlorinated organic compounds, redox metals, and non-redox metals. FeS has a high metal 'exchange' capacity for non-redox metals (Coles et al., 2000). These metal 'exchange' reactions, however, may be more accurately described as the precipitation of highly insoluble metal sulfide phases as follows:

$$FeS_{(S)} + Pb^{2+} \rightarrow PbS_{(S)} + Fe^{2+} \quad (2.1)$$

$$FeS_{(S)} + Cd^{2+} \rightarrow CdS_{(S)} + Fe^{2+} \quad (2.2)$$

FeS is also an effective reductant so that oxidized forms of some metals are reduced and subsequently removed by adsorption or formation of mixed-metal sulfide phases (Patterson, 1997). Hexavalent chromium is more soluble and mobile than Cr(III) compounds. Cr(VI) is negatively charged and does not tend to not absorb to negatively charged mineral surfaces. Since Cr(VI) is very soluble, removal of chromium by precipitation requires that it first be reduced to Cr(III), which readily precipitates as $Cr(OH)_{3(s)}$. FeS can sequester Cr(VI) by a single step combining reduction and precipitation shown in equation 2.3 (Chung, 1989).

$$Cr_2O_7^{2-} + 2FeS + 7H_2O \rightarrow 2Cr(OH)_{3(S)} + 2Fe(OH)_{3(S)} + 2S + 2OH^- \quad (2.3)$$

FeS has demonstrated abiotic reducing potential for the dechlorination of chlorinated organic contaminants such as tetrachloroethylene (PCE) and trichloroethylene (TCE) (Butler and Hayes, 1998 and 1999; Jeong and Hayes, 2003). Butler and Hayes (1999) reported that PCE and TCE transformed to acetylene and *cis*-1,2-dichloroethylene

(*cis*-DCE) by abiotic reductive dechlorination by FeS. The reported pseudo first-order rate constants for TCE and PCE transformation by FeS at pH 8.3 were (1.49 ± 0.14) × 10^{-3} h^{-1} and (5.7 ± 1.0) × 10^{-4} h^{-1}, respectively. These rate constants were an order of magnitude smaller than those for dechlorination by ZVI (Matheson, 1994; Liu et al., 2006). The dechlorination rate constants for TCE by ZVI were 0.011 to 0.084 h^{-1} under various test conditions, i.e. ZVI surface treatment by acid washing and various ferrous iron concentrations. This slower dechlorination rate may be caused by slower electron transfer rates of ferrous sulfide than zerovalent iron.

Many researchers (Liou et al., 2006; Choe et. al, 2000; Li and Zhang, 2006) have recently employed nanoscale ZVI particles to take advantage of the large surface area and high surface reactivity that it offers for many target contaminants. Liou et. al. (2006) reported that smaller grained ZVI would have greater reactivity due to its large specific surface area (SSA) through nitrate reduction kinetic experiments. Their laboratory synthesized nanoscale ZVI, having an average diameter of 9.5 nm, 56.67 m^2 g^{-1} SSA, and up to 8.6 times greater nitrate reduction rate constants compared to 45 nm nanoscale ZVI, which had 16.16 m^2/g of SSA.

Furthermore, *in situ* synthesized FeS particles have smaller size than ZVI. Synthetic iron monosulfide has a tetragonal mackinawite structure which forms tabular crystals (Vaughan and Craig, 1978; Wolthers et al. 2003, see Figure 2.2). Ohfuji and Rickard (2006) estimated particle sizes of mackinawite from 2 to 5.7 nm (3.6nm in average) in thickness (the direction parallel to the c axis) and from 3 to 11 nm (5.6nm in average) in length using high resolution transmission electron microscopic (HSTEM)

study. The mean specific surface area by calculation based on particle size was 380 ± 10 m^2 g^{-1} which agrees with Wolthers et al. (2003), 350 m^2 g^{-1}. However, this value is much higher than previously reported values, 7 to 80 m^2 g^{-1}, based on BET and conventional TEM studies (Taylor et al., 1979; Benning et al., 2000; Widler and Seward, 2002). The lower SSA may result from the aggregation of the mackinawite particles. The large SSA values are a result of the layered structure of mackinawite and the high internal surface area between the layers (see Figure 2.2). However, the separation distance between Fe-Fe layers is as small as 0.5 nm, and the internal surface area may not be available for sorption of contaminants if the interlayer spacing is not extendable.

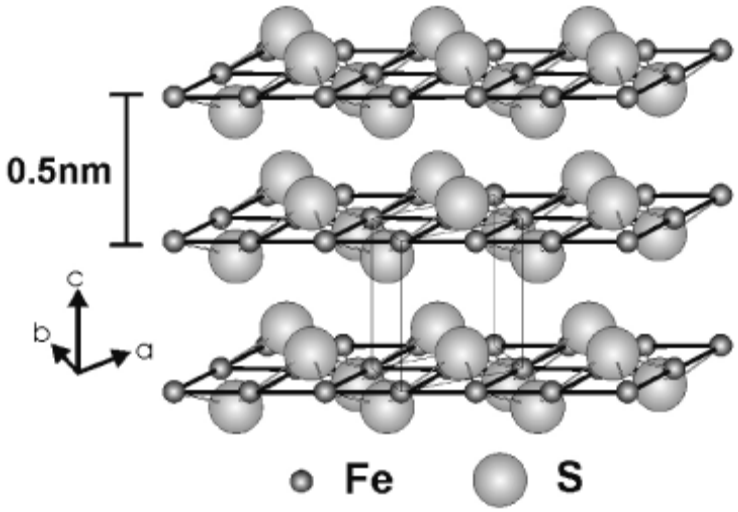

Figure 2.2 Sketch of mackinawite structure (Wolthers et al., 2003). Mackinawite possesses a tetragonal layer structure, where the Fe atoms are linked in a tetrahedral coordination to four equidistant S atoms. Fe-Fe layers are separated by ca. 0.5 nm.

2.2.2 Metastability of Mackinawite

Among various iron sulfide minerals such as troilite (FeS), pyrrhotite (FeS), greigite (Fe_3S_4), pyrite (FeS_2), and marcasite (FeS_2), mackinawite (FeS) is the first precipitated iron sulfide in the reaction of sulfide and ferrous iron (Schoonen and Barnes, 1991; Wilkin and Barnes, 1996; Benning et. al., 2000; Hunger and Benning, 2007). Mackinawite is commonly referred to as amorphous FeS or poorly crystalline iron sulfide. During aging, less crystalline mackinawite can be transformed into more stable and more crystalline iron sulfides such as pyrite.

Schoonen and Barnes (1991) showed that mackinawite is a precursor for the formation of pyrite and marcasite which are the most stable forms of iron sulfides. Their aging experiments upon mixing of ferrous iron ($FeCl_2$ or Mohr's salt) and hydrogen sulfide (NaSH or Na_2S_4) at 65^{o}C showed that sulfidation of the precursor proceeds progressively through the formation of more sulfur-rich FeS phases as follows:

Amorphous FeS	→	Mackinawite	→	Greigite	→	Pyrite/Marcasite
(FeS)		(FeS)		(Fe_3S_4)		(FeS_2)

This conversion occurs at a significant rate only in the presence of intermediate sulfur species, such as zerovalent sulfur, polysulfides, polythionates, or thiosulfate. If there is no sulfur contributor even if hydrogen sulfide or bisulfide present, no significant FeS_2 formed. These results suggest that the conversion rates from amorphous FeS to iron disulfide depend on the solution redox state and pH. More oxidizing solutions favor the formation of important sulfur intermediates. When the molar Fe/SH ratio was less than

unity, greigite never formed due to an excess of reduced sulfur species. In neutral to alkaline pH experiments, the formation rates of FeS_2 from FeS were slowed than acidic experiments due to the low solubility of Fe (II).

Benning et al. (2000) also demonstrated that the transformation of mackinawite to pyrite occurs only in slightly oxidizing environments in experiments at low temperature (25 – 100 ^{o}C). Mackinawite was stable for 4 months in reduced sulfur solution. The conversion to pyrite occurred only after oxidation was induced, and the rate of transformation increased as the oxidation degree increases.

Wilkin and Barnes (1996), in contrast, postulated that the conversion of mackinawite to pyrite proceeds via iron loss, not by sulfur addition, based on sulfur isotopic experiments. The composition of $\delta^{34}S$ in the formed pyrite and the precursor mackinawite was the same as in the presence of a variety of sulfur species, i.e. H_2S, HS^-, S_x^{2-}, $S_2O_3^{2-}$, SO_3^{2-}, colloidal elemental sulfur, and the organic sulfur species at neutral pH at 70^{o}C. They concluded that a key factor governing pyrite formation is the near-surface oxidation state of iron monosulfides. Oxidized iron monosulfides, by air exposure prior to aging in sulfide solution, were converted to pyrite in the absence of intermediate sulfur species, even in excess of sulfide.

In summary, based on the available literature, the conversion of FeS to pyrite proceeds either by addition of excess sulfur from solution (equation 2.4, Schoonen and Barnes, 1991) or by loss of ferrous iron from surface (equation 2.5, Wilkin and Barnes,

1996). In both pathways, the transformations are more favorable as solution conditions become more oxidizing.

$$3FeS \xrightarrow[+S^{2-}]{-2e^-} Fe_3S_4 \xrightarrow[+2S^{2-}]{-4e^-} 3FeS_2 \quad (2.4)$$

$$4FeS \xrightarrow[-Fe^{2+}]{-2e^-} Fe_3S_4 \xrightarrow[-Fe^{2+}]{-2e^-} 2FeS_2 \quad (2.5)$$

This metastable nature of FeS may significantly affect its reactivity in a PRB. Weerasooriya and Dharmasena (2001) and Lee and Batchelor (2002), for example, have both demonstrated that FeS_2 is significantly less efficient in degrading TCE than FeS. Such reactivity comparisons in terms of metal and trace element removal, however, are not available. In addition, the metastability of FeS can interfere with analytical characterizations of its properties and these interferences may contribute to the wide range of reported literature values for some of its properties.

2.2.3 Surface Charge Characteristics of Mackinawite and Quartz Sand

An understanding of the surface charge characteristics of iron sulfide is crucial to understanding the aggregation rates of FeS suspensions or their deposition rates on porous media since both processes are governed by the electrostatic forces between interacting surfaces. The net interaction force between two charged surfaces is determined by the balance of either repulsive or attractive coulombic forces and attractive van der Waals forces between them. Only the coulombic interaction forces, however, are a function of solution chemistry. Coulombic interaction forces between *like* colloidal

particles in a suspension are naturally repulsive, except when the surface is uncharged. The coulombic interaction force between a colloidal particle and filter grain surface is either repulsive or attractive, depending on whether their surface charges are similar or dissimilar in sign, respectively. Both FeS and quartz sand are ionizable surfaces for which protons are potential-determining. The surface charge of both minerals, therefore, is pH dependent.

Near a charged surface, the ions in solution re-distribute themselves into what is referred to as an electrical double-layer, consisting of a compact Stern layer and a diffuse layer (see Figure 2.3A). Within this electrical double layer counter ions (opposite charge of the surface) are in higher concentration than the bulk solution while co-ions (same charge as the surface) are at lower concentration. The surface potential of such an interface represents the electrical work required to bring a co-ion from the bulk solution to the surface. The electrostatic interaction forces between particles can be modulated chemically by changing the surface potential or screening the surface charge such as by adding salt (see Figure 2.3B). Although surface potentials cannot be directly measured in aqueous systems, electrokinetics techniques for colloidal particles, such as electrophoresis, provide estimates of the potential at the plane of shear, or 'zeta potential'. This parameter is often used to characterize the coulombic state of a charged interface.

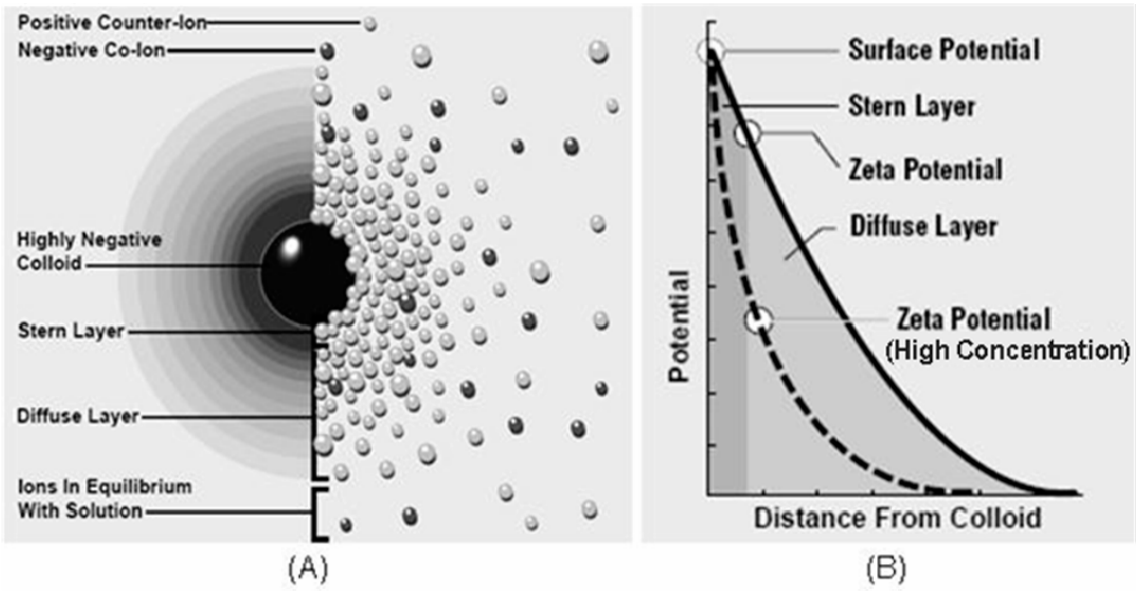

Figure 2.3 Schematic diagrams for double layer and electrical potential of a charged colloidal particle. (A) The left view shows the change in charge density around colloid. The right shows the distribution of positive and negative ions around the charged colloid. (B) The relationship between zeta potential and surface potential depend on the ion concentrations in solution. (Zeta-Meter Inc., www.zeta-meter.com)

For surfaces such as FeS and silica sand, surface potentials are a function of pH. The surface charge of quartz monotonically becomes more negative at pH greater than 2 (see Figure 2.4). The surface potential of mackinawite is less understood, however, since the literature data are not in close agreement. Gallegos (2007) found, based on electrokinetic measurements, that charge reversal of the FeS surface occurs near pH 5 and thus it was negatively charged at pH > 5. Figure 2.5 presents the reported FeS zeta potential as a function of pH from this study. Potentiometric titrations were used by other researchers (Wolthers et al., 2005) to estimate the point of zero charge (pH_{PZC}) of the FeS surface, at which the net surface charge density at the shear plane on a surface becomes zero. They reported that the pHpzc is pH 7.5, and these results are presented in Figure 2.6.

This alkaline pH_{PZC} is in disagreement with pH isoelectric points (pH_{iep}) of various metal sulfides reported by others. Bebie et al. (1998) investigated the surface charge development on a variety of metal sulfides such as sphalerite (ZnS), galena (PbS), chalcopyrite ($CuFeS_2$), pyrrhotite (FeS), pyrite (FeS_2), vaesite (NiS_2), cattierite (CoS_2), and hauerite (MnS_2) based on an electrokinetic study, i.e. electrophoresis. The isoelectric points of these metal sulfides are expected to be between pH 0.6 and 3.3. Widler and Seward (2002) also reported the potentiometrically determined pH_{PZC} of pH 2.9 for a very crystalline mackinawite aged at 130°C for 20 hours. This disagreement of the point of zero charge of mackinawite may result from different synthesis methods, the high solubility of FeS at acidic pH, or the metastability of FeS.

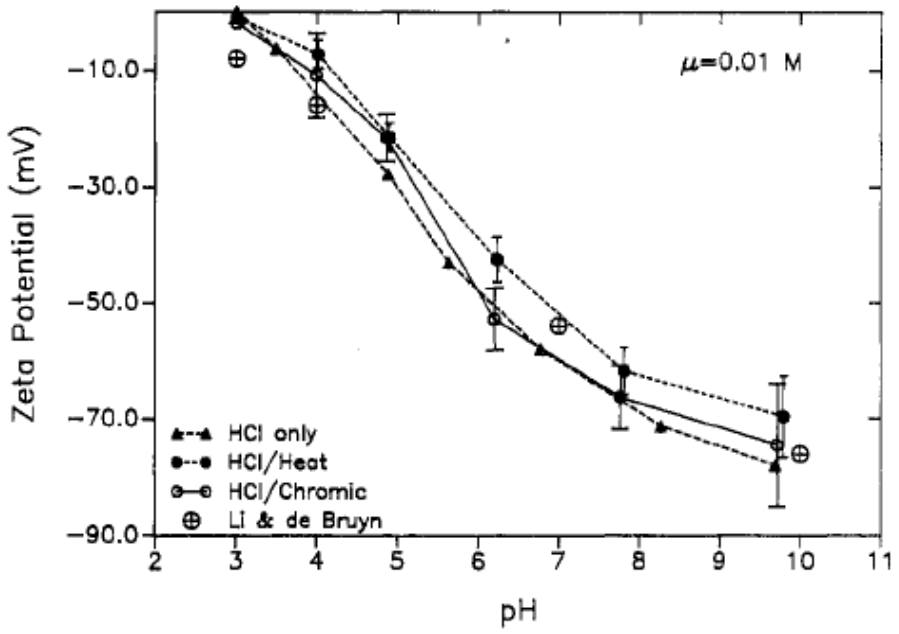

Figure 2.4 Zeta potential of quartz as a function of pH at an ionic strength of 0.01 M. Different curves represent different quartz cleaning methods. (Litton and Olson, 1993)

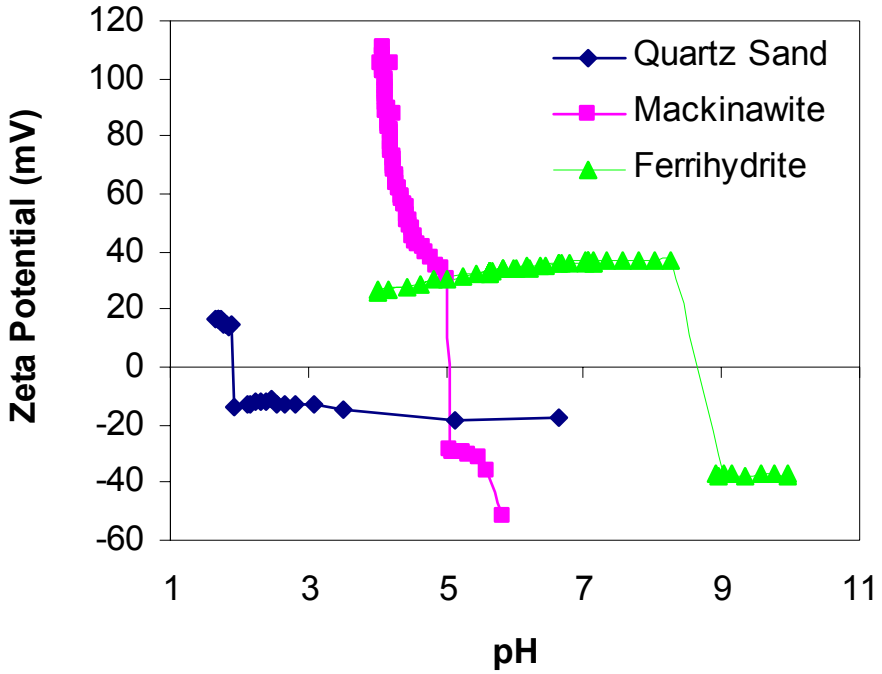

Figure 2.5 Zeta potential measurement for mackinawite, quartz sand, and ferrihydrite in 0.001 M NaCl background electrolyte. (Gallegos, 2007)

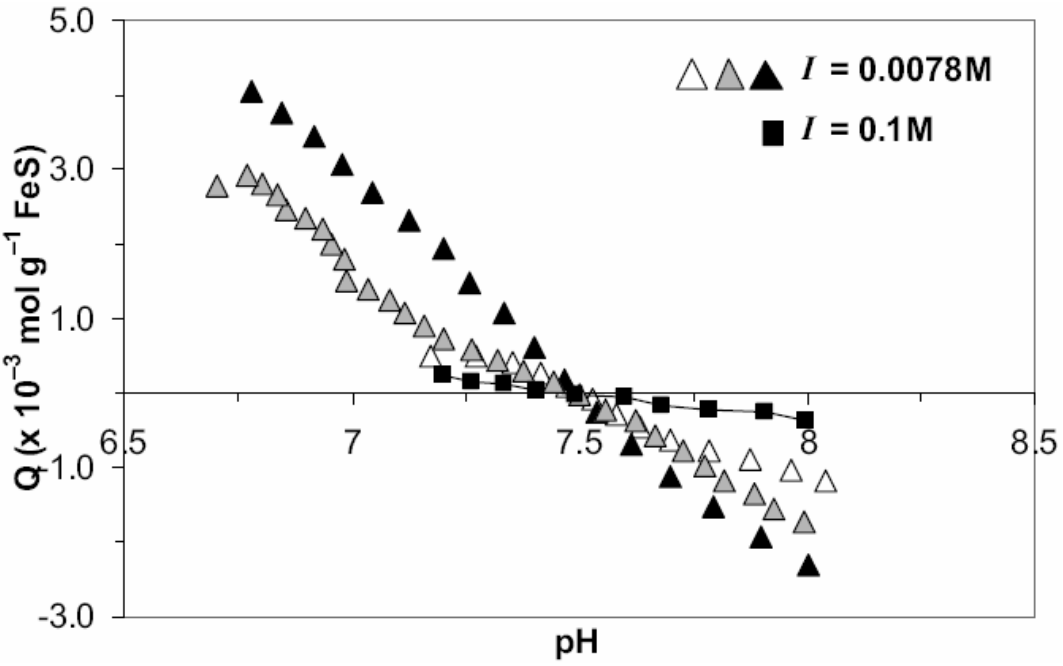

Figure 2.6 Surface titration of disordered mackinawite (Wolthers, et al., 2005)

2.2.4 Surface Functional Groups of FeS Nanoparticles

Surface functional groups on FeS surfaces determine the surface potentials and reactivity of iron sulfide. Although it is a generally accepted hypothesis that metal sulfides have multiple types of surface functional groups, detailed surface spectroscopic data to support this hypothesis is not yet available. Two suggested surface functional groups at iron sulfide surface are iron hydroxyl ($\equiv FeOH^0$) and sulfide ($\equiv SH^0$) functional groups (Bebie et al., 1998). Theoretically, however, there are a number of possible functional groups on the surface of FeS as follows (Wolthers, 2005; Bebie et al., 1998):

$$\equiv Fe^+ + SH^- \leftrightarrow \equiv FeSH \quad (2.6)$$

$$\equiv Fe^+ + OH^- \leftrightarrow \equiv FeOH \quad (2.7)$$

$$\equiv S^- + H^+ \leftrightarrow \equiv SH \quad (2.8)$$

$$\equiv S^- + Fe^{2+} \leftrightarrow \equiv SFe^+ \quad (2.9)$$

$$\equiv SFe^+ + SH^- \leftrightarrow \equiv SFeSH \quad (2.10)$$

$$\equiv SFe^+ + S^{2-} \leftrightarrow \equiv SFeS^- \quad (2.11)$$

Wolthers et al. (2005) suggested that the $FeSH^+$ complex should be dominant over the $FeOH^+$ complex (see Figure 2.7) in solutions saturated with FeS at pH<10. Figure 2.7 shows the reversal of surface charge at pH 7.5, which is consistent with the pH_{PZC} ~ 7.5 they reported. Since the pH_{PZC} is uncertain, however, the functional group distribution is as well.

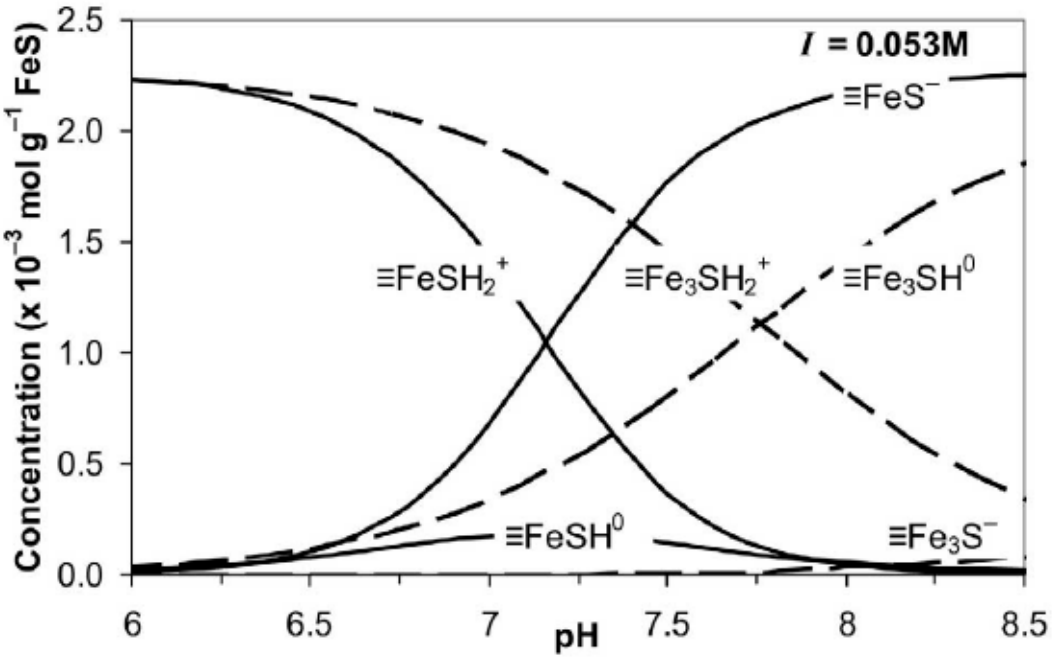

Figure 2.7 Surface complexes proposed for saturated FeS solutions at 0.053 M of ionic strength by Wolthers et al. (2005)

2.3 Stability of Suspensions

Although the aggregation kinetics of FeS nanoparticles has not been specifically studied, colloidal particle aggregation in suspension can be generally controlled by adjusting the surface charge of particles and/or suspension chemistry. Aggregation rates of colloidal particles are commonly described by classical DLVO theory (named after two independent groups who developed the framework, Derjaguin, Landau, Verway, and Overbeek, Derjaguin and Landau, 1941; Verwey and Overbeek, 1948), which explains the balance of electrostatic repulsion and van der Waals attraction forces between particles.

In order to avoid high deposition rates of FeS particles at the point of injection and consequently reductions in hydraulic conductivity or plugging during FeS emplacement by injection, influent FeS suspensions must be sufficiently stable with respect to aggregation. The net repulsive energy, in other words, the interaction energy barrier, between colloids should be sufficiently large (see Figure 2.8).

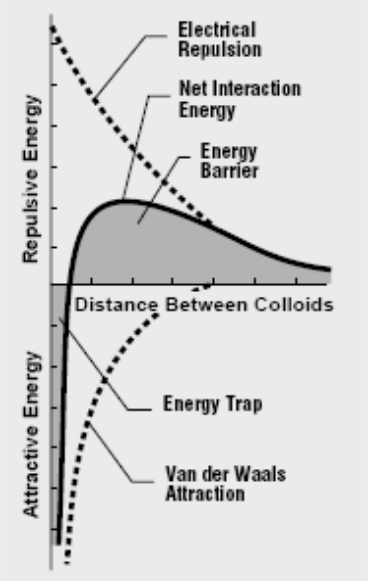

Figure 2.8 Typical net interaction curve between charged colloids as a function of particle separation distance for the case of a net repulsive energy barrier. (Zeta-Meter Inc., www.zeta-meter.com)

The repulsive energy barrier can be controlled by modifying solution chemistry such as ionic strength and pH (Mylon et al., 2004), or directly changing the surface charge of colloids by adding surface active materials to specifically adsorb on to the colloid surface. Shear thinning materials can also be used to prevent the particles from aggregating, settling or precipitating from suspension.

Mylon et al. (2004) studied the aggregation kinetics of hematite nanoparticles (43 ± 3 nm) by adjusting ionic strength using NaCl and $CaCO_3$. In both of background electrolytes, the zeta potentials of hematite colloids decreased (i.e., became less negative) as ionic strength increased. The rate of change in the mean aggregate radii increased with ionic strength until a maximum aggregation rate was reached. The minimum cation concentration required for diffusion limited aggregation, i.e., the critical coagulation concentration (CCC), is commonly to be correlated with colloid release. CCC for NaCl and CaCO3 was 30 mM and 2.4 mM, respectively.

In this research the aggregation rates of FeS nanoparticulates were examined to understand their stability in aqueous suspensions as a function of pH and ionic strength. Photon correlation spectroscopy (PCS) was utilized to measure changes in aggregate radii in time. Detailed is discussed in chapter 4.

2.4 Colloid Filtration

Under conditions in which migrating colloids are filtered through granular bed media, high rates of deposition quickly lead to plugging at the point of injection. In order to avoid plugging or loss of permeability, the deposition rates must be optimized. Several factors affect the deposition rate of colloids, among which are colloidal properties such as size, shape, density, aggregation state and surface charge, and fluid properties such as viscosity, density and velocity, and bed grain properties such as grain size, shape and surface charge (Ward, 1987).

2.4.1 Filtration Theory

For colloidal particles which are much smaller than the pores of the medium, depth filtration is a dominant process. In this concept of filtration, the migrating particles in porous media can be captured on surface of the media by collision mechanisms. Particle deposition rates depend on the rate of physical contact with the granular media, and the rate of successful attachment. For submicron-sized particles, the frequency of colloidal encounter with a grain is diffusion controlled. Figure 2.9 shows conceptual diagrams of mechanisms of particle capture in depth filters. Figure 2.9.C illustrates particles captured on a single media by diffusion. More detail filtration theory will be discussed in Section 5.2 later.

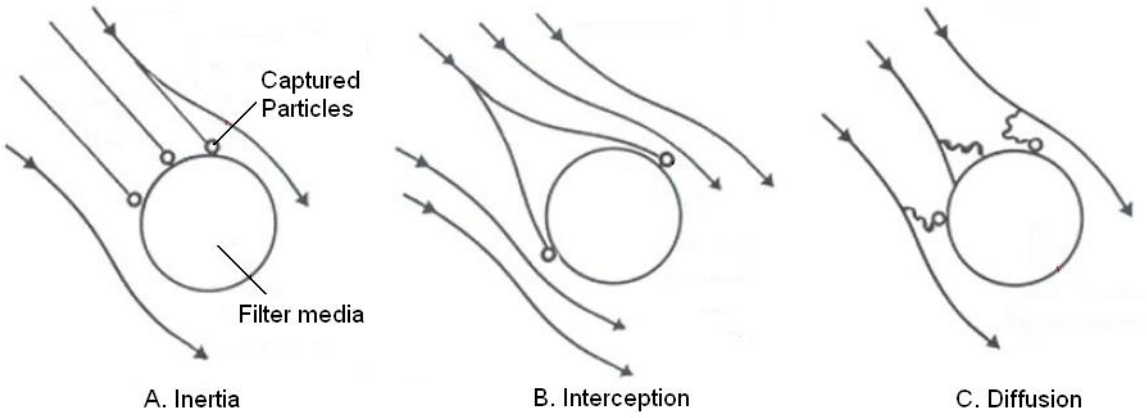

Figure 2.9 Particle capture mechanisms in depth filtration

The rate of successful attachment depends on the net interaction energy profile as a function of separation distance from the collector as electrical double layers overlap. The deposition rates of particles, therefore, are affected by electrokinetics of both the

migrating colloids and the porous media. The deposition rates can be increased if repulsive forces are decreased. In order to achieve colloid penetration and more uniform deposition conditions over practical PRB thicknesses, therefore, it is essential to establish sufficiently favorable deposition conditions between FeS particles and the porous media surface while sufficiently unfavorable interaction between FeS particles. Unfavorable deposition conditions arise when repulsive interaction forces between negatively charged particles and granular media are sufficiently large. In contrast, favorable deposition conditions are enhanced if the repulsive forces between the particles and the porous media are minimized.

2.5 Remobilization of Deposited Colloids in Porous Media

Despite the advantages PRB processes offer, there is uncertainty about their effectiveness over relatively long operation periods due to their relatively short history of field application. In PRBs constructed by *in situ* emplacement of injected colloids, the eventual loss of the reactive colloids by detachment or dissolution could limit the service life of the barrier. Even FeS-type PRBs constructed by trench-and-fill approaches, for example by using FeS-coated sand, could have reduced service lives if significant losses of the coating occur. The factors that are likely to control FeS loss are discussed in the following sections.

2.5.1 Detachment of Reactive Particles by Repulsive Interaction Forces

Release of colloidal particles is largely controlled by the solution chemistry of pore water and hydrodynamics of the flow field (Ryan and Elimelech, 1996; Khilar and Fogler, 1998; Grolimund and Borkovec, 1999, 2006; Abadzic and Ryan, 2001). The pH and ionic strength of pore water are thought to be major factors that affect particle mobilization. A number of experiments have demonstrated that the release of subsurface colloidal particles, i.e. clays, is enhanced under low ionic strengths of pore water conditions (Ryan and Gschwend, 1994; Roy and Dzombak, 1996; Grolimund and Borkovec, 2006). The release of particles is generally governed by DLVO theory by which the balance of forces between colloidal particles and aquifer grains is described in terms of electrostatic repulsion and the van der Waals attraction forces within the double layer. A decrease in ionic strength causes changes in net potential by expansion of the double layer around like-charged colloids and aquifer grains. If the net interaction energy is repulsive, the particles may be released. In addition, many researchers reported that pore water containing monovalent ions causes more release than divalent ions for a particular ionic strength (Khilar and Fogler, 1998; Roy and Dzombak, 1996).

The release of colloidal particles is generally enhanced with an increase in pH due to the greater development of negative charge on the colloid and grain surface (Khilar and Fogler, 1998; Bunn et al., 2002). However, pH effects on electrostatic forces between colloids and grains may be less sensitive than that of ionic strength (Grolimund and Borkovec, 1999), unless the pH changes by several orders of magnitude or a charge reversal of the particles occurs.

2.5.2 Particle Loss by Dissolution

The solubility of mackinawite has been investigated by many researchers since Berner (1967) first reported its thermodynamic stability, although the values in the literatures are also not in close agreement. The dissolution reactions of mackinawite are generally described as a function of pH according to equations 2.12 and 2.13:

$$FeS + 2H^+ \rightarrow Fe^{2+} + H_2S_{(aq)} \quad (2.12)$$

$$FeS + H^+ \rightarrow Fe^{2+} + HS^- \quad (2.13)$$

The dominant form of sulfide is as a function of pH due to acid dissociation, and the first equilibrium constant in aqueous solution is $10^{-6.98}$ (Suleimenov and Seward, 1997) as follows:

$$H_2S_{(aq)} \rightarrow H^+ + HS^- \qquad \log K_{a1} = -6.98 \quad (2.14)$$

Under acidic pH conditions, equation (2.12) will govern the solubility of FeS and equation (2.13) controls it at alkaline pH. The reported solubility constants for mackinawite are summarized based on the equation (2.13) in Table 2.1. From this review of the literature, it appears that there is more than an order of magnitude range in the reported solubility of FeS. For example, a factor of 20 difference in the equilibrium dissolved iron concentration is predicted with the highest and lowest solubility constants at pH 5 and $[H_2S] = 10^{-4}$ M.

Table 2.1 Solubility constants for mackinawite

pK_{sp}	pH tested	Temperature	Reference
3.00 ± 0.12	3.1 – 7.9	20 ^{o}C	Davison et al., 1999
3.89 to 3.99	3.3 –12	25 ^{o}C	Benning et al., 2000
2.11 ± 0.27	6 –8	25 ^{o}C	Wolthers et al., 2005
3.48 ± 0.25	3.16 –9.66	23 ^{o}C	Rickard, 2006

$$pK_{sp} = p\{Fe^{2+}\} + p\{HS^{-}\} - pH$$

This difference of solubility constants might be due to its metastable nature. The state of mackinawite used in various research studies may differ since it ages relatively quickly to more crystalline forms, and can further be transformed to more stable iron sulfides, i.e., greigite and pyrite, in the presence of aqueous oxidant species. Also the transformation rate to more stable iron sulfides can increase under more acidic pH conditions since one of the conversion mechanisms, to greigite from mackinawite, is the iron loss pathway (Wilkin and Barnes, 1996, see equation 2.5). Accurate experimental measurements of the solubility of mackinawite can be hindered if surface corrosion of mackinawite occurs since the solubility of greigite is much less than that of mackinawite (Berner, 1967; Benning et al., 2000; Rickard and Morse, 2005). Also Gallegos (2007) postulated that the solubility of FeS is significantly sensitive to the oxidation state of solution.

Rickard (2006) recently reported that an aqueous FeS cluster complex is the dominant dissolved species at alkaline pH. The aqueous FeS clusters ($Fe_nS_n \cdot 4H_2O$, where n = 2 or 4) are independent of pH, with a formation constant, log K, of -5.7.

The dissolution of FeS, therefore, at relatively acidic pH conditions may be an important process limiting the longevity of PRBs. In this study, FeS release rates from model quartz sand were investigated under varying pore water chemistry, i.e. ionic strength and pH, to examine the longevity of FeS sand coatings.

Chapter 3

General Methods, Materials, and Characterization

In this chapter general experimental methods and materials used throughout the dissertation are discussed. Specific experimental methods and materials that were employed in each of the FeS stability, deposition, and release studies are discussed separately in Chapters 4, 5, and 6, respectively. All sample preparations were performed in an anaerobic chamber (4 ± 1 % hydrogen gas + 96 ± 1% nitrogen gas) where other conditions are not noted. All chemicals used were reagent grade. Deoxygenated and deionized water was prepared by boiling of deionized water (18 MOhm·cm) from a Millipore Milli-Q system (Billerica, MA) to remove dissolved oxygen. Then the boiled water was cooled in a water bath while bubbling high purity (99.99%) nitrogen gas to prevent the dissolution of atmospheric oxygen until the temperature dropped to about 50^{o}C. The warm, deoxygenated Milli-Q water was then stored in the glovebox for at least 24 hours before use.

3.1 FeS Synthesis

Nanoparticulate mackinawite (FeS) was synthesized by a precipitation method in which $FeCl_2 \cdot 4H_2O$ and $Na_2S \cdot 9H_2O$ (Fisher Scientific, Certified ACS) solutions were

reacted in an anoxic chamber following the method of Butler and Hayes (1998). 1.2 liters of 1.1 M Na_2S were slowly added to 2.0 L of 0.57 M $FeCl_2$. The resulting slurry was mixed on a magnetic stir plate for 4 days to age the particles. Upon aging, the pH of the suspension increased from 8 to 11. The 4 day aged FeS particles were in equilibrium with the solution at a pH of 11.3. The aged suspension was decanted into polypropylene centrifuge bottles that were tightly sealed and centrifuged at 11,000 rpm for 15 min. The supernatant was discarded. Fresh deoxygenated water was added, and the bottles were shaken, equilibrated, and re-centrifuged a total of eight times over 2-3 days. The FeS was then freeze-dried under vacuum for 5 ± 1 days. The freeze-dried FeS particles were stored in airtight vials in the anoxic chamber until used. All synthesis procedures were conducted in an anaerobic chamber except during the short periods of centrifugation and freeze drying.

3.2 Structure Characterization of FeS using X-ray Diffraction

X-ray diffraction analyses were conducted to verify that the synthetic iron sulfide powder was crystalline mackinawite. Prior to analysis, the freeze dried FeS particles were crushed to a fine powder using an agate mortar and pestle. The diffraction patterns were obtained from a Rigaku (The Woodlands, Texas) 12 kW rotating anode generator at 40 kV and 100 mV with a Cu Kα radiation source. Spectra were collected over a 2-theta range of 0 to 95 degrees and analyzed using JADE analysis software (Materials Data Inc., CA). As shown in Figure 3.1, the spectra were consistent with the reported peak

reflections of mackinawite at 17.62°, 30.06°, 34.47°, 38.96°, 50.43° and 59.09° (Kouvo et al., 1963). The red line in Figure 3.1 shows the reported XRD peaks for mackinawite.

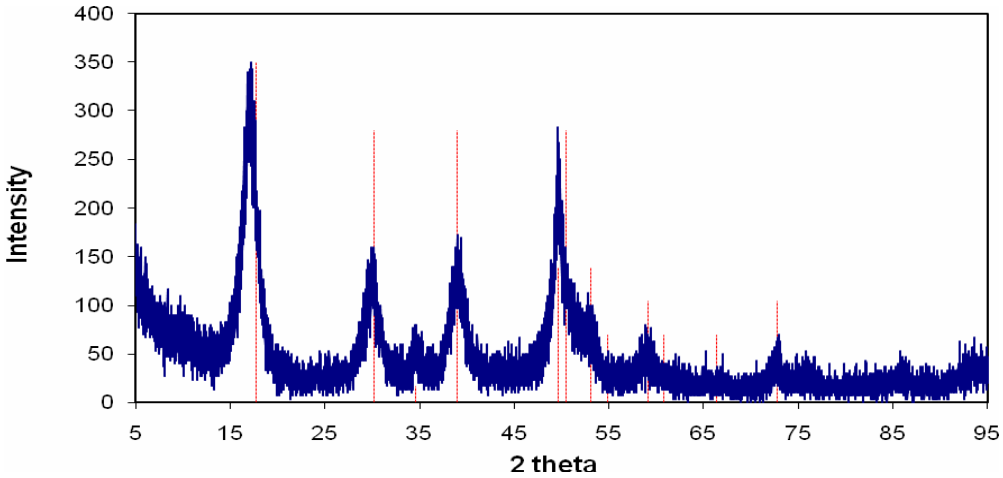

Figure 3.1 XRD analysis of synthesized FeS nano-particles

3.3 Size Analysis of FeS using Photon Correlation Spectroscopy

Photon correlation spectroscopy (PCS) was used to characterize the size of the synthetic FeS particles. This technique relies on dynamic light scattering measurements of Brownian, submicron particles in a suspension. Since particle diffusion rates are determined by their size, size information is obtained from the measured rates of fluctuation of the scattered light. The lower size limit by this technique is a few nanometers, depending on the difference in the refractive index of the solvent and the particle. The method requires that light be scattered only once, and to minimize multiple scattering, dilute suspensions are required. For this reason, the technique could not be

applied to suspensions at the concentrations used in the deposition experiments (1 g L^{-1} FeS). Size determinations of 20 mg L^{-1} suspensions were performed instead.

The PCS instrument (Model N4 Submicron Particle Size Analyzer, Coulter, Fullerton, CA) was installed in an anaerobic chamber to conduct the size measurements in order to minimize oxidation. Stock suspensions of freeze-dried FeS (1 g L^{-1}) were dispersed by vigorously mixing with a magnetic stirrer for 24 hours prior to the measurement. With dispersing times shorter than 24 hours, the size analysis indicated that the particles are significantly aggregated and not well dispersed as single nanosized particles. The conductivity of the stock suspension was 92 μS cm^{-1}, which is approximately equivalent to 7×10^{-4} M KCl. The dispersed stock suspension was then further diluted to 20 mg L^{-1} just prior to PCS analysis. The sample pH was 7.5 and suspension remained stable for several days at these conditions. The samples were measured at 90 degree of scattering angle for 200 seconds of acquisition time with weight distribution analysis mode. Results of the PCS analyses indicated that the FeS colloidal suspensions had a mean diameter of 3 nm. Since this value is close to the detection limit of the instrument, the mean diameter may be slightly over-estimated by the method.

3.4 Quartz sand

Since the objective of this study was to characterize the nature of the interaction forces between the FeS colloids and granular porous media, a relatively well-characterized granular media, clean quartz sand, was selected in order to better understand the surface charge characteristics of the FeS surface. Clean quartz surfaces

have a negative surface potential over ambient groundwater pH conditions, repulsive electrostatic forces between the sand and FeS particles would be expected, therefore, if the surface of the FeS was negatively charged as well.

The quartz sand (#1 Dry (65), U.S. Silica, Pacific, MO) had a mean grain diameter ranging from 150-210 μm (typical size range of 75 to 600 μm) and a relatively round shape. Typical size distribution is shown in Table 3.1 and Figure 3.2. The sand was used without further size grading since mechanical sieving is known to impart impurities on the surface of quartz sand that are difficult to remove (Litton and Olson, 1993). Prior to use in the column experiments, the sand was cleaned by sequential rinses of dithionite and hydrogen peroxide to remove surface metal oxides and organic matter (American Society of Agronomy and Soil Science Society of America, 1982).

Table 3.1 Typical size distribution of Dry #1 (65) quartz sand (US Silica, Missouri)

USA Standard Sieve Size		Typical Values		
		% Retained		% Passing
Mesh	Millimeters	Individual	Cumulative	Cumulative
20	0.850	0.0	0.0	100.0
30	0.600	0.1	0.1	99.9
40	0.425	4.5	4.6	95.4
50	0.300	15.0	19.6	80.4
70	0.212	31.0	50.6	49.4
100	0.150	34.0	84.6	15.4
140	0.106	13.0	97.6	2.4
200	0.075	2.3	99.9	0.1
270	0.053	0.1	100.0	0.0
Pan	Pan	0.0		

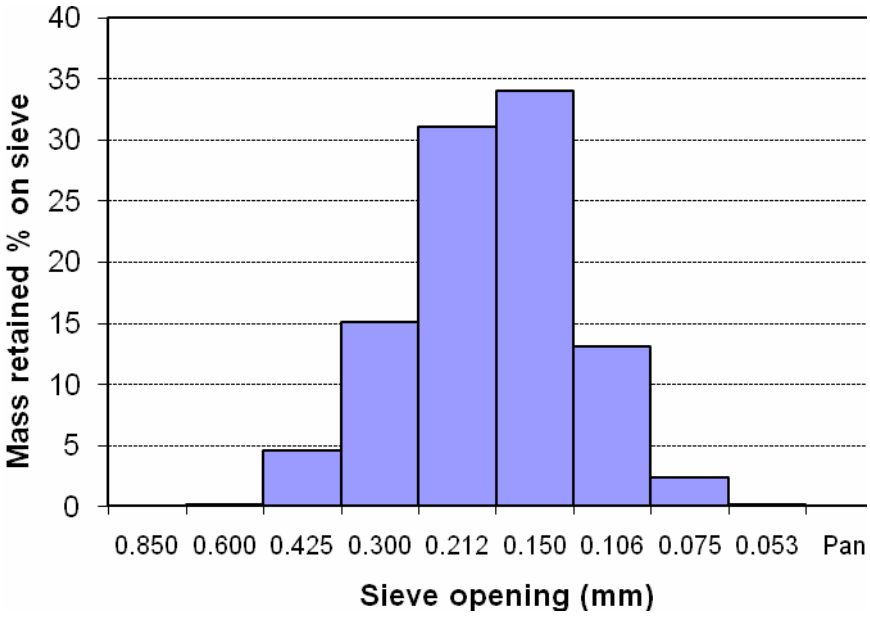

Figure 3.2 Typical size distribution of Dry #1 (65) quartz sand (US Silica, Pacific, MO)

3.5 Buffers

In both the FeS deposition and release studies, chemical buffers were used to maintain the pH of FeS suspensions and electrolytes. The synthesized mackinawite equilibrates with hydrogen and sulfide ions in suspension, and the time for equilibrium is extremely long for open systems or at low $H_2S_{(g)}$ partial pressure. Thus, the buffers were used to minimize unexpected pH changes over long equilibration periods due to processes such as oxidation, aging, or phase change. Borate or boric acid buffer was used over the pH range of 8.2 to 10.0. MOPS (3-(N-Morpholino)propanesulfonic acid, sodium salt) buffer was used for pH 6.5 to 7.5. Acetate buffer was used for pH 5 to 5.9. Desired concentrations of buffers and ionic strengths were calculated by MINEQL+ (Version 4.5,

Environmental Research Software, Hallowell, ME). Effects of buffers on the stability of FeS particles were tested in Chapter 4.

3.6 Iron Analysis

Iron sulfide suspensions were acidified to a 2% nitric acid concentration prior to analyses using concentrated trace metal nitric acid (approximately 70% HNO_3, Fisher Scientific). 1/35 of the sample volume of the 70 % nitric acid was added to FeS sample suspension. The acidified FeS suspension was completely dissolved using a vortex mixer before further dilution. The acidified solution was further diluted to an appropriate concentration for iron analysis using 2% HNO_3 using a colorimetric method (AWWA, APHA, WEP, 1995) or Ion Coupled Plasma – Mass Spectroscopy (ICP-MS, Perkin Elmer, Waltham, MA)

Chapter 4

Aggregation Kinetics of FeS Suspensions

4.1 Introduction

A study of the self interaction dynamics of FeS particles in suspension provides both a direct determination of the solution conditions that favor their stability with respect to aggregation and an indirect method of probing their surface charge characteristics as a function of solution chemistry. As the surface charge on an FeS colloid increases, whether negatively or positively, the interaction forces between the particles become more repulsive, resulting in a more slowly aggregating (i.e., stable) suspension. Because of the known pH-dependent surface charge of metal sulfides, FeS aggregation rates were studied here as a function of pH.

The few attempts to characterize the surface charge-pH dependence of mackinawite have not yielded a precise estimate of its pH point of zero charge, pHpzc, (Mullet et al., 2004; Wolthers, et al., 2005; Gallegos, 2007). The analytical approach and mackinawite synthesis methods used by these researchers vary, however. Mullet et al. (2004) carried out electrokinetic measurements (electrophoretic mobility) with synthetic mackinawite, which was aged for 24 hours and freeze dried for storage prior to use over

the range of pH 4 – 10. The zeta potential was negative over the entire pH range tested and thus, the pH_{iep} was less than 4. Wolther et al. (2005) conducted potentiometric titrations with freshly precipitated FeS to estimate its surface charge, over the pH range of 6 to 8.The pH_{PZC} estimated was near 7.5. The analysis of their titration data required complex corrections and speciation assumptions to account for the significant solubility of FeS in this pH range. Gallegos (2007) performed electrokinetic analyses and reported zeta potentials (potential at the plane of shear) over the pH range of 4 to 6. The suspensions were also aged longer than those studied by the Wolthers group. These experiments suggested the pH_{PZC} of FeS was near 5. The significant solubility of FeS in this pH range, however, can be expected to confound measurements of its electrokinetic velocity. The resulting increases in solution ionic strength with dissolution, for example, would also contribute to a reduction in the electrokinetic mobility of colloidal FeS. Nevertheless, Gallegos' estimate of the pH_{PZC} is more consistent with the surface acidity reported for metal sulfides generally. Iron sulfide mineral surfaces such as pyrite (FeS_2) and pyrrhotite (FeS) were negatively charged above pH value of 2 and 3.3, respectively (Bebie et al., 1998). These investigators also demonstrated that the addition of soluble ferrous iron, resulted in an alkaline shift in their isoelectric points. An even greater alkaline shift would be expected for mackinawite, since it is even more soluble than pyrrhotite. The pH_{PZC} estimated by Gallegos, therefore is consistent with that prediction.

Aggregation kinetic studies of FeS suspensions were visually conducted by Gallegos (2007). Noticeable aggregation and settling were observed in these experiments as the pH approached pH 5 (starting from more alkaline pH). FeS particle aggregation,

however, has not been quantitatively studied. In this research the temporal changes in light scattering of nanoparticulate FeS suspensions, as measured by photon correlation spectrometry (PCS), were quantitatively related to the change in FeS particle size with time over the pH range of 6.5 to 9. The theoretical basis for these relationships and the approach used to analyze the PCS data sets are outlined here.

4.2 Theory

For initially monodisperse suspensions, i.e., suspensions consisting of particles of all the same type and diameter, the aggregation kinetics can be expressed by as a second-order decay process (von Smoluchowski, 1916):

$$\frac{dN}{dt} = -k_{11}N^2 \qquad (4.1)$$

where N is the number concentration of singlet particles and k_{11} is the rate constant for doublet formation. The rate constant, k_{11}, depends on the frequency of collisions and the efficiency with which collisions successfully produce a doublet. Namely,

$$k_{11} = \beta_{11}\alpha \qquad (4.2)$$

where β_{11} is the collision frequency function between two singlets, and α is the dimensionless sticking coefficient. For nano-sized colloids, the collision frequencies are governed by their Brownian motion. von Smoluchowski (1916) derived the following relationship for the collision frequency of two identical particles due to Brownian diffusion:

$$k_{smol} = \frac{8K_B T}{3\mu} \qquad (4.3)$$

where K_B is the Boltzmann constant, T is the absolute temperature, and μ is the viscosity of the medium. For a monodisperse suspension, the Smoluchowski constant is independent of particle size and depends only on fluid properties. Under conditions when all collisions successfully produce an aggregate, i.e., α is unity, then $k_{11} = k_{smol}$, and aggregation proceeds at its maximum rate. This condition is referred to as diffusion-limited colloid aggregation (DLCA).

Electrostatic repulsive forces between interacting particles can reduce the aggregation efficiency of collisions, wherein $\alpha < 1$. These conditions are often referred to as reaction-limited colloid aggregation (RLCA). The relationship of α to solution composition and surface properties is typically described in terms of classical DLVO theory. This theory describes the balance between the repulsive coulombic energy, V_R, and attractive van der Waals energy, V_A, of two interacting charged spheres. The relationship between α and the net interaction energy, $V_T = V_R + V_A$, is expressed according to the theory as:

$$\frac{1}{\alpha} = W = 2a \int_{2a}^{\infty} \exp(V_T / K_B T) \frac{dr}{r^2} \qquad (4.4)$$

where W is the stability ratio, a is the radii of interacting particles and r is the distance between the centers of interacting particles.

The V_A contribution to V_T, is independent of solution composition. The solution chemistry dependent term, V_R, for two interacting spheres is:

$$V_R = \frac{64K_BTn_0}{\kappa}\frac{(a+\delta)^2}{r}\left[\tanh\frac{ze\varphi_d}{4K_BT}\right]^2 e^{-\mathrm{K}(H-2\delta)} \qquad (4.5)$$

where, n_o is ion number concentration, δ is the depth of the stern layer, and H is the distance of the interacting particles at closest approach ($H = r - 2a$).

Since H^+ is a potential-determining ion for the FeS surface, the pH affects the magnitude of its zeta potential and therefore V_R. The second effect of solution composition on V_R is revealed through the parameter, κ in equation 4.6. Solution ionic strength controls the characteristic thickness of the electrical double layer, also known as the DeBye length, $1/\kappa$. κ is related to the ionic strength as follows:

$$\kappa = \left(\frac{2000F^2}{\varepsilon_0\varepsilon RT}\right)^{1/2}\sqrt{I} \qquad (4.6)$$

where κ is in m^{-1}, F is Faraday's constant, ε_0 is permittivity in vacuum, ε is the relative dielectric permittivity and I is the ionic strength ($=\frac{1}{2}\Sigma C_i Z_i^2$ where C_i is the ionic concentration in mol L^{-1}).

The approach to obtain experimental estimates of the attachment efficiency at a particular solution condition, was to first determine initial rates of aggregation (after significant doublet formation, the suspension is no longer monodisperse) and the rate constant, k_{11}. Based on theoretical estimates of k_{smol}, α can be calculated as:

$$\alpha = \frac{k_{11}}{k_{smol}} \qquad (4.7)$$

In aggregation studies, it is conventional to express the stability of a suspension in terms of the symbol, W, which is the inverse of α and known as the stability ratio,

$$W = \frac{1}{\alpha} \qquad (4.8)$$

$$\text{or } W = \frac{k_{smol}}{k_{11}} \qquad (4.9)$$

Large values of W correspond to stable suspensions, whereas α approaches zero. For unstable suspensions aggregating at DLCA conditions, W = 1.

When light scattering intensity measurements and initial aggregation rates are monitored to study RLCA kinetics, the aggregation rate constant can be estimated as follows (Virden and Berg, 1992):

$$k_{11} = \frac{1}{r_0 \cdot n_0} \frac{2I_1(q)}{I_2(q)} \frac{r_{h2}}{r_{h2} - r_{h1}} \left(\frac{dr}{dt} \right)_{t=0} \qquad (4.10)$$

where r_0 is the radius of particles at $t = 0$, n_0 is the particle number concentration at $t = 0$, $I_1(q)$ and $I_2(q)$ are the scattered intensity of singlet and doublet, respectively, $q = (4\pi/\lambda)\sin(\theta/2)$ is the magnitude of the scattering vector, where λ is the wavelength of the light in the medium and θ is the scattering angle, and r_{h1} and r_{h2} are the hydrodynamic radii of the singlet and doublet, respectively.

Based on the Rayleigh-Gans-Debye theory (RGD), Virden and Berg (1992) demonstrated the ratio of the intensity of singlet and doublet can be obtained as:

$$\frac{I_2(q)}{2I_1(q)} = 1 + \frac{\sin(2r_0 q)}{2r_0 q} \quad \text{when } \frac{2\pi d}{\lambda}|m-1| \ll 1 \qquad (4.11)$$

where d is the longest linear dimension through the particle and $m = n_{particle}/n_{medium}$ is the ratio of the complex refractive index of the particle to the refractive index of the surrounding medium. This equation is valid when the particle diameter is appropriately small. Mackinawite suspensions used here meet this criterion; the longest linear dimension of the FeS particle is 5.6 nm on average, and the wavelength of helium-neon laser of the instrument used in the research is 632.8 nm. The refractive indices for water and mackinawite are 1.333 and 2.5-2.8 at 20°C, respectively (Kyprianidou-Leodidou et al., 1997). From the experimental initial growth rates, $(dr/dt)_{t=0}$, the aggregation rate constant for slow aggregation can be obtained by substituting equation 4.11 into 4.10 which yields:

$$k_{11} = \frac{\beta}{r_0 \cdot n_0}\left(\frac{dr}{dt}\right)_{t=0} \qquad (4.12)$$

$$\text{where } \beta = \frac{2r_0 q}{2r_0 q + \sin(2r_0 q)} \frac{r_{h2}}{r_{h2} - r_{h1}} \qquad (4.13)$$

4.3 Methods and Materials

All aggregation experiments were conducted in an anoxic chamber. Photon correlation spectroscopy (PCS) by N4 Submicron Particle Size Analyzer (Coulter, The Woodlands, TX) was utilized to measure the change of particle sizes over time. Particle free deoxygenated/deionized water was prepared by filtering deoxygenated/deionized

water (18MΩ·cm, see chapter 3) with 0.1 μm syringe filters (GE Healthcare, Piscataway, NJ). 2 g L^{-1} of FeS suspensions were prepared using deoxygenated/deionized water (18MΩ·cm) and freeze dried FeS. The suspensions were completely re-dispersed on a magnetic stirrer for 4 days, and then filtered twice with 0.1 μm syringe filters (GE) to remove any undesired impurities or possible large FeS aggregates. The filtered stock suspensions had particle concentrations in the range of 60.0 to 80.9 mg FeS L^{-1} and a pH of 9.4 ± 0.3. Sample suspensions were prepared by adding proper amounts of buffers and salt solution (KCl) with the stock suspension. The desired ionic strength of solutions includes contributions of the buffer and additional salt. The added salt concentration to maintain the desired ionic strength was determined using MINEQL+. The pH was adjusted using MOPS for pH < 8 and borate for pH > 8. Potassium chloride was added to obtain the desired ionic strength. The sample particle concentrations used in PCS measurement were 13 ± 1 mg L^{-1} in FeS concentration and 40 ± 10 nm of mean diameter based on the scattered light intensity by PCS analysis. The equivalent particle number concentration was (6.49 ± 0.71) × 10^{10} cm^{-3}. All plastic wares, i.e., cuvettes and sample tubes, were rendered dust free by rinsing with filtered deoxygenated/deionized water (0.01 μm syringe filters). All solutions including buffers and salt were also filtered prior to use. The particle size changes were monitored until particles grew to approximately 250 nm in diameter. Most tests were replicated at least twice.

4.4 Results and Discussion

The changes in FeS aggregate diameter were measured over time at various pH and ionic strength using PCS. Figure 4.1 shows the aggregation rates of FeS as a function of pH at a constant ionic strength of 0.05 M. The initial aggregation rates clearly decrease as pH increases. The diameter of the aggregates was measured until they attained an aggregate size of about 250 nm. A complete experiment required 40 to 90 minutes over the pH range of 6.5 to 8.3 and an ionic strength of 0.05 M. At pH 9 and an ionic strength of 0.05 M, the total PCS measurement time was about 7 hours to attain a particle size of about 200 nm (complete data not shown in Figure 4.1). The data acquisition time for a

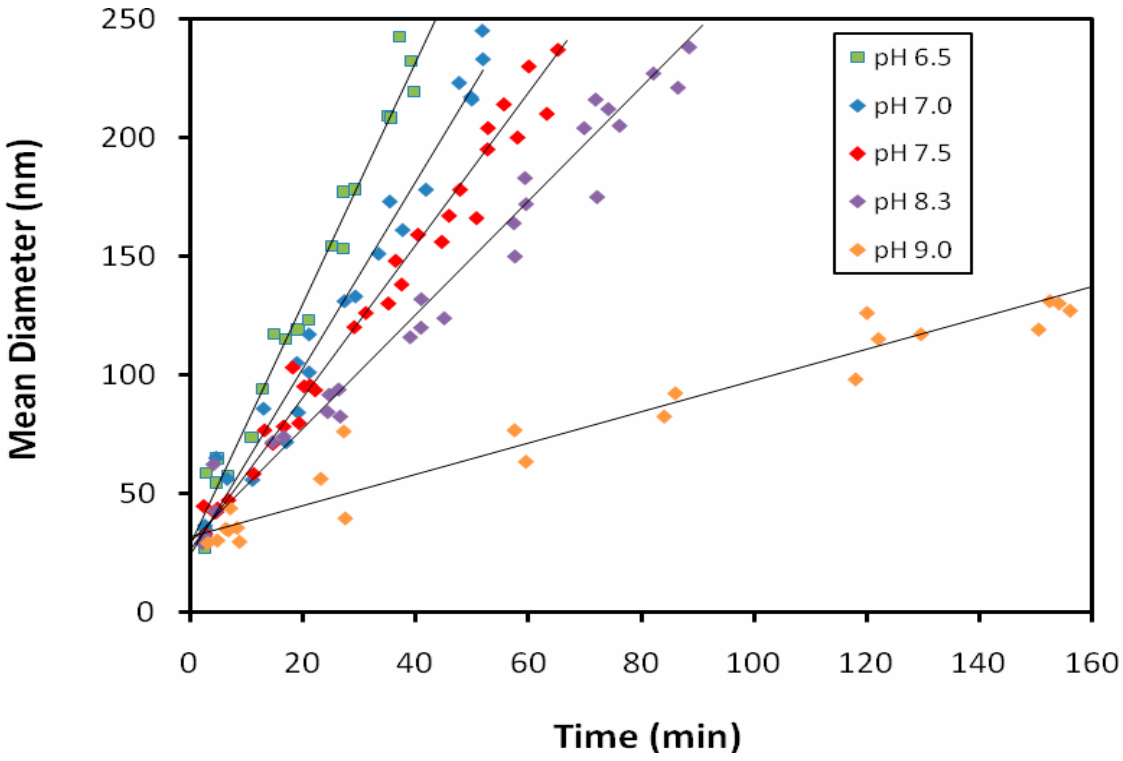

Figure 4.1 Initial aggregation rates of nanoparticulate FeS at various pH at a constant ionic strength of 0.05 M. The diameter of mackinawite were measured over time using Photon Correlation Spectroscopy

reading was 100 seconds for most samples. Over the course of an entire aggregation experiment, the suspensions were stable and no discoloration was observed due to the possible oxidation of FeS. For the fastest coagulation condition considered, ionic strength of 0.1 M at pH 8.3, in which the stability ratio (W) was 5.5 ± 0.3, and particles grew to a size of 300 nm in 3 minutes. In this case, particle size was measured every 30 seconds. At an ionic strength of 0.025 M, the particle coagulation rate was extremely slow. Approximately 120 hours were required to grow the particles to 190 nm. Over such long periods, the particles might undergo other reactions, such as oxidation, although no visual evidence of any precipitation or color change was observed.

The stability ratios (W) were calculated from the slopes, $(dr/dt)_{t=0}$, of the initial aggregation rate tests based on equations 4.12, 4.13 and 4.9. Table 1 summarizes the slope data and the stability ratios at various chemical conditions. For the pH 8.3 and ionic strength of 0.05 M suspension, the initial particle coagulation rate, $(dr/dt)_{t=0}$, was determined to be 1.21 nm min^{-1} in average from Figure 4.1. The initial particle concentration was 13.7 mg L^{-1}, and the initial particle size was 43.7 nm in diameter. From these data the initial particle number concentration, n_0, was calculated with a typical value of the mackinawite density, 4.5 g cm^{-1}. β was estimated from equation 4.13 as follows:

$$\beta = \frac{2r_0 q}{2r_0 q + \sin(2r_0 q)} \frac{r_{h2}}{r_{h2} - r_{h1}} = 1.9$$

where $q = (4\pi/\lambda)\sin(\theta/2) = 0.0169$

and λ = 632.8 nm and $\theta = 90^o$ for a PCS light source of 4 mV helium-neon laser

Table 4.1 The stability ratios of FeS nanoparticles as a function of suspension composition: pH, ionic strength, and buffer concentration.

Sample ID	pH	Ionic Strength (mM)	MOPS (mM)	Borate (mM)	HCl (mM)	$(dr/dt)_{t=0}$ (nm/min)	W (±σ)
65-50	6.48	50	10	0	0	2.7 (±0.16)	119 (±7.2)
70-50	6.99	50	10	0	0	2.0 (±0.14)	164 (±12.0)
75-50	7.48	50	10	0	0	1.5 (±0.11)	201 (±13.9)
83-50	8.32	50	0	10	0	1.2 (±0.12)	267 (±26.3)
90-50	9.03	50	0	10	0	0.33 (±0.018)	976 (±51.2)
65-50A	6.75	50	0	0	0.167	2.7 (±0.075)	119 (±3.3)
70-50A	7.06	50	0	0	0.125	2.3 (±0.13)	137 (±7.6)
75-50A	7.50	50	0	0	0.094	1.8 (±0.039)	181 (±3.9)
83-50A	8.12	50	0	0	0.070	0.94	188
83-50A1	8.41	50	0	0	0.076	1.0	250
90-50A	8.97	50	0	0	0.031	0.40 (±0.006)	802 (±12.1)
83-100	8.28	100	0	10	0	39 (±2.2)	5.5 (±0.3)
83-75	8.30	75	0	10	0	10 (±0.091)	20.6 (±0.2)
83-45	8.31	45	0	10	0	0.37 (±0.015)	585 (±24.2)
83-40	8.32	40	0	10	0	0.15	1423
83-35	8.29	35	0	10	0	0.075	2884
83-25	8.29	25	0	10	0	0.009 (±0.0004)	33769 (±1295)
70-50M5	7.00	50	5	0	0	1.7 (±0.0075)	128 (±0.6)
70-50M15	6.96	50	15	0	0	1.3 (±0.058)	166 (±7.6)
70-50M20	6.96	50	20	0	0	0.98 (±0.053)	218 (±11.8)
70-50M50	6.98	50	50	0	0	0.17 (±0.0085)	1258.5 (±63.2)
83-50B15	8.40	50	0	15	0	0.62	343
83-50B20	8.38	50	0	20	0	0.61	347
83-50B25	NM*	50	0	25	0	0.52	409
83-50B44	8.35	50	0	44	0	0.47	457

* NM is not measured

The rate constant obtained using equation 4.5 is:

$$k_{11} = \frac{\beta}{r_0 \cdot n_0}\left(\frac{dr}{dt}\right)_{t=0} = 2.49 \times 10^{-14}\ \text{cm}^3\ \text{sec}^{-1}$$

Therefore, the stability ratio is

$$W = \frac{1}{\alpha} = \frac{k_{smol}}{k_{11}} = 267.2$$

where $k_{smol} = \frac{4K_BT}{3\mu} = 6.63 \times 10^{-12}\ \text{cm}^3\ \text{sec}^{-1}$ at 28°C

Most samples were 2 – 3 times replicated, and the standard deviations of the initial aggregation rates and the stabilities are also reported in Table 4.1.

4.4.1 FeS Stability as a Function of pH

The pH dependence of the FeS suspension stability ratios tabulated in Table 4.1 is graphically presented in Figure 4.2. Over the pH range studied, the stability of FeS monotonically increases as pH increases, suggesting the FeS surface is negatively charged in the pH range tested. In the case of a positively charged surface, the charge density would be expected to decrease with increasing pH. Thus, the pH_{PZC} of mackinawite must be less than pH 6.5.

The sensitivity of FeS suspension stability to pH varied over the pH range studied. Buffer concentrations of 0.01 M were used to maintain the pH of suspensions; MOPS buffer for 6.5 < pH < 7.5, and borate buffer for 8.2 < pH < 9.0. In the region of pH 6.5 – 8.3, the stability ratios gently increased from 119 (±7.2) to 267 (±26). Bebie and coworkers (1998) showed that all metal sulfides are negatively charged above their pH_{PZC},

0.6 to 3.3, and their surface potential gradually increased in the neutral pH region. Also the zeta potential of the iron sulfides is weakly negative, -20 to -40 mV (Bebie et al., 1998), compared to iron oxides which easily go down to -100 mV (Kallay et al., 2005; Preocanin et al., 2006) which results in relatively low stability ratios. This may explain the relatively low and pH-insensitive stability of FeS suspensions in this pH region.

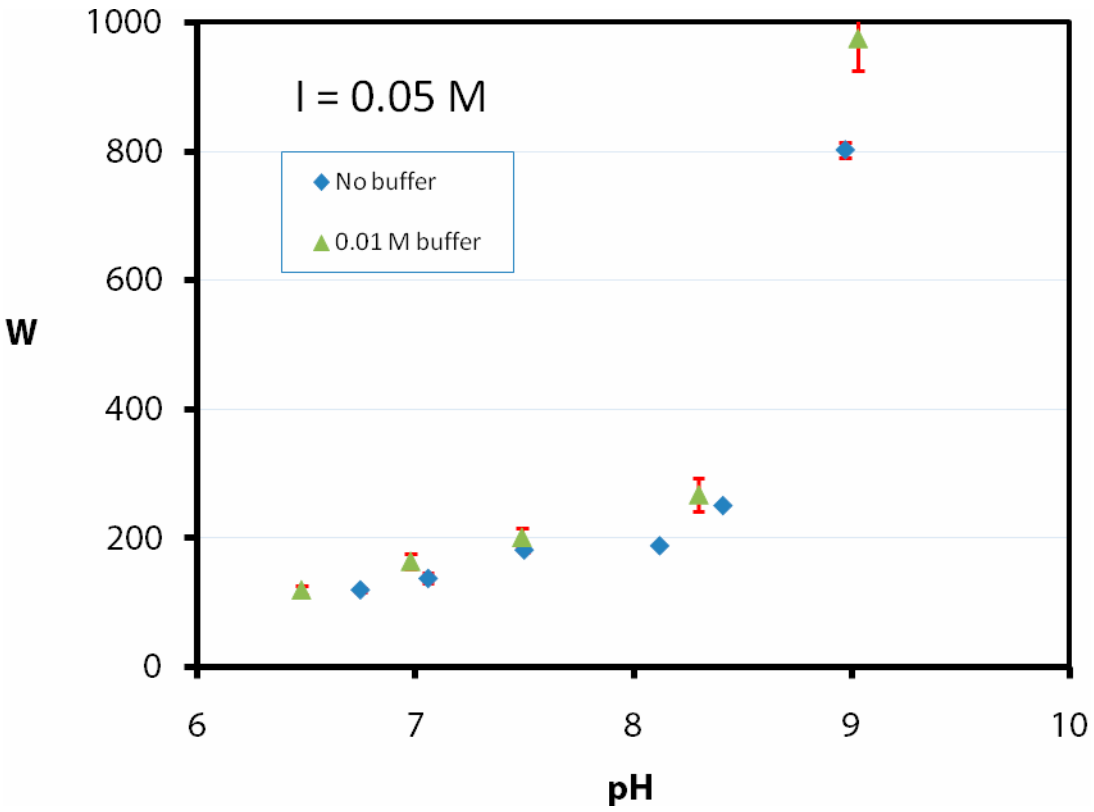

Figure 4.2 Stability ratios as a function of pH at a constant ionic strength of 0.05 M. Diamond markers present FeS suspensions in which the pH was adjusted with hydrochloric acid. Triangular markers represent suspensions in which the pH was adjusted with 0.01 M buffers: borate buffer for pH > 8, MOPS buffer for pH < 8. Red error bars indicate one standard deviation based on 2 to 3 replicates. Error bars where not visible, are smaller than the symbols.

A much more sensitive pH dependence of suspension stability is observed at more alkaline conditions. The stability ratio increased sharply between pH 8.3 and 9.0. These results appear to disagree with the pH independence of FeS electrophoretic mobilities reported by Mullet et al. (2004) over the pH range of 4 to 10, although such a large range of pH insensitive surface charge has not been reported in other studies. Possible explanations for the pronounced increase in observed stability in this study could involve either extensive deprotonation of surface functional groups or oxidation of the surface to form iron hydroxide phases. It should be pointed out, however, that in the preparation of FeS suspensions for all of the stability experiments, the original stock suspensions were dispersed for four days at somewhat alkaline conditions (pH = 9.4±0.3) before adjusting the pH and measuring aggregation rates. If oxidation near pH 9 was relatively rapid, it is unlikely that the effect would have been reversible and hence the particles should likely have behaved as iron hydroxides. It is unlikely that a fresh iron hydroxide phase, however, would be negatively charged at pH values as low as 6.5. Based on this reasoning, the deprotonation of surface functional groups is a more likely mechanism to explain the increase in stability at pH > 8.3.

Experimental determinations of FeS aggregation rates at pH < 6.5 were attempted, however, the dissolution of FeS was thought to interfere with the measurements in this pH range. The experimental data was characterized by considerably more scatter and a lack of reproducibility. These sample suspensions were also discolored after a few hours. The solubility of FeS begins to increase as pH decreases below pH 6.5 while its solubility

at neutral and alkaline pH is not pH dependent and the soluble iron concentration is quite low. For example, according to Richard (2006), the dissolved iron concentration is $10^{-5.7}$ M above pH 7. Thus, the dilute FeS suspension of about 13 mg L^{-1} ($10^{-3.8}$ M) employed in this experiment and the increased phase change rates to greigite by iron loss mechanism hindered accurate measurement of particle coagulation rates at acidic pH.

Aggregation rates were also studied in a buffer-less system in which the pH was adjusted using only hydrochloric acid. The stabilities of the suspensions that were pH adjusted using hydrochloric acid was slightly less than that of the pH buffered suspensions, but statistically not significant at this buffer concentration (0.01 M). Buffer effects on the stability along with buffer concentrations will be discussed later in this chapter.

4.4.2 Effect of Ionic Strength

The dependence of stability ratio on the ionic strength of the FeS suspension was also examined at pH 8.3. Figure 4.3 showed a sharp decrease in W from 33,800 (±1300) to 5.5 (±0.3) as the ionic strength increased from 0.025 M to 0.1 M. This decrease would be expected by a simple calculation of Debye length, κ^{-1} (see equation 4.6). The characteristic thickness of double layer was decreased from 1.93 to 0.96 nm with the increase of the ionic strength from 0.025 to 0.1 M. The net effect of double layer compression is to reduce the net interaction energy barrier, V_T, and thus W (see equations 4.6). As a rule of thumb, energy barriers greater than $15k_BT$, or so, are sufficient to stabilize a suspension such that 1 in ~10^6 (W = 10^6) collisions are effective (Stumm and

Morgan, 1996). At pH ≤ 8.3, the interaction energy barriers between FeS particles are probably smaller than this value for the range of ionic strengths used in this study.

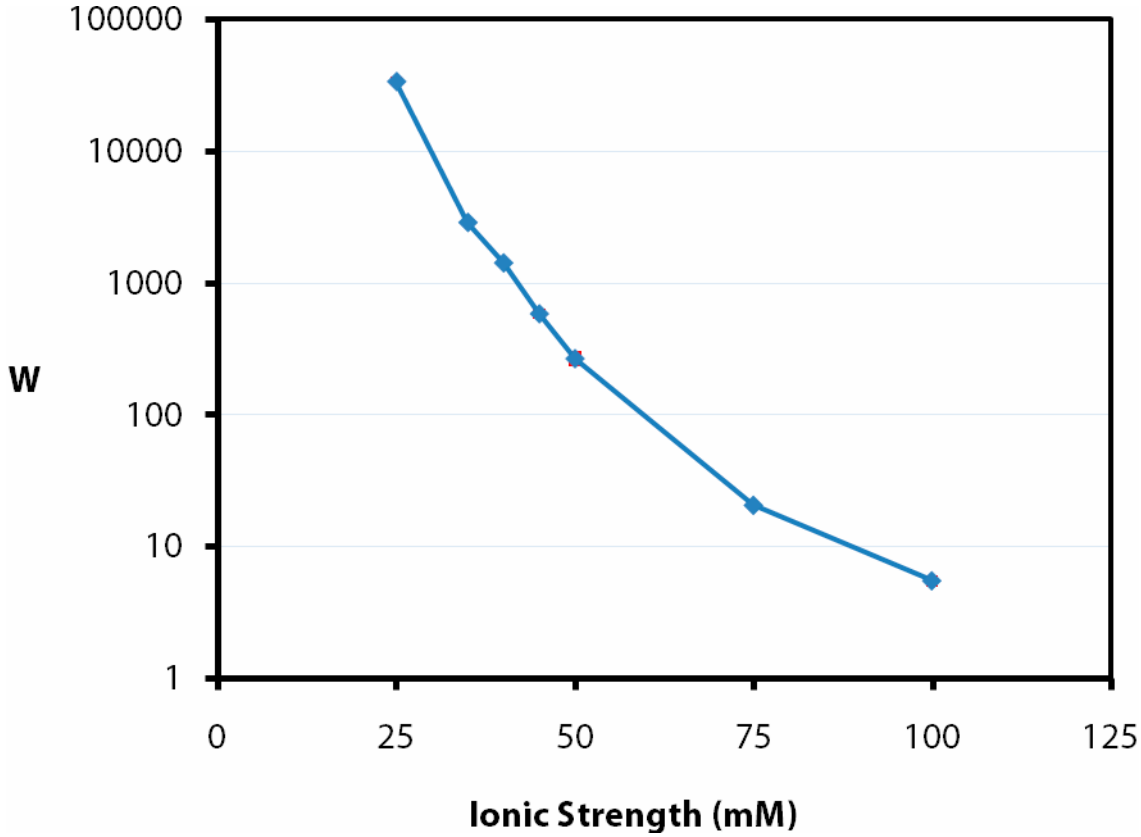

Figure 4.3 Semi-logarithmic plot of stability ratios of mackinawite as a function of ionic strength at pH 8.3 with 0.01 M borate buffer. Error bars are smaller than symbols.

4.4.3 Effects of Buffers on FeS Stability

With the addition of buffers to a suspension, there is a general concern that specific adsorption of buffer ion species could change the surface charge of the colloids being studied. In these aggregation studies, the pH buffers used were MOPS (3-(N-

Morpholino)-propanesulfonic acid, MW = 209.3) for the pH range 6.5 to 7.5 and boric acid ($B(OH)_3$, MW = 61.8) for pH 8.2 to 9.0. The effects of buffer concentration on FeS suspension stability were studied at a constant pH and ionic strength for each of the two buffer systems. Aggregation rates were also studied in buffer-less solutions in which the pH was adjusted with only hydrochloric acid.

Buffer effects on the particle stability are shown in Figure 4.4a and Figure 4.4b for the MOPS and borate buffers, respectively. In general there is an increase in particle stability with increasing buffer concentration. In the case of the MOPS system at pH 7, stability ratios increased only slightly from 131 ± 7.3 in the absence of buffer, to 218 ± 12 at 20 mM MOPS, but *W* then increased sharply to 1258 ± 63 at 50 mM MOPS. This might be explained by adsorption of high molecular weight organic compound to the surface of FeS (Joanny et al., 1979; Liang and Morgan, 1990; Zherenkova et al., 1998). MOPS buffer has molecular weight of 209.26. It should be pointed out, however, that if the FeS particle concentrations were larger than those used here, the sorbed concentration of MOPS would decrease, and the effect of MOPS on particle surface charge would likely diminish as well.

For the inorganic borate buffer, the stability of FeS gradually increased as the borate concentration increased at pH 8.3 and I = 0.05 M. *W* increased by a factor of 2, from 219 to 457, over the buffer concentration range tested, 0 to 0.044 M, respectively. MOPS affected the stability of FeS more than the borate at high concentrations.

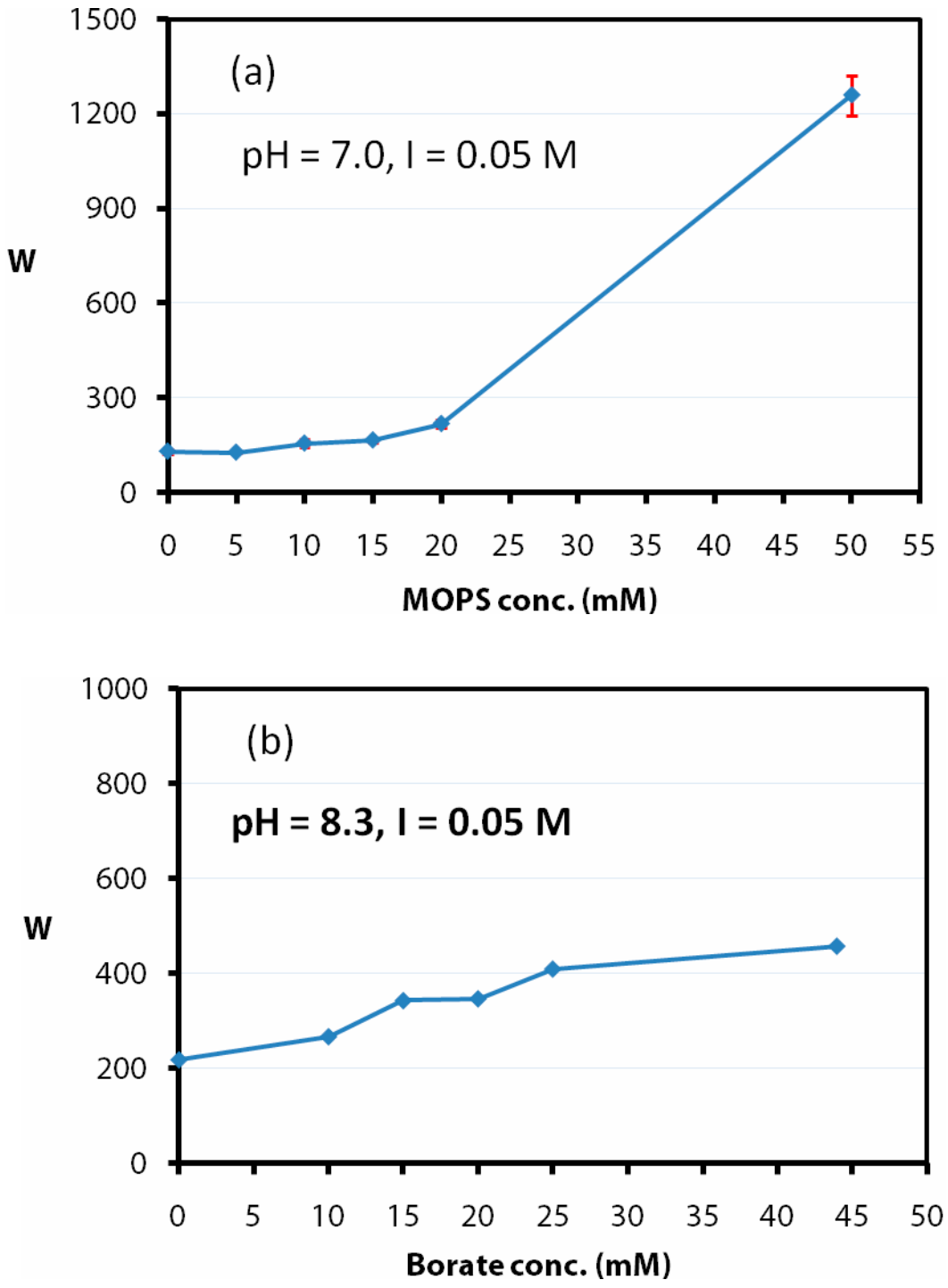

Figure 4.4 FeS suspension stability as a function of buffer concentration; (a) *W* as a function of MOPS buffer concentration at pH 7.0 and 0.05 M ionic strength. (b) *W* as a function of borate buffer concentration at pH 8.3 and 0.05 M ionic strength.

4.5 Conclusions

In this research, the stability of nanoparticulate mackinawite suspensions was characterized as a function of solution chemistry under anaerobic condiitons. The results demonstrate that the surface of mackinawite is negatively charged above pH 6.5 and thus its pH_{PZC} must be lower than pH 6.5. The stability is relatively pH-insensitive in the neutral pH range, pH 6.5 to 8.3. Values of the stability ratios (W) are relatively small and range from 120 to 270 as pH increases from 6.5 to 8.3. These W values suggest that 1 in 120 to 270 collisions result in the formation of an aggregate. By inference, the surface charge of FeS in this pH region becomes only slightly more negative as pH increases. The surface of FeS becomes sharply more negatively charged, however, between pH 8.3 and 9.0 in which the stability ratio increases from 270 to 980 at an ionic strength of 0.05 M. The presence of functional groups with varying acidity on the mackinawite surface is hypothesized to account for these pH regimes of weak and strong surface charge.

If MOPS is used as a pH buffer, the stability of FeS suspensions sharply increases as the MOPS concentration exceeds 0.02 M. This may be due to specific adsorption of this relatively high molecular weight organic compound on the particle surface, resulting in greater repulsive interactions between particles. The FeS stability is relatively insensitive to the presence of MOPS, however, below 0.015 M. Therefore, a careful selection of MOPS concentration is required to minimize specific adsorption effects of MOPS. Since the FeS particle concentrations were relatively dilute in these aggregation studies compared to the suspension concentrations that would be required for in situ emplacement systems, adsorption effects of MOPS might be negligible in such an

application. The stability of FeS increased only slightly as borate concentrations were increases.

Salt concentration strongly affects FeS stability. The stability of FeS suspension approaches unity at an ionic strength of 0.1 M and pH of 8.3. However, the suspension was significantly stable at an ionic strength of 0.025 M, as the stability ratio was more than 30,000. The sensitivity of FeS stability to ionic strength is expected in terms of classical electrical double layer compression. In order for FeS particles to penetrate the porous media without clogging at the injection point, the particles must stable themselves. The stability ratio must be sufficiently large, at least larger than hundreds. Therefore the FeS deposition tests were tested in the range of ionic strength 25 to 50 mM.

Chapter 5

Chemical Optimization of FeS Deposition on Granular Quartz Sand

5.1 Introduction

In this chapter the feasibility of *in situ* emplacement of FeS nanoparticles by direct injection into porous media is evaluated. These particle filtration experiments were conducted at the bench scale, in which columns of well defined granular quartz were used as the bed material. Although actual aquifer mineralogy will be more geochemically complex than the media used here, the motivation of these experiments was to demonstrate that the FeS deposition rates could be chemically controlled and optimized, and to improve our understanding of FeS-bed media interactions.

To successfully inject and emplace iron sulfide nanoparticles in porous media, deposition rates of the particles must be rapid enough to obtain coatings with sufficient reactive area, but plugging by high rates of deposition at the injection point must be prevented. In this set of experiments, the optimal deposition rates were evaluated by modulating the chemistry of nanoparticulate iron sulfide suspensions. It was hypothesized that optimal deposition conditions can be achieved when the interaction force between particle and porous media surfaces is sufficiently favorable to obtain good

coverage, while the interaction between suspended particles is sufficiently unfavorable. Favorable interactions between suspended particles would lead to rapid aggregation and plugging at the injection point. In addition, injected particles can be deposited on the surface of previously deposited FeS particles if particle-particle interactions are favorable, which again would promote plugging at the injection point.

It is envisioned that *in situ* emplacement of FeS would be most applicable in zones of relatively high permeability, such as sandy aquifers. Natural sand sediments are likely to have a wide variability of surface mineral coatings, however, such as metal oxides, carbonate minerals, aluminosilicates, clay particles, and organic matter, and often combinations thereof. Inevitably, these site-specific coatings will have an important influence on the mobility of suspended particles as they flow through the media. Despite the recognized complexity and variability of natural sands, there is a need to select bed materials that would more easily allow a mechanistic interpretation of the factors controlling FeS particle deposition. For this reason, a decision was made to use a well characterized clean quartz sand as the bed media. The results of those laboratory scale packed column tests are discussed in this Chapter.

5.2 Theory

The particle deposition rates in granular media depend on the rate of physical contact with the media and the rate of successful attachment. Yao et al. (1971) developed a clean bed filtration model based on earlier air filtration models of Friedlander (1958).

This classical filtration model was developed by considering particle deposition on a single spherical filter media (a collector). This theory assumes no interaction of colloids with previously deposited colloids such that the steady state deposition rates are given by:

$$\frac{dC}{dL} = -\frac{3}{2}\frac{(1-f)}{d}\alpha\eta C \qquad (5.1)$$

where C is the local concentration of suspended colloid, L is the bed depth, f is the bed porosity, d is the filter media diameter. α is the attachment efficiency factor which reflects the chemistry of the system shown as equation 4.7 – 4.9. η is the collection efficiency of the media which is the ratio of the rate at which particles strike the collector divided by the rate at which particles flux toward the media. According to Yao et al., the collection efficiency, η, by diffusion can be estimated as:

$$\eta_D = 0.9\left(\frac{kT}{\mu d_p d \upsilon_0}\right)^{2/3} \qquad (5.2)$$

$$\eta_I = \frac{3}{2}\left(\frac{d_p}{d}\right)^2 \qquad (5.3)$$

$$\eta_G = \frac{(\rho_p - \rho) g d_p^{\,2}}{18\mu\upsilon_0} \qquad (5.4)$$

where, η_D, η_I, and η_G represent single collector efficiency when the sole transport mechanism is diffusion, interception, and inertia, respectively (see Figure 2.9). k is Boltzmann's constant, T is the absolute temperature, μ is viscosity of fluid, d_p is the particle diameter, d is the media diameter, and υ_o is the pore velocity. The collection efficiency can be estimated by the sum of the equation 5.2 to 5.4, $\eta = \eta_D + \eta_I + \eta_G$.

For the FeS nanoparticles, $\eta = \eta_D$ because the deposition rates solely depends on diffusion for small particles less than 1 μm. FeS particles have diameters ranging from 2 to 10 nm, thus only diffusion controls their physical collection. When the FeS suspension becomes more unstable, i.e., at low pH, high ionic strength and/or high particle concentration, however, the particles aggregate appreciably, and the size distribution will broaden to include much larger particles. Under such conditions the particle deposition rates might be controlled by other mechanisms, i.e., interception and sedimentation. Other researchers (Fitzpatrick and Spielman, 1973) showed that the filtration theory can successfully describe in favorable particle deposition rates in model porous media, i.e., latex suspension and well glass beads.

The system at more complicated conditions, however, cannot be predicted by the simple clean bed filtration model, i.e., unfavorable chemical conditions, and heterogeneous and complex natural porous media (Grolimund et al., 1998; Kuhnen et al., 2000; Tufenkji and Elimelech, 2004; Kulkarni et al., 2005). Mechanistic descriptions of the deposition behavior under these conditions have not been elucidated. The deposition rates may be affected by previously deposited particles. Heterogeneous surface properties on colloids and distributed interaction energies between colloids and collectors may be possible causes of this observation. Interactions between the injected particles and the previously deposited particles may alter the deposition behavior. Heterogeneity of quartz sand, even after cleaning, may cause non-uniform coverage of colloids. At high aggregation rates of suspension, the injected particles can be deposited on the previously deposited particles. The most common approaches to modeling this filtration behavior are

based on empirical macroscopic physical models (Iwasaki, 1937). Such models described the rate of particle removal per unit depth of filter as proportional to the local concentration of suspended solids;

$$-\frac{\partial C_{SS}}{\partial L} = \lambda C_{SS} \qquad (5.5)$$

where C_{SS} is the concentration of suspended solids at any time and depth in the filter, L is the depth of the filter, and λ is the filter coefficient, which varies with time and depth in the filter.

In the porous media, the deposited (filtered) particles on the filter media are related to the rate of particle removal from suspension. The mathematical mass balance of migrating suspended solids is represented as follows (Weber Jr., W., 1972);

$$\upsilon \frac{\partial C_{SS}}{\partial L} = \frac{\partial \Omega_d}{\partial t} + (\varepsilon - \Omega_d)\frac{\partial C_{SS}}{\partial t} \qquad (5.6)$$

where υ is superficial velocity, Ω_d is volume of specific deposit per unit volume of filter, and ε is porosity of the clean bed. A general relationship between the filter coefficient, λ, and specific deposit, Ω_d, has been developed by Ives (1969). It is based on the hypothesis that the filter coefficient is a function of the changing specific filter surface available for deposition and the increasing interstitial velocity. At the initial stage of a filter run, the specific surface is represented by a porous bed of individual filter media. As the media is coated with deposited particles, the specific surface and the filter coefficient increase. As the deposit continues accumulating, however, the flow paths tend to straighten and the specific surface is represented by an assembly of individual cylindrical capillaries. The

specific surface decreases as the capillaries become smaller, and the filter coefficient decreases. The interstitial velocity increases as the deposits accumulates, and the filter coefficient decreases.

5.3 Methods and Materials

5.3.1 Column Apparatus for FeS Deposition Tests

A 2.6 cm-diameter and 25 cm-long glass column was used in the FeS deposition experiments. Clean quartz sand was packed with a dry packing method and the porosity was 0.34±0.01. The dry packed column was pre-equilibrated by processing 10 pore volumes of particle-free electrolyte solution which has the same composition as influent FeS suspension expect FeS particles. Figure 5.1 shows the schematic diagram of the column experiment. Influent suspensions of 1 g L^{-1} FeS were pumped into the quartz bed in an upflow direction using an HPLC pump (Series I, Lab Alliance, State College, PA) at 3 mL min^{-1}. Ten pore volumes of the suspension were injected to the pre equilibrated quartz packed column during the deposition experiment. Effluent fractions were collected in 15mL polypropylene tubes using an automatic fraction collector. Since the column length and influent suspension concentrations were the same in all of the deposition experiments, the breakthrough and specific deposit concentration profiles of FeS in the bed are intercomparable.

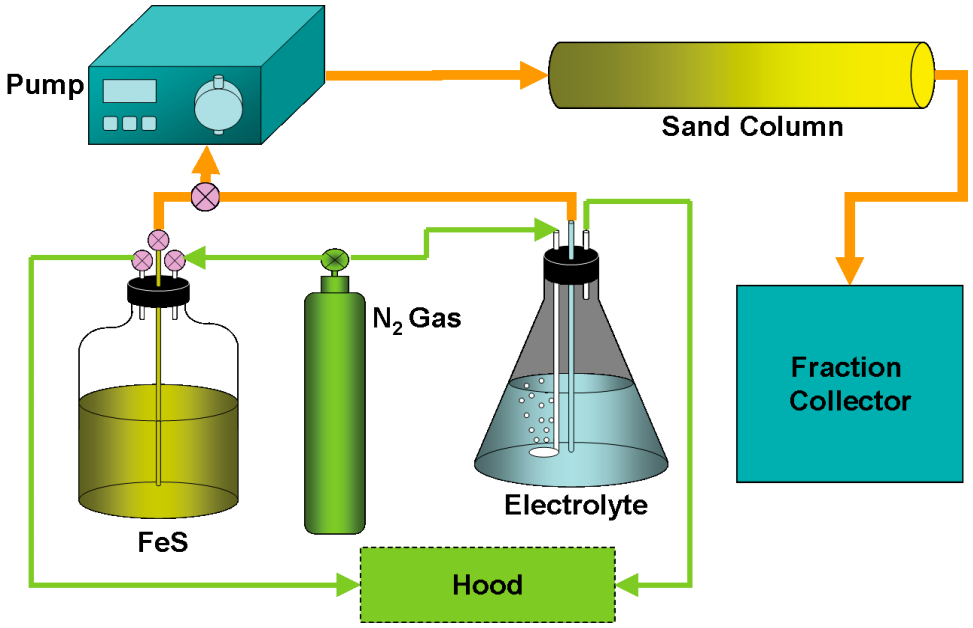

Figure 5.1 Schematic of column apparatus used in FeS deposition experiments

5.3.2 FeS Suspension

One gram of freeze-dried FeS was re-dispersed in 1 liter of deoxygenated deionized water for each column experiment. The suspensions were mixed with a stirrer for 48 hours in an anaerobic chamber before adding pH buffers and salt. The 1 g L^{-1} FeS suspension without the addition of chemical has an alkaline pH of 10.3 and a conductivity of 92 µS cm^{-1} which is equivalent to 0.71 mM of KCl. The mean size of the FeS particles after dilution of the suspension was 2 – 4 nm. Borate (0.0125 M) and MOPS (0.015 M) buffers were used to adjust the suspension over the range of pH 8.3 to 9.0, and pH 6.5 to 7.5, respectively. Sodium chloride (NaCl) was used to adjust the ionic strength as necessary. Calculations of the concentration of NaCl needed to achieve the desired ionic strength were performed with MINEQL+, in which the contributions of the

buffer system to the ionic strength were also calculated. After chemical adjustment, the 1 g L^{-1} FeS suspension was further mixed for 24 hours prior to each column injection test.

5.3.3 Sectioning of FeS-deposited Sand and Iron Analysis

In order to investigate deposition rates of FeS through the column length, the bed media were destructively sectioned after the 10-pore volume injection period. A hydraulic extrusion approach was developed in which the 25-cm bed depth could be precisely separated into 10 sections (see Figure 5.2). Concentrations of deposited FeS on the sand were obtained by drying and extracting the sand sections with 6N HCl. The extracts were analyzed for total iron by either ICP-MS or colorimetric method based on standard methods, 3500-Fe. D (AWWA, APHA, WEP, 1995).

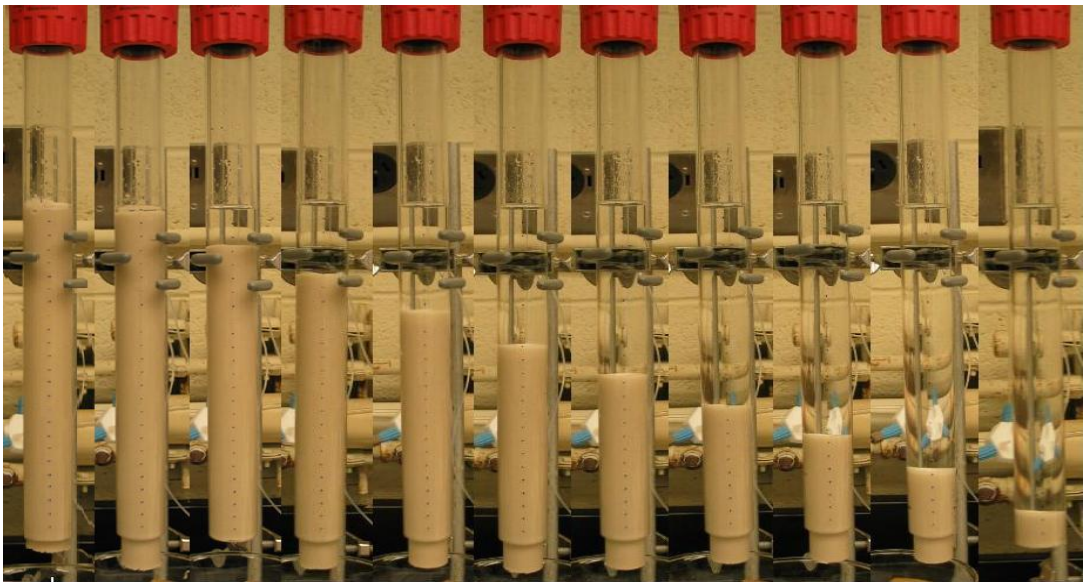

Figure 5.2 Sequential photographs of the column illustrating the progressive hydraulic extrusion of the sand bed (from left to right) for sectional analysis of the specific deposit concentration of FeS on the sand.

5.4 Results and Discussion

5.4.1 Feasibility of Emplacement of FeS on Quartz Sand by Injection

To validate that chemical control of FeS particle filtration rates was possible, deposition experiments were conducted at an alkaline pH and minimum ionic strength. In these initial experiments, one gram of dried FeS was dispersed in a liter of deoxygenated, deionized (DI) water. The resulting pure FeS suspension has a pH of 10.3. At this pH condition, FeS particles are negatively charged and repulsive interaction forces between the particles and the sand should be present since the quartz is also negatively charged at this pH condition. The conductivity was 92 $\mu S\ cm^{-1}$, which equivalent to the conductivity of a 7.1×10^{-4} M KCl solution. In this initial experiment, the effluent or the deposited FeS concentrations were not made quantitatively, rather the goal was to determine if the expected rapid breakthrough of particles was visually observable. Sequential photographs of the column were taken over the course of the injection. A total ten pore volumes of the pure 1 $g\ L^{-1}$ FeS suspension were introduced to a 25 cm-long model quartz sand column at 3 $mL\ min^{-1}$.

At this pH, and without salt addition, rapid breakthrough of FeS was observed after one to two pore volumes. Photographs showing the progression of the FeS particle 'front' in the injection experiments are shown in Figure 5.3. Figure 5.3 shows a sequence of the injection experiment of the pure FeS suspension. Columns 1 through 6 in this Figure show a progression of the front during the first pore volume, which indicates rapid breakthrough. The seventh column photo was taken immediately after 10 pore volumes

of the suspension were introduced. The entire length of the colujmn appeared dark after 10 pore volumes, due to the high concentration of FeS in the pore liquid. An additional 2 pore volumes of particle-free deoxygenated DI water was injected to subsequently wash out the FeS suspension in the pore liquid in order to visualize the extent of particle deposition. The sand was visibly but slightly discolored relative to the clean column (see column photo (8) in Figure 5.3).

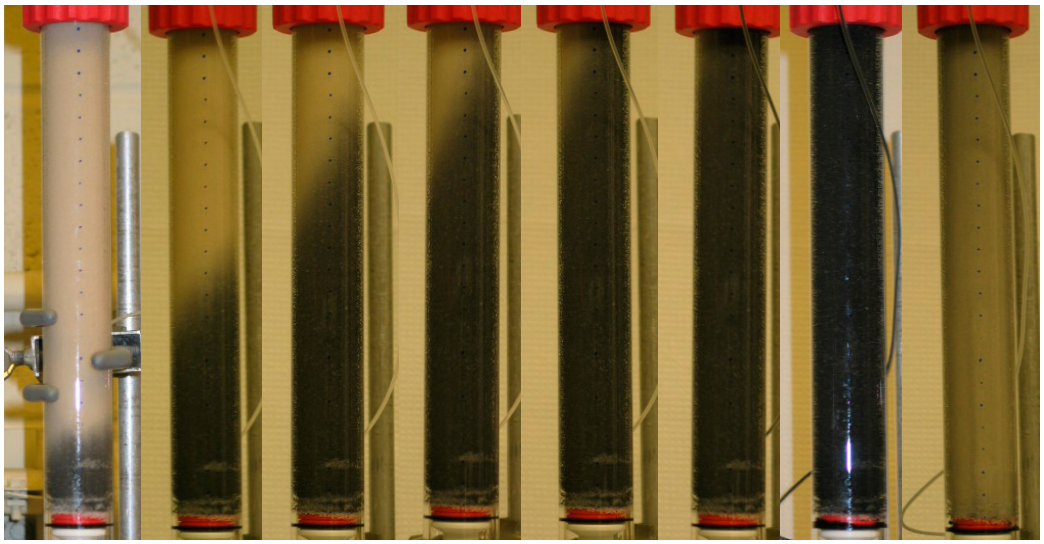

(1) (2) (3) (4) (5) (6) (7) (8)

Figure 5.3 Visual breakthrough behavior of 1 g L^{-1} FeS suspension in columns containing clean quartz sand without pH adjustment (pH = 10.3) and no added salt. Columns (1)-(6): progression during 1st pore volume of FeS suspension injection; Column (7): after 10 pore volumes; Column (8): after injecting additional 2 pore volumes of particle-free DI water

The nearly unretarded breakthrough and slight FeS coverage of the sand indicates significant repulsive interactions must exist between the FeS colloids and the sand. If repulsive interactions did not exist, most of injected FeS nanoparticles injected would be deposited through the column, a claim which can be demonstrated by calculations using the traditional clean bed filtration theory (Yao et al., 1971, equation 5.1). Assuming no interaction of colloids with previously deposited colloids, the hypothetical steady state effluent concentration can be calculated for the case when particle-grain interactions are completely favorable and simply diffusion-limited, i.e., attachment efficiency, α, was unity in Equation 4.7, and the collection efficiency parameter, η, is approximated by the diffusion-limited collection rate, η_D, of Equation 5.2. This calculation, using the values of parameters given in Table 5.1, yields a normalized effluent breakthrough concentration, C/C0, of 1.3×10^{-20}. These calculations demonstrate that without repulsive interactions, particle breakthrough concentrations would not be visually detectable. In the preliminary experiment shown in Figure 5.3, however, breakthrough effluent concentrations were visually similar to the influent particle concentration, suggesting that FeS nanoparticle interactions with the sand were unfavorable at these solution conditions.

The pH 10.3 experiment in which FeS suspensions were injected resulted in rapid breakthrough and significantly low FeS coverage on the sand. This result suggests that significant electrostatic repulsive interactions exist between the sand and the colloids. Since sand and FeS particle surface charge are a function of solution chemistry, i.e., pH and ionic strength, more favorable interactions can be achieved by reducing the repulsive forces with changes in solution chemistry. Self interactions between colloids, however,

Table 5.1 Variables used in sample calculation for deposition rates using clean bed filtration theory with negligible repulsive barrier

Variables	Values
Porosity, f	0.34
Mean sand diameter, d (m)	2×10^{-4}
Column depth, L (m)	0.25
Particle diameter, d_p (m)	1×10^{-8}
Temperature, T (K)	298
Water viscosity, μ (kg/m·s)	8.91×10^{-4}
Velocity, v (m/s)	2.77×10^{-4}
Boltzmann constant, k ($m^2 \cdot kg/s^2 \cdot K$)	1.38×10^{-23}
Collision efficiency, α	1
Contact efficiency, μ	3.70×10^{-2}

must be significantly unfavorable to prevent aggregation and plugging in the inlet region. The optimal conditions of FeS deposition rates on the sand can be achieved if the interactions between the colloids and the sand are sufficiently favorable while the interactions between the colloids themselves are sufficiently unfavorable. Subsequent experiments were performed to quantitatively ascertain the optimal pH and ionic strength and optimal deposition conditions.

5.4.2 Chemical Optimization of Deposition of Colloidal FeS

FeS deposition experiments were conducted at varying pH conditions from pH 6.5 to 10.3, and three ionic strengths, 0.025 M, 0.05 M, and 0.077 M of the 1 g L^{-1} particle

suspension. 0.0125 M Borate buffer solutions were used to buffer the pH 8.3 and 9.0 experiments. 0.036 M organic MOPS buffer was used to adjust pH of FeS suspension to 6.5 and 7.5. This MOPS concentration was the minimum concentration needed to buffer the desired pH with a 1 gL^{-1} FeS suspension. Most of the column tests were duplicated. The resulting profiles of deposited FeS concentrations after 10 pore volumes, as well as effluent iron breakthrough concentrations were measured at three ionic strengths, and at a series of pH conditions for each of those ionic strengths.

FeS deposition at 0.05 M ionic strength

As the visual FeS deposition experiment in Figure 5.3 demonstrated, very little FeS retention was noted at the most unfavorable deposition conditions (pH 10.3, no salt). In the presence of 0.05 M NaCl, however, an appreciable and relatively uniform FeS deposition was observed over the entire length of the column as shown in Figure 5.4 (a), with a mean FeS deposit concentration of 5.1 $\times 10^{-6}$ mol Fe g^{-1} sand (see Table 5.2). The effluent breakthrough curve (see Figure 5.4 (b)) approached 80% of the influent concentration of particles after 3 to 4 pore volumes, suggesting that there is an apparent unfavorable deposition condition between the FeS nanoparticles and quartz sand as well as repulsive interaction forces between the deposited and suspended FeS particles.

At an ionic strength of 0.05 M, the deposition and breakthrough of 1 g L^{-1} FeS suspensions were further examined in duplicate at relatively alkaline pH 9.0 and 8.3. At these alkaline and moderate ionic strength conditions, FeS deposition profiles exhibited highly uneven distributions throughout the length of column. Furthermore, the profiles

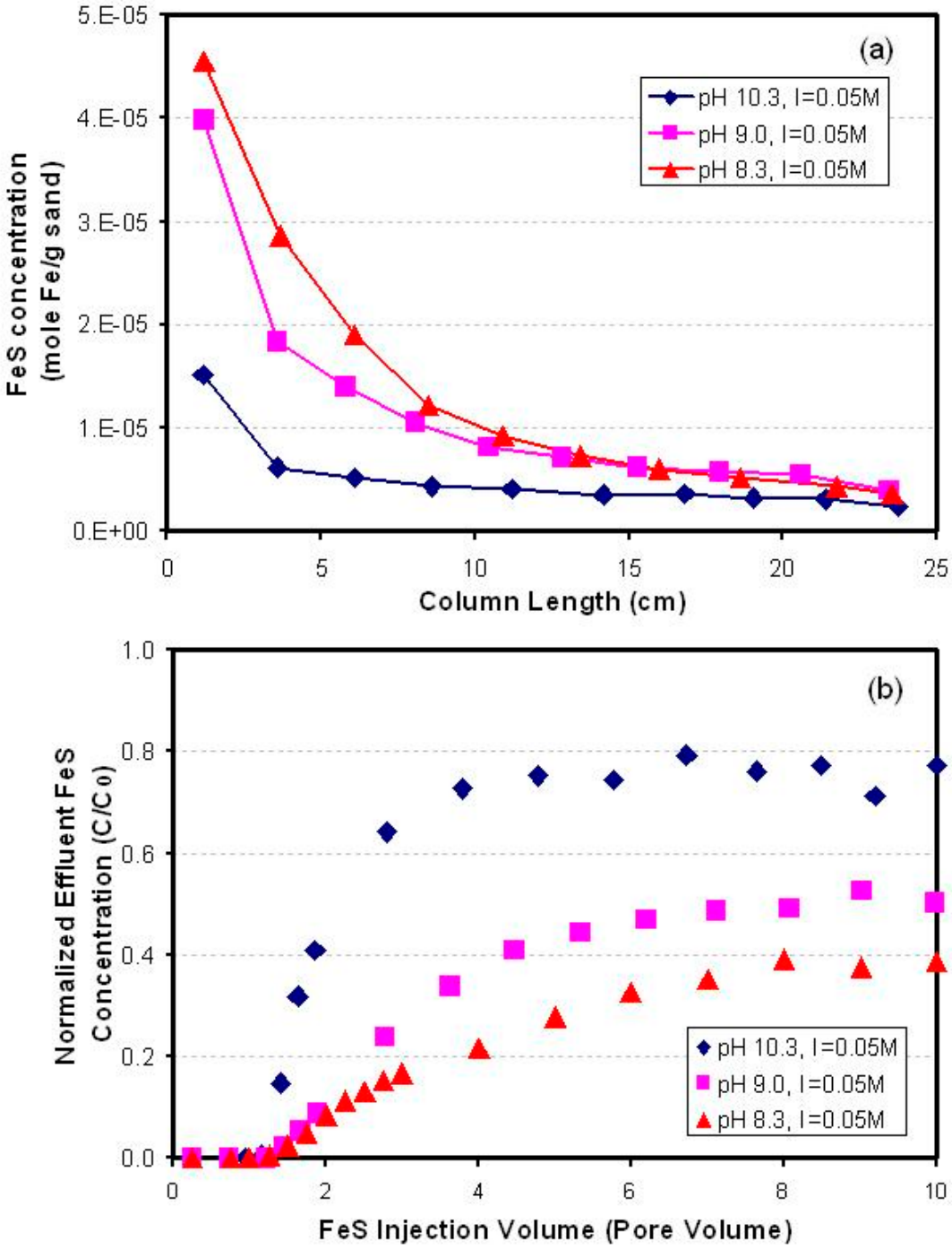

Figure 5.4 Deposition experiments of 1 g L^{-1} FeS suspension at various pH, pH 8.3 to 10.3 at an ionic strength of 0.05M. (a) Deposited FeS concentration profiles after injection of 10 pore volumes of 1 g L^{-1} FeS, (b) Effluent breakthrough curves during the injection of FeS suspension

show an accumulation of particles near the inlet. This accumulation is likely due to relatively favorable FeS particle-particle interactions at this ionic strength and pH. Figure 5.4b presents the corresponding breakthrough curves during particle injection. The effluent iron concentrations reached a maximum at 40 and 50 % of the influent suspension concentration at pH 8.3 and 9.0, respectively. The incomplete breakthrough suggests that the amount of FeS deposition should continue to increase over longer injection periods. The pH effect, therefore, was to increase FeS deposition rates as pH decreases. These results are consistent with the stability study findings of FeS suspension in Chapter 4, in which FeS particle stability was found to monotonically increase with pH over the same pH range. Additional experiments were therefore conducted at a lower ionic strength, 0.025 M, to investigate whether more uniform deposition through the column is possible. In addition, near neutral pH (pH 6.5 and 7.5) conditions were employed to see if greater deposition rates can be achieved due to more favorable interactions between the particles and the sand.

FeS deposition at 0.025 M ionic strength

At a lower ionic strength of 0.025 M, it was possible to consider a wider range of pH conditions (pH 6.5 to 10.3) since the FeS suspensions were then sufficiently stable at the lower end of this pH range. The deposition profiles and effluent breakthrough behavior of FeS suspensions in these column experiments are presented in Figure 5.5. In Figure 5.5 (a) two groups of deposition profiles are evident; at neutral pH, pH 6.5 to 8.3, deposition rates were similar, while they were significantly higher than those obtained

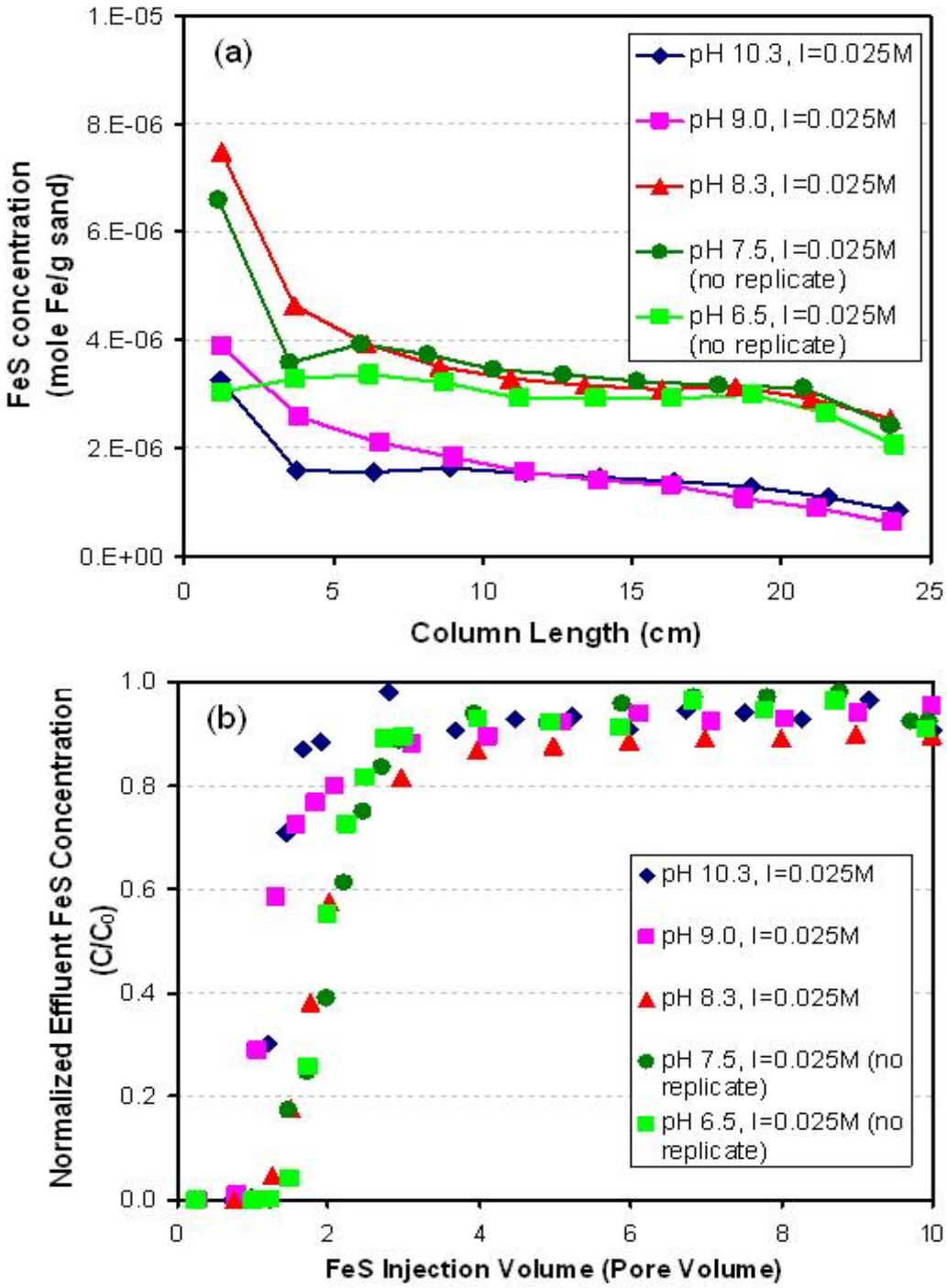

Figure 5.5 Deposition experiments of 1 g L^{-1} FeS suspension at various values of pH, pH 6.5 to 10.3 with ionic strength of 0.05M. (a) Deposited FeS concentration profiles after 10 pore volume injection of 1 g L^{-1} FeS, (b) Effluent breakthrough curves during injection of FeS suspension

under alkaline pH, 9.0 and 10.3. The sharper sensitivity of FeS deposition rates to pH between pH 8.3 and 9.0 is similar to the pH range at which the stability of FeS suspensions becomes increasing sensitive to pH as discussed in Section 4.4.1. The deposition profiles are further evidence that the surface charge of FeS is insensitive to pH in the neutral pH region and that there is a pronounced increase in surface ionization of the FeS surface at a pH > 7.5.

The deposited FeS profile near the column inlet at pH 6.5 reveals slightly lower coverage than the profile at pH 7.5, although it was expected to be higher based on the stability studies. Given that the solubility of FeS is significantly higher at pH 6.5 relative to pH 7.5 (Richard, 2006), these trends may be related to FeS dissolution. Since the influent suspensions are saturated, however, the exact role of dissolution is unclear. Dissolution may, for example, change the particle size distribution of the influent suspension and thereby affect the rates of deposition near the inlet. It should be noted that the net effect of lower particle coverage near the inlet would be a decreased risk of plugging. In a field application, these injection conditions could therefore be advantageous.

The breakthrough curves (Figure 5.5 b) also indicate that FeS particles at alkaline pH were less favorably attached to the quartz grain surface. The effluent concentrations (C) at alkaline pH, 9.0 and 10.3, more rapidly approached the influent concentration (C_0) after the injection of two pore volumes of the FeS suspension while the effluent concentrations at neutral pH, 6.5 to 8.3, approached the initial concentration (C_0) after the injection of three pore volumes. Since the breakthrough concentration approached the

influent concentration, further significant FeS deposition would not be expected if the injection period was increased.

FeS deposition at 0.077 M ionic strength

Additional deposition tests at higher ionic strength were performed to establish conditions leading to plugging in the injection region of column. Because of the insensitivity of FeS deposition to pH over the neutral pH range, only on pH condition was considered, pH 8.2. Ten pore volumes of 1g L^{-1} FeS suspension, adjusted to pH 8.2 using 0.0125M borate buffer and achieved by the total ionic strength of 0.077 M based on $MINEQL^{+}$ analysis with an addition of 0.05M NaCl, was injected through the column at 3 mL min^{-1}.

Figure 5.6(a) shows a high deposition rates at the injection point as high as 8×10^{-5} mole Fe per gram sand, and a considerably less uniform Fe deposition profile than those at lower ionic strengths. Figure 5.6(b) indicates the breakthrough curve reached a plateau after 2 pore volumes were injected, followed by a decrease in effluent FeS concentration until 6 pore volumes were introduced, followed by no penetration of FeS particles after the injection of 7 pore volumes. This breakthrough curve and deposition profile suggest that favorable or near favorable deposition conditions exist between FeS and the previously deposited FeS particles, since almost all of the particles were retained in the column after 7 pore volumes were injected. By the seventh pore volume, deposited particles were sufficiently numerous as to retain all of the approaching particles. At this ionic strength of 0.077 M and pH 8.2, significant plugging was also observed at the

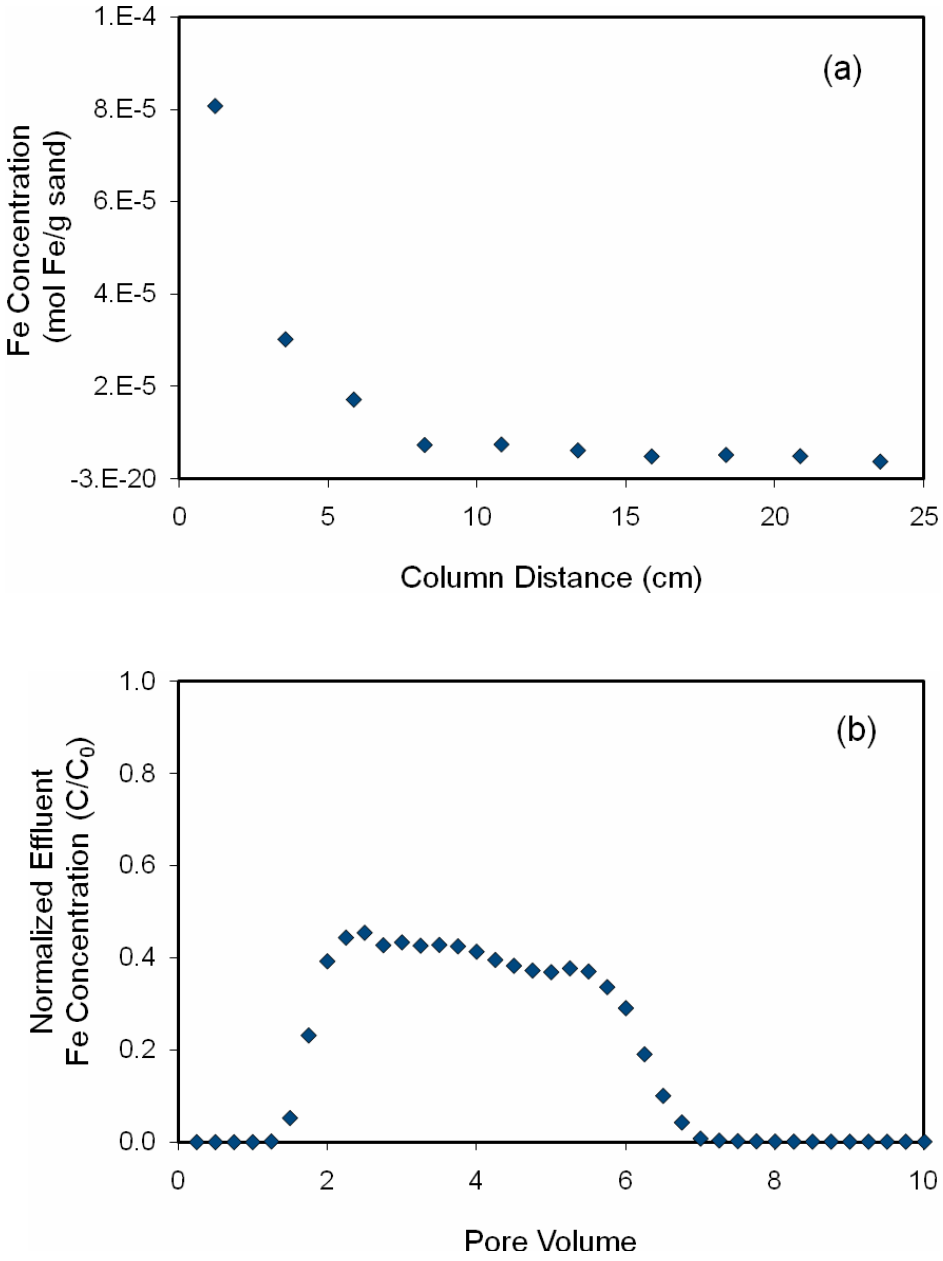

Figure 5.6 Deposition experiments of 1 g L^{-1} FeS suspension at pH 8.2 with ionic strength of 0.075M. (a) Deposited FeS concentration profiles after the injection of 10 pore volumes of 1 g L^{-1} FeS, (b) Effluent breakthrough curves during the injection of FeS suspension

injection region of the column due to the sufficiently favorable interactions between the particles and the previously deposited particles. An increase in back pressure was noted during the experiment.

5.5 Chemical Optimization Conclusions for FeS Deposition

Based on sectional measurements of deposited FeS in each of the column experiments, the average coverage and variance of the deposited FeS after 10 pore volumes was calculated to assess the optimal solution conditions for uniformity and maximum coverage. A summary of these calculations is presented in Table 5.2. As the normalized standard deviations for the data indicate, the greatest uniformity of coverage was obtained at the lowest ionic strength, 0.025 M and greater spatial differences in coverage were observed with increasing ionic strength. Neutral pH conditions lead to the greatest FeS particle deposition rates, an average of 3×10^{-6} mole iron per gram of sand, and therefore would represent optimal injection conditions. Experiments conducted at these optimal deposition conditions are shown in boldface type in Table 5.2. Due to the high solubility of FeS at pH < 6.5, more acidic conditions than the pH range suggested here would be problematic.

Both the stability and deposition rates of FeS suspensions in sand columns were relatively independent of pH over a range that is typical of many natural aquifer pH conditions (pH 6.5 - 8.3). This finding is likely to be helpful in terms of implementing injections of FeS suspensions at a field site, since it suggests that pH adjustment of the

FeS suspension to values outside the range of the natural groundwater pH conditions would not be necessary or desired. A significant pH shift in an aquifer could cause new mineral phases to precipitate and reduce its hydraulic conductivity and therefore should be avoided. The results of these deposition studies suggest that FeS suspensions for injection into most aquifers could be designed to match the local groundwater pH conditions while still yielding approximately optimal deposition rates.

Table 5.2 Summary of deposition rates at various pH and ionic strength

1g/L FeS Suspensions		Average FeS Coverage (mol Fe/g sand)	FeS deposition in first 2.5cm (mol Fe/g sand)	FeS deposition in last 2.5cm (mol Fe/g sand)	Normalized standard deviation*
pH	Ionic strength (M)				
10.3	0.025	1.56×10^{-6}	3.25×10^{-6}	1.08×10^{-6}	0.41
9.0	0.025	2.43×10^{-6}	3.87×10^{-6}	8.81×10^{-7}	0.55
8.3	**0.025**	**3.76×10^{-6}**	**7.48×10^{-6}**	**2.91×10^{-6}**	**0.38**
7.5	**0.025**	**3.66×10^{-6}**	**6.50×10^{-6}**	**3.12×10^{-6}**	**0.30**
6.5	**0.025**	**2.93×10^{-6}**	**3.04×10^{-6}**	**2.65×10^{-6}**	**0.13**
10.3	0.050	5.08×10^{-6}	1.52×10^{-5}	3.01×10^{-6}	0.73
9.0	0.050	1.19×10^{-5}	3.98×10^{-5}	5.40×10^{-6}	0.69
8.3	0.050	1.45×10^{-5}	4.55×10^{-5}	4.31×10^{-6}	0.93
8.3	0.077	5.74×10^{-6}	**8.06×10^{-5}****	4.93×10^{-6}	1.42

* Normalized standard deviation = standard deviation/mean of data from 10 sections in the column

** 100% retention of FeS particles occurred

Chapter 6

Release of Deposited FeS

6.1 Introduction

An important factor that could limit the useful design life of PRBs that contain nanoparticulate FeS as the reactive media is gradual loss mechanisms of the FeS. The cost-effectiveness of the technology would be significantly reduced if frequent reinstallation or rejuvenation of the reactive material was required in order to replace lost FeS. These considerations would be the case whether the PRB was constructed by *in situ* emplacement of injected particles or trench-and-fill approaches. In addition, remobilization of the reactive materials could seriously degrade the treatment performance of the PRB if sequestered contaminants are also remobilized. An understanding of the release mechanisms of nanoparticulate iron sulfide coatings in porous media will be critical, therefore, to FeS-type PRB applications. Two important FeS release mechanisms include particle detachment and FeS dissolution. Since it was hypothesized that hydrogeochemical solution conditions would control the rates and relative importance of these two release mechanisms, the experiments described in this Chapter were designed to study FeS release as a function of solution chemistry.

The rate of particle detachment from the surface of a granular packed bed is governed in part by the interaction forces between the particles and the subsurface grain, which are a function of pH and solution ionic strength of the suspension. The detachment rate is reported to increase as the pH increases when both of the particles and the subsurface grain are negatively charged, such as in the case of iron sulfides and quartz in neutral to alkaline pH conditions, since the interacting surfaces become even more negatively charged as the pH increases (Ryan and Elimelech, 1996; Sen and Khilar, 2006). In response to variations in ionic strength, particle detachment rates can generally be expected to decrease as the ionic strength increases due to a decrease in repulsive interaction forces between the colloid and grain surfaces (Kallay, 1986; Ryan and Gschwend, 1994; Roy and Dzomback, 1996).

Iron sulfide dissolution may be another significant loss mechanism, especially at acidic pH conditions. Literature values of the solubility of mackinawite suggest it is a relatively soluble metal sulfide at acidic pH, although the equilibrium constants are not in close agreement (see Table 2.1). In this research the mechanisms of FeS loss were investigated, by distinguishing iron loss due to dissolution from loss by particle detachment as a function of pH and ionic strength. In conjunction with the experimental results, mathematical modeling was proposed to characterize the dissolution kinetics where dissolution is shown to be a significant mechanism of FeS particle release. A mathematical model was employed to simulate the transport and dissolution of iron and assess whether FeS dissolution is limited by mass transfer. In order to test the mass transfer limitation, effects of flow rate variations were also tested. The results of these

experiments and modeling further helped to characterize the solubility of FeS. A pH range of 5.5 to 10 and an ionic strength range of 0.001 to 0.1 M were considered in order to bracket the range of natural groundwater conditions.

6.2 Methods and Materials

The method of FeS application to sand, say by *in situ* injection or by precoating the sand for trench-and-fill use, is likely to effect the loss rate of FeS from the sand. Iron release experiments from coatings obtained by particle filtration and batch application on sand were compared in this study, although due to the difficulty in analyzing the former systems, more extensive studies were conducted with batch-coated FeS sand columns. The primary complexity introduced with coatings generated by particle deposition was an inability to characterize the spatially non-uniform FeS content of the sand as an initial starting condition of FeS release experiments.

6.2.1 FeS Release Tests using Deposited FeS Sand

Release of FeS was initially studied in sand columns where the FeS coating was deposited from flow-through suspensions. This column experiment was conducted outside a glovebox using the same systems described in Section 5.3.1. The FeS-coated sand was prepared by injecting suspension into a clean sand column under one of the same conditions in which deposition had previously been studied. This condition corresponded to a pH 8.3, 0.025 M ionic strength solution, which yields a relatively uniform deposition profile in earlier experiments, as shown in Figure 5.5. Based on the

previous estimates of the average FeS coverage for these conditions in Table 5.2, approximately 3.76×10^{-6} mol FeS per gram of sand would be expected by these FeS injection procedures.

Using the same starting column, FeS release was studied by sequentially reducing the pH of the particle-free influent solution (in 11 pore volume increments), while maintaining the ionic strength at 0.025 M. In the first stage, pH 8.3 particle-free electrolyte solution was injected in the FeS-coated sand column for eleven pore volumes, followed by an additional eleven pore volumes of pH 7.5 electrolyte solution, and finally pH 6.5 electrolyte was injected over another eleven pore volumes.

6.2.2 FeS Release Tests using FeS Pre-coated Sand

The FeS pre-coated sand was prepared according to a method developed by Han (2009) that included mixing of 50 grams clean quartz sand (Chapter 3.4) and 30 mL of 3.70 ± 0.05 g L^{-1} of well-dispersed FeS suspension in 50 mL polypropylene air tight centrifuge tubes. The mixture of sand and FeS was acidified by adding 3.8 mL of 1 N hydrochloric acid. The tubes were mounted on tube rotators and mixed for 48 hours. The pH of the slurry at the end of mixing was about 5.2. It was then filtered using 45 μm filters to remove excessive water, and the bottom portion of filtered sand on the filter membrane was discarded to avoid the incorporation of FeS particles remained in suspension. The wet FeS coated sand was spread on a plastic plate and air-dried in the glovebox for 72 hours. The completely dried FeS-coated sand was stored in airtight

bottles until used. An average coating of 2.02 ± 0.056 mg FeS per gram of sand was obtained by this procedure.

The release tests were carried out in an anoxic glovebox to avoid the oxidation of the effluent samples before separation of the particulate FeS from dissolved iron. The FeS pre-coated sand was packed into a 16 mm-diameter and 100 mm-long glass column for these experiments. The FeS pre-coated sand was dry-packed and the resulting porosity was 0.32±0.01. The dried packed column was saturated by processing 25 pore volumes of an electrolyte solution through the column at 2.95 ± 0.05 mL min^{-1} prior to the release tests. The conditioning electrolyte was a pH 9 solution containing only 3.5 mM total borate buffer. The ionic strength was 5 mM, due only to the buffer, based on a MINEQL+ calculation. Iron concentrations in the effluent over the course of conditioning were less than detection limit, ~50 µg L^{-1} as Fe.

After the column conditioning period, deoxygenated particle-free electrolytes of the desired ionic strength were introduced and total and dissolved iron concentration in the effluent were monitored. These solutions were pumped into the packed bed using a peristaltic pump (Masterflex, Vernon Hills, IL) at a nominal flow rate of 2.9 ± 0.05 mL min^{-1}. To examine the effect of flow rate, an additional experiment were conducted at a slower flow rate of 0.3 mL min^{-1}. Effluent samples were collected in 15 mL polypropylene tube using an automatic fraction collector (Frac-100, Amersham Biosciences, Uppsala, Sweden). Effluent sample fractions contained 1 to 2 pore volumes. The electrolyte solutions were buffered with 0.01 M borate buffer for pH 9.0 and 10.0,

0.01 M MOPS buffer for pH 6.5 and 7.5, and 0.01 M acetate buffer for pH 5.5 electrolyte conditions. Effluent samples were filtered using 0.02 μm syringe filters (Whatman, Florham, NJ) to separate dissolved iron from particulate FeS particles. The filtration step was performed immediately upon collection of a fraction to minimize the loss of suspended particulate FeS by further dissolution prior to separation.

6.3 Results and Discussion

6.3.1 FeS Release Tests with FeS-coated Sand by deposition

At initial stage of FeS release studies, FeS coating sand was obtained from deposition of FeS particles by flow the FeS suspensions through clean quartz sand columns which is the same method employed in FeS deposition studies in Chapter 5. Initially, a total of 34.4 mg of iron was deposited through the sand column based on previously determined values from deposition tests. Based on the mass of iron released in each stage of the elution experiment, 31.2 mg of iron remained in the column after the completion of the release test, as shown in Table 6.1. The retained iron mass represents about 90% of the initially deposited iron. Since a relative small fraction of the total iron was eluted over each of the 11 pore volume injection periods, the iron loss in any one period was unlikely to have affected subsequent elutions.

Figure 6.1 presents the iron release profiles over the total injection of 33 pore volumes, showing the three different pH stages of the elution test. Comparing the profiles

Table 6.1 Iron elution using columns of FeS-coated sand obtained by prior filtration in flow-through columns

	Initial condition* (Fe deposited)	Fe released			Fe remained
		pH 8.2	pH 7.5	pH 6.5	
Fe mass	34.35 mg	0.84 mg	0.64 mg	1.69 mg	31.17 mg
Percentage**		2.4%	1.9%	4.9%	90.7%

* Initial FeS mass was assumed to be same as previously determined value from deposition test at pH 8.3, 0.025 M ionic strength conditions.

** Percentage refers to the mass of released or retained iron divided by initial iron mass times 100

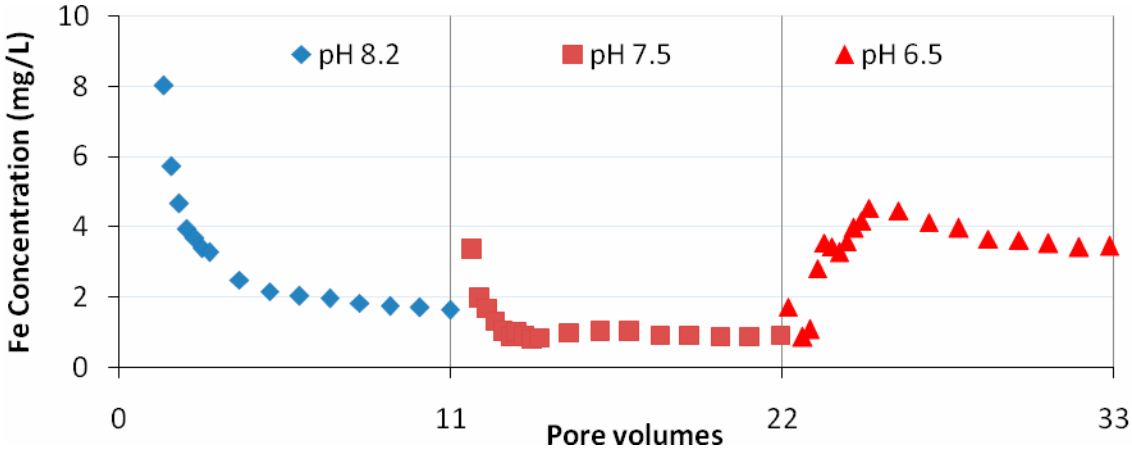

Figure 6.1 Fe release profiles; 1g L^{-1} FeS particles injected at pH 8.3 and ionic strength of 0.025 M. After the injection completed, 11 pore volumes of electrolyte of pH 8.3 solution was injected to release the deposited FeS particles following by 11 pore volumes of each pH 7.5 and 6.5 electrolyte in sequence.

at pH 8.3 and 7.5, the steady-state iron concentrations appear to decrease as pH is decreased from pH 8.3 to ph 7.5. This decrease in eluted iron as pH decreases might be due to the increased electrostatic repulsion between the particles and the sand grains as other researchers have observed (Khilar and Fogler, 1998; Grolimund and Borkovec, 1999). When the pH is decreased further to pH 6.5, however, higher total steady-state iron concentrations were measured in the effluent. It was initially hypothesized that the increased release of iron at low pH was due to FeS dissolution. Since only total iron concentrations were measured in the effluent samples, it was not possible to distinguish the forms of iron that were released. In view of the need to conduct the experiments in an anaerobic chamber to preserve effluent samples for further processing that enable measurements of both particulate and dissolved iron concentrations, subsequent release experiments were conducted in shorter columns (sized to fit in an anaerobic chamber).

Based on literature values of the solubility constants of mackinawite (see Table 2.1), the calculated (using MINEQL+) range of expected total dissolved iron concentrations at pH 6.5 (0.78 – 5.2 mg L^{-1} as Fe) were much higher than its solubility at pH 7.5 (0.21 – 0.75 mg L^{-1} as Fe). These calculations support the hypothesis that dissolution of FeS can be appreciable at pH 6.5.

6.3.2 FeS Release Tests with FeS Pre-coated Sand

The two different mechanisms of iron release, particle detachment and dissolution, were further examined using FeS pre-coated sand in packed columns. A smaller column (16mm in dia. × 100mm in length) than that used in deposition tests was

used to perform the tests in anoxic glove box for successful separation of dissolved iron from particulate in the effluent.

Release of dissolved iron

Dissolved iron concentrations in the effluent were measured as a function of pH over the range of pH 5.5 to 10.0 and a Darcy velocity of 0.024 cm sec^{-1}. Above pH 9, iron release was not observed, and the measured total iron concentrations were below the detection limit, ~50 μg L^{-1} as Fe. At neutral to acidic pH conditions, the dissolved iron concentrations tended to increase as the influent pH decreased, as shown in Figure 6.2. This result is consistent with the literature with respect to the increase in solubility of FeS below around pH 6.5 (Gallegos, 2007; Richard, 2006).

Unlike the elution experiments in Figure 6.1, steady-state effluent breakthrough iron concentrations were not achieved even after processing 60 pore volumes in the pre-FeS coated sand experiments. This slow approach to steady state might be explained by phase changes that occur over the course of the injection of electrolyte solution. Mackinawite oxidizes to other iron sulfur minerals, such as greigite or green rust, under more oxidizing conditions (Schoonen and Barnes, 1991; Wilkin and Barnes, 1996; Benning et al., 2000). At the initial conditions of the test, the oxidation state of pore water in the FeS coated-sand column is likely to be more reduced than the particle free electrolyte influent solutions even though these solutions were deoxygenated, since the pore water pe in the column prior to the elution experiment was controlled by the FeS coating. As electrolyte solution is injected, a higher pore water pe, especially near the

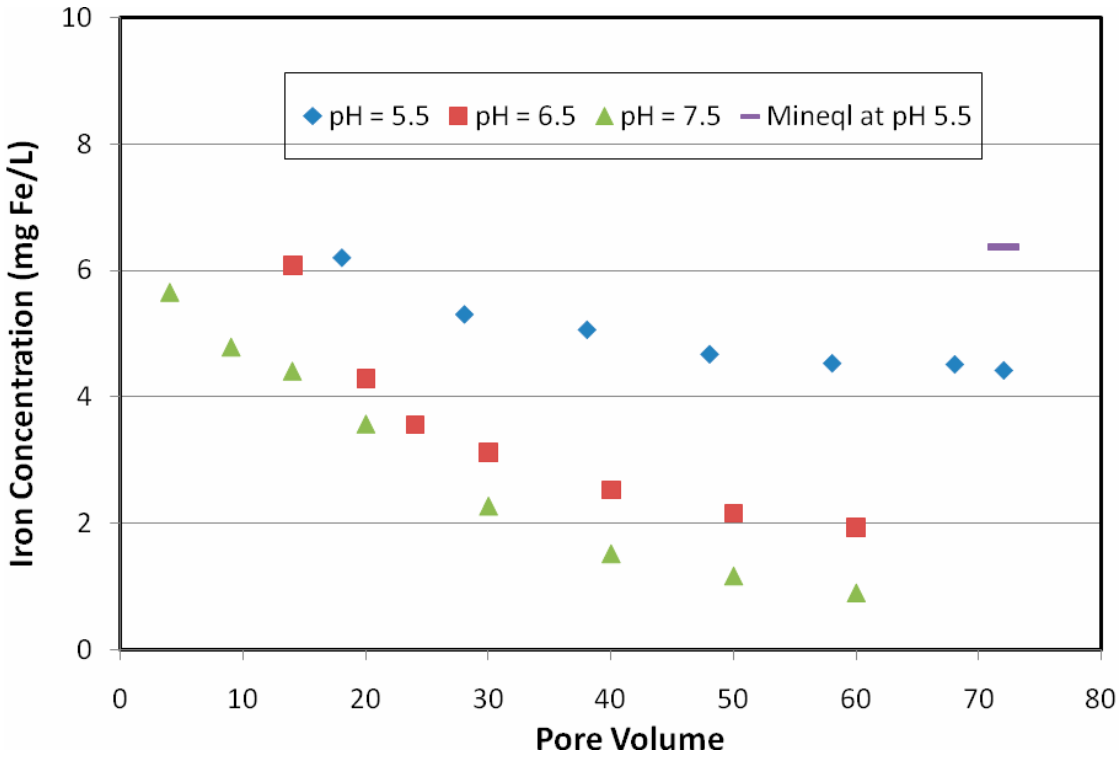

Figure 6.2 Effluent dissolved iron concentrations as a function of pH at constant ionic strength of 0.01 M and Darcy velocity of 0.024 cm sec^{-1}. Effluents were filtered using a 0.01 μm filters to remove particulate iron.

influent end of the column, could cause oxidation of the FeS. The effluent dissolved iron concentration at pH 5.5 at near steady-state, 4.4 mg L^{-1}, was slightly lower than that calculated by MINEQL+ using the lowest mackinawite solubility constant in the literature, 6.4 mg L^{-1} as Fe. A lower iron solubility would be expected if mackinawite became extensively oxidized. Griegite and other iron sulfides mineral have lower solubilities than mackinawite (Berner, 1967; Benning et al., 2000; Rickard and Morse, 2005).

Release of particulate iron

In addition to the dissolved iron concentration measurements in the experiment described above, effluent samples were also analyzed for their total iron content. The differences between total and dissolved iron concentrations were then calculated to estimate the particulate iron content of the samples. Effluent particulate FeS concentrations are plotted versus pore volume of electrolyte injected in Figure 6.3. Over the range of pH tested, particulate release was a maximum at pH 6.5. The release rate at pH 7.5 was smaller than that at pH 6.5. The effluent particulate iron concentrations, like the eluted dissolved iron concentration, were slow to achieve steady values. Although it was expected that electrostatic forces might control particulate release rates, the release of particulate FeS due to the repulsive interaction forces does not appear to explain the enhanced release of FeS at acidic pH conditions. At even more alkaline pH, pH 9 and 10, the total iron concentrations, both of particulate and dissolved iron, were below the detection limit of 50 μg L^{-1}. The complex pH dependence of particulate iron release may be the result of dissolution-driven, not repulsive, detachment. If the FeS coating, as a

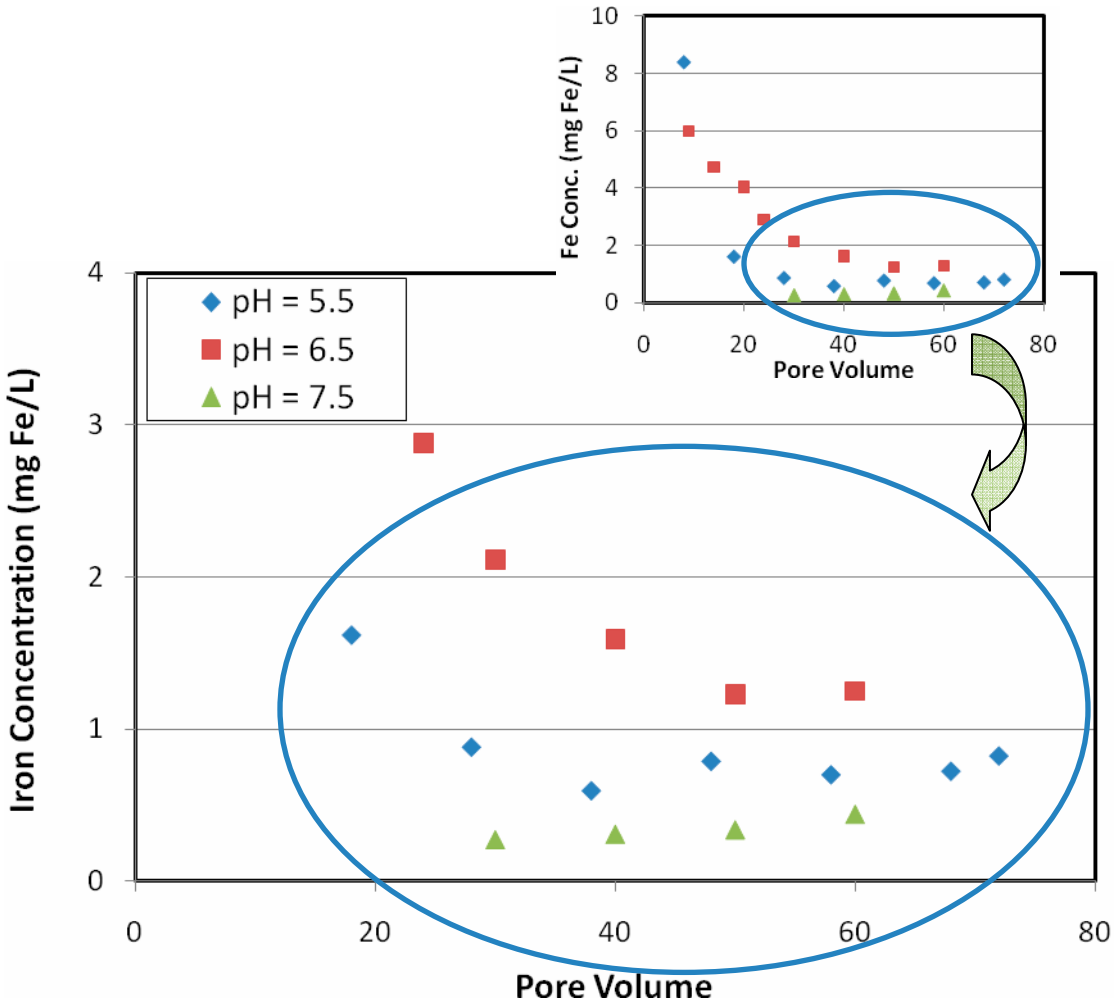

Figure 6.3 Particulate iron release as a function of pH at a constant ironic strength of 0.01 M. Particulate concentration was calculated by subtracting dissolved iron (filtered) from total iron concentration in the effluent. Small embedded picture shows expanded y-axis scale.

result of the batch coating process, exhibited a fine structure in which particulate fragments of the coating could be shed as portions dissolve, acidic conditions could promote particle release. At sufficiently acidic pH, the particles released by this dissolution-driven mechanism may themselves dissolve before exiting the column. Such a mechanism could explain why maximum rates of FeS particle release were observed at pH 6.5. Although detachment of FeS particles by repulsive interaction forces does not appear to significantly explain particle release in the batch-coated sand columns, it may be more important when FeS is applied by deposition in a flow-through packed bed. Unlike the batch-coated sand, the rates of detachment of FeS applied by deposition appeared to increase as pH was increased above pH 7.5. The drying step in the batch-coating process of the sand may cause particles on the sand surface to aggregate as the solvent evaporates, rendering them less able to detach.

Effect of ionic strength

Using batch-coated FeS sand, iron release was also examined at a higher ionic strength of 0.1 M over the pH range of 5.5 to 10.0. Over the entire range of pH conditions tested, no particulate iron was observed. Figure 6.4 compares the effluent iron concentrations at the two different ionic strengths, 0.01 and 0.1 M, at pH 5.5. The filled markers are total iron concentrations, and the unfilled symbols are dissolved iron concentrations. At higher salt concentrations the dissolved iron concentrations were similar to the total iron concentrations. Although particulate release was evident at low

ionic strength, it is likely that any particles generated by the hypothesized dissolution-driven process would be re-deposited readily at the higher ionic strength of 0.1 M.

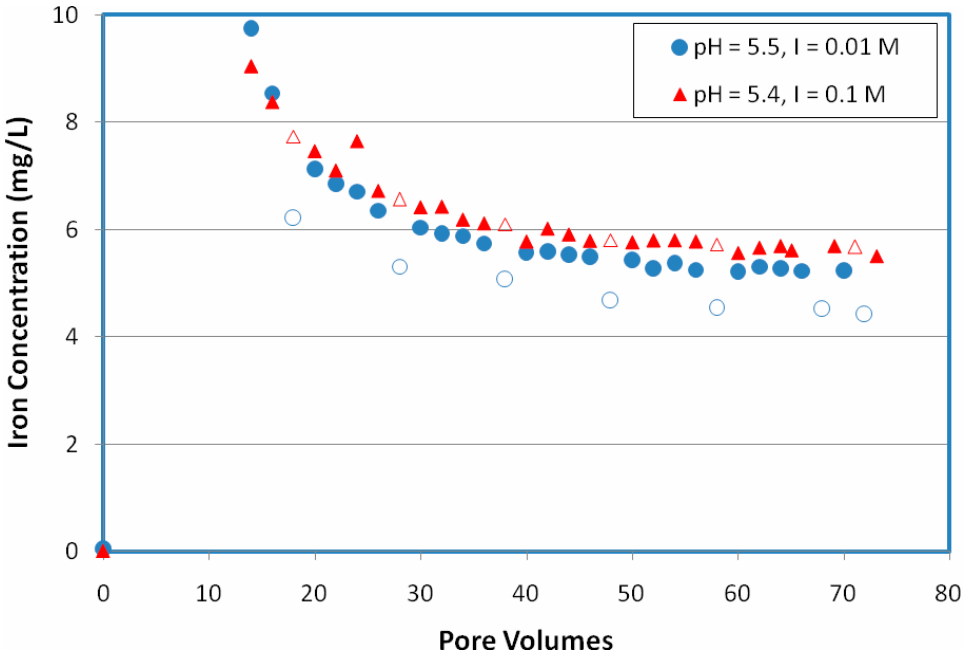

Figure 6.4 Ionic strength effect on FeS release at acidic pH. Filled markers are total iron concentrations, and unfilled symbols are dissolved iron concentrations. At high ionic strength, I = 0.1 M, no particulate iron was observed in effluent.

Effect of flow rates

When the flow rate of the eluent was reduced by an approximate order of magnitude, 2.9 mL min^{-1} to 0.3 mL min^{-1}, the total rate of FeS release increased and the steady-state effluent concentration of dissolved iron was achieved earlier at slow flow rates as shown in Figure 6.5. Calculations based on a simple mathematical transport

model were performed to rule out the possibilty of mass transfer limited FeS dissolution in packed beds. The model used for calculation is described in Appendix. A possible explanation for the increase in total iron concentrations when the flow rate is reduced might be related to its influence on the redox conditions in the column. At slower flow rates, the porewater pe may be more easily controlled by the FeS, resulting in less oxidation, the more rapid attainment of a steady-state effluent concentration, and a higher iron solubility.

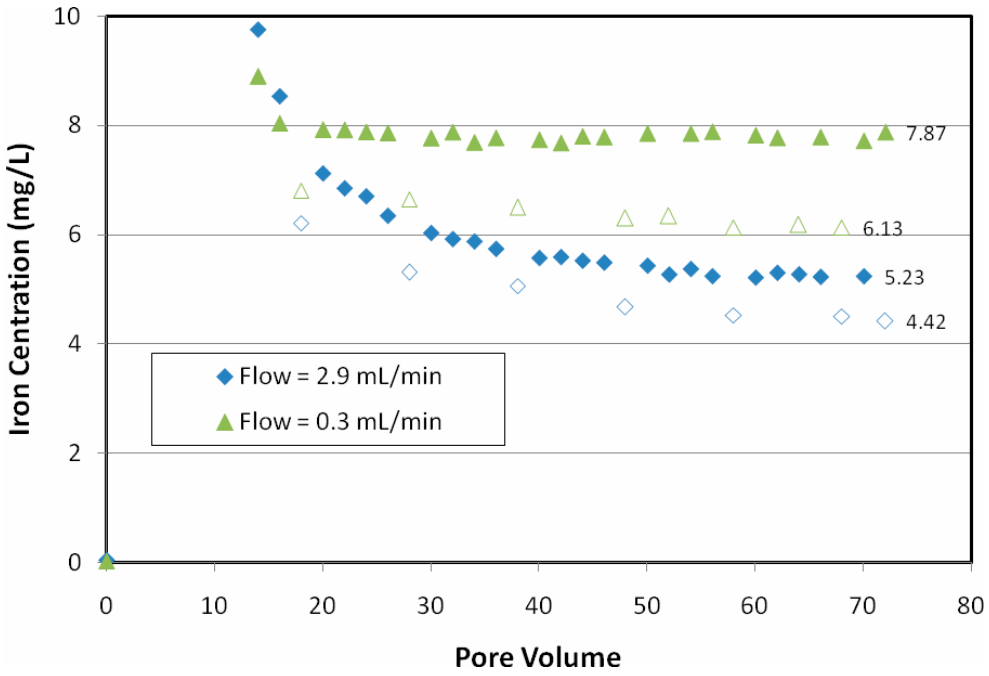

Figure 6.5 FeS release at different fluid velocities. Filled markers are total iron concentrations, and unfilled symbols are dissolved iron concentrations. The numeric values next to curves are iron concentrations at steady states.

6.4 Conclusions

The loss of iron sulfide coatings from quartz sand can occur by multiple mechanisms; particle detachment by repulsive forces between particles and particle and media surface, and mineral dissolution. Dissolution appeared to be the dominant mechanism of FeS loss under acidic pH conditions. The dissolution rate of FeS from coated sands column increased as pH decreased, a trend that is consistent with reported studies of FeS solubility (Davison et al, 1999; Benning et al, 2000; Richards, 2006). The dissolution rate, however, does not reach steady state even after injecting more than 60 pore volumes, nor does the observed iron solubility in the effluent match the solubility reported in the literature. It was hypothesized that the slow approach to steady-state was an indication of slow oxidation of FeS in the column. The oxidation rate, however, is reduced when the flow rate is slowed. The FeS-type PRBs may undergo relatively fast corrosion under the faster flow rate. The dissolution rates under acidic pH conditions are relatively significant. A simple calculation of FeS loss by dissolution was performed in the case of a hypothetical FeS-type PRB; the calculation was based on the following assumptions: a coating containing 2 mg FeS coated per gram sand, a Darcy velocity of 1×10^{-3} cm sec, and an FeS barrier thickness of 5 meters. The loss of iron sulfide per year will be 2.4, 5.2, and 11.9% at pH 7.5, 6.5, and 5.5, respectively. The higher rates of dissolution at pH < 6, may preclude their use in acidic aquifers.

Particulate FeS was released at low ionic strengths at neutral to acidic pH conditions when the sand was batch-coated with the FeS. Particle detachment by repulsive interaction forces did not appear to be an important mechanism of FeS loss, however, for the FeS batch-coated sand. Repulsive interaction forces may, however, more significantly contribute to iron loss if the deposited FeS were applied by injection. In batch-coated sand, the release of FeS particles was hypothesized to be due to the release of coating fragments as the coating dissolves.

Chapter 7

Conclusions and Recommendations

7.1 Conclusions

The feasibility of *in situ* emplacement of nanoparticulate iron monosulfide (FeS, mackinawite) by direct injection techniques was investigated. The deposition rates of the nanoparticles in porous media largely depend on the surface chemistry of the interacting colloids and filter media, which can be modulated by solution chemistry. To understand the surface characteristics of mackinawite, the stability of FeS suspensions was investigated by monitoring the initial aggregation kinetics. This study of the self interaction dynamics of FeS particles in suspension provided both a direct determination of the solution conditions that favor their stability with respect to aggregation and an indirect evaluation of their surface charge characteristics as a function of solution chemistry.

The iron sulfide particles used herein are negatively charged over the pH range studied, pH 6.5 to 9.0. The sensitivity of FeS suspension aggregation rates to pH varied over the pH range tested. Between pH 6.5 and 8.3, the FeS stability gently increased as pH increased, suggesting that the surface of FeS is negatively charged and becomes

slightly more negative with an increase of pH. The stability ratios were relatively low: 120 and 270 at pH 6.5 and 8.3, respectively. These low stability ratios indicate that the surface of FeS is relatively weakly charged. This finding is in agreement with the behavior of other metal sulfide minerals which are weakly negatively charged above their pH_{PZC}, pH 0.6 – 3.3 and whose surface potential gradually increases in the neutral pH region (Bebie et al., 1998). At more alkaline pH conditions, the stability was much more sensitive to pH. The stability sharply increased between pH 8.3 and 9.0. This behavior might be explained by the extensive deprotonation of surface functional groups at this pH, although the surface functional groups of FeS are not well characterized. The monotonic increase of the stability indicated that the pH_{PZC} must be below pH 6.5. Some limitations exist in the measurement of the aggregation rates at acidic pH conditions, pH<6.5, due to the increased solubility of FeS. At alkaline pH conditions, pH>9, the aggregation rates are quite slow, requiring measurement times in excess of a week. Over such a long measurement time, FeS might undergo other reactions, such as oxidation. These limitations hindered the estimation of FeS aggregation rates at more alkaline or more acidic pH conditions.

The stability of FeS suspensions was much more sensitive to the ionic strength of the suspension. The stability ratio, *W*, sharply decreased from 33,800 to 5.5 as the ionic strength increased from 0.025 to 0.1 M at pH 8.3. To obtain sufficient penetration of FeS particles in a sandy porous media and prevent clogging the injection zone, the particles must be stable themselves. This criterion requires that the stability ratio be greater than a few hundred. FeS deposition tests, therefore, were tested in the range of ionic strength 25

to 50 mM. MOPS buffer used in this research. The MOPS buffer system exerted a significant effect on the stability of FeS particles at concentration above 0.02 M, This result, however applies to experiments with relatively dilute concentrations of FeS particles, about 13 mg L^{-1}; the adsorption effects of MOPS is probably negligible in deposition studies where the FeS particle concentration was almost a hundred-fold higher, i.e., approximately 1000 mg L^{-1}. Careful selection of the MOPS concentration, therefore, is required to minimize specific adsorption effects.

The feasibility of *in situ* emplacement of FeS nanoparticles in porous media was evaluated using a model packed bed column of clean quartz sand. The influent suspension of 1 g L^{-1} FeS particles was quite stable in the absence of any added reagents due to its high pH of 10.3 and low conductivity of 92 μS cm^{-1} which is equivalent to 0.71 mM of KCl. At this high pH and low ionic strength, the deposition rate was also relatively slow due to the significant repulsive forces between the FeS particle and quartz media, as well as between FeS particles. The deposition rates are probably increased as pH decreased over the pH range studied, $6.5 < pH < 10.3$. The observed variations in sensitivity of FeS deposition rates to pH was consistent with pH dependence of FeS particle aggregation rates. Both deposition and aggregation rates were insensitive to pH over the pH region of neutral to relatively alkaline pH, and more pH-sensitive at alkaline pH, between pH 8.3 to 10.3. The FeS coverage on the sand was greater by more than two-fold in the neutral pH region, below pH 8.3, than that at pH 10.3 at an ionic strength of 0.025 M. The coverage of deposited FeS particles on quartz sand increased only slightly as the pH decreased from 8.3 to 7.5. However, the average coverage slightly

decreased as the pH further decreased to pH 6.5. This might be due in a complex manner to the increased dissolution of FeS at this pH, perhaps by changing the particle size distribution.

The deposition rates are particularly sensitive to the ionic strength of the FeS suspension. At an ionic strength of 0.05 M, the deposition profiles along the length of the column were relatively less uniform than the profiles obtained at 0.025 M. The non-uniformity also increased as pH decreased. Since FeS coverage on the quartz column was relatively uniform at an ionic strength of 0.025 M over the entire pH range tested, pH 6.5 to 10.3, deposition at this ionic strength is considered the optimal solution condition for *in situ* deposition. The pH dependence of FeS deposition rates on natural sands is likely to vary based on the type of mineral coatings on the sand. These variations would have to be characterized on a site-specific basis. The optimal design pH range for injection, therefore, could be more restrictive than the range found in this study, depending on these natural variations.

Two different mechanisms can contribute to the gradual loss of FeS particles over the long operation of a PRB, particle detachment and dissolution. These FeS loss mechanisms were investigated as a function of solution chemistry and flow rate. The loss of FeS particles by detachment due to repulsive forces was not significant on FeS pre-coated sand. No particulate iron was detected in the effluent when multiple pore volumes of an alkaline, particle-free electrolyte solution were introduced. Iron sulfide particle detachment was expected to increase as the solution pH increased as a result of increased repulsive forces since both surfaces of FeS particles and quartz sand become more

negatively charged. This mechanism might be more important in FeS-coated sand generated by direct injection. Consistent with the expected effect of greater repulsion, more iron release was observed at pH 8.3 than at pH 7.5 in the experiment when the FeS was applied to the sand by direct injection.

FeS dissolution was the dominant mechanism of FeS loss at relatively acidic values of pH. The dissolved iron concentrations increased as the pH of the eluent electrolyte solution decreased from 7.5 to 5.5. The dissolution rate was significantly rapid at relatively acidic pH. At pH 5.5, for example, 12% of the initially installed FeS could be lost per year in a 5 meter-thick PRB zone, with and assumed 2 mg FeS per gram of sand coating, and a groundwater flow velocity of 10^{-3} cm sec^{-1}. The dissolution rate of FeS, however, is slightly lower than the rate predicted from literature values of mackinawite solubility. This might be due to the corrosion of mackinawite to more stable metal sulfides, i.e., greigite and pyrite, which are also less soluble iron sulfides, or other phases such as green rust. The oxidation of mackinawite occurs in a slightly oxidized environment. Since the apparent release of iron decreased slowly with time, it is hypothesized that corrosion results in a gradually slower loss of the coating due to dissolution. At slower flow rates, a more rapid steady-state iron release was observed. More reducing conditions are likely to be established in the pore water as the particle-free solution passes through the FeS-coated sand at slow flow rates. The groundwater flow rate is expected to have an important effect on the redox potential in a barrier, and in the case of FeS-type PRBs, the flow rate could determine whether the reactive media is lost more quickly due to corrosion or by dissolution.

7.2 Recommendations for Future Study

The findings in this work demonstrated the feasibility of nanoparticulate FeS deposition onto clean sand media by controlling solution chemistry within a range of pH, 6.5 to 8.3, and ionic strength, 0.025 to 0.05 M. Natural sand media in an existing contaminated aquifer, however, likely to have a wide variety of surface mineral coatings, such as oxides carbonate minerals, aluminosilicates, clay particles, and organic matter. For further field implementation, feasibility studies of FeS deposition onto natural sand media are also needed to demonstrate the effectiveness of the colloidal emplacement technique. Surface minerals on natural sand grains are expected to exert an important influence on the attachment rate of colloidal FeS. These surface minerals, for example, may be positively charged metal oxides, and would then represent more favorable sites for negatively charged FeS. Future experiments to examine the role of various common mineral coatings on FeS deposition are recommended to improve the design of FeS-type PRBs installation methods.

Additional studies are also necessary to examine the wider effects of natural corrosion processes on the treatment efficiency of FeS-type PRBs. Mackinawite corrosion products, such as greigite, may provide additional treatment depending on the contaminants involved. A greater understanding of all the effects of FeS corrosion will be necessary to predict the longevity of FeS-type PRBs.

Appendix

Modeling of FeS Dissolution in a Fixed Bed

An interface transport model in a fixed bed was employed to estimate the solubility of iron sulfide particles. The solubility of FeS may play an important role in particle loss of FeS-type PRBs especially at acidic pH condition. The dissolved iron concentration in the effluent can be simulated by a film model in which the iron dissolution rate is limited by diffusive mass transfer through a quiescent microscale domain (i.e. film). Figure A.1 shows the film theory that diffusive mass transfer occurs in the film from solid surface to bulk fluid by concentration gradient.

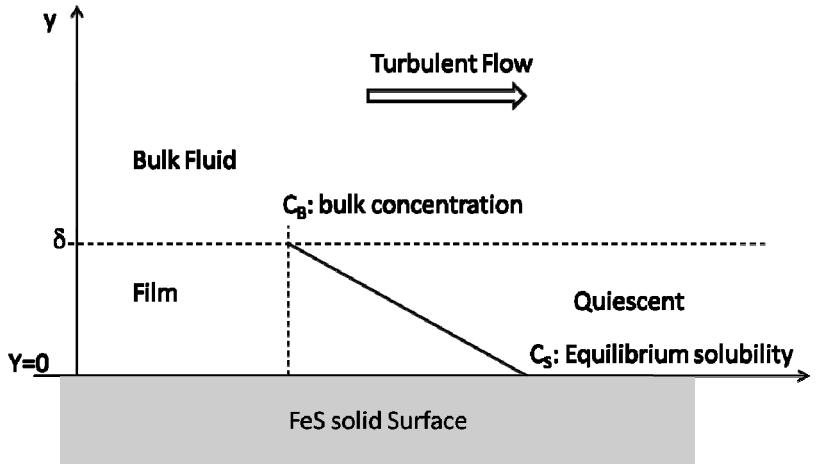

Figure A.1 Film model for mass transfer from solid surface to bulk fluid

The diffusive iron mass transfer through the film can be illustrated by diffusional flux as following:

$$N = D_l \frac{dC}{dy} = D_l \left(\frac{C_S - C_B}{\delta} \right) = \frac{D_l}{\delta} (C_S - C_B) = k_f (C_S - C_B) \quad \text{(A.1)}$$

$$\text{where, } k_f = \frac{D_l}{\delta} \quad \text{(A.2)}$$

N is flux of dissolved iron (Fe^{2+}) from surface to bulk solution by diffusion, D_l is diffusivity of ferrous iron, δ is the film thickness, k_f is the film mass transfer coefficient, C_S is the iron concentration on the surface of FeS particle at the equilibrium by the solubility, and C_B is the iron concentration in the bulk fluid.

If we assume that the iron dissolution rate is limited by the mass transfer, the dissolution rate can be determined by the concentration difference between the C_S and C_B. The equilibrium concentration of dissolved iron (C_S) at the surface of FeS solid will be a fitting parameter as a function of pH by varying the velocity (or flow rate) of pore water. The fitted equilibrium iron concentrations as a function of pH will be utilized to estimate the solubility of FeS.

The mass transfer coefficient, k_f, depends on velocity in the vicinity of the interface and upon the film thickness (sees equation A.2). Although the film thickness may not be measured directly, it is inversely proportional to turbulence at the phase interface. The film thickness, δ, decreases and the mass transfer coefficient increases with

bulk turbulence. The mass transfer coefficient can be estimated by dimensionless parameters, i.e. Sherwood number as following.

$$N_{Sh} = \frac{K_f L_c}{D_l} \tag{A.3}$$

where L_c is a characteristic length. Several mass transfer correlations have been reported for liquids in fixed beds (Wilson and Geankoplis, 1966, eq. (A.4); Williamson et al., 1963, eq. (A.5); Gnielinski, 1978, eq. (A.6)). In the correlations, the Sherwood number is related to Reynolds number, $N_{Re}=d_p v\rho/\mu$, and Schmidt number, $N_{Sc}=\mu/\rho D_l$, where d_p is the particle diameter, v is the fluid velocity, ρ is the fluid density, and μ is the fluid viscosity. The flow velocity in a fixed bed is directly related in mass transfer coefficient and thus it is would be a variable in this proposed modeling.

$$N_{Sh} = \frac{1.09}{\varepsilon_B} N_{\mathrm{Re}}^{0.333} N_{Sc}^{0.333} \qquad \text{for } 0.0016 < N_{\mathrm{Re}} < 55, \text{ and } 950 < N_{Sc} < 70,000 \tag{A.4}$$

$$N_{Sh} = 2.4 N_{\mathrm{Re}}^{0.34} N_{Sc}^{0.42} \qquad \text{for } 0.08 < N_{\mathrm{Re}} < 125, \text{ and } 150 < N_{Sc} < 1300 \tag{A.5}$$

$$N_{Sh} = (2 + 0.644 N_{\mathrm{Re}}^{0.5} N_{Sc}^{0.333})[1+1.5(1-\varepsilon_{\mathrm{B}})] \qquad \text{for } N_{\mathrm{Re}} < 100 \tag{A.6}$$

The mass balance model for a fixed bed can be described as following one dimensional advection – diffusion model:

$$\frac{\partial C}{\partial t} = -v_z \frac{\partial C}{\partial z} + D_d \frac{\partial^2 C}{\partial z^2} + R \tag{A.7}$$

where v_z is the flow velocity and D_d is the dispersion coefficient which can be estimated by an transient experiment using an inert trace. The reaction rate term, *R*, can account for diffusive iron mass transfer through the film on surface of solid.

$$R = N(a_s^\circ)_R = k_f(C_S - C)(a_s^\circ)_R \tag{A.8}$$

where $(a_s^\circ)_R$ is the specific interfacial area per unit volume of system.

In this modeling, several assumptions were necessary to facilitate the model. (1) The initial concentration of deposited FeS particles on the quartz is homogeneous through the column length. (2) Size and number of the coated FeS particle does not change by dissolution. (3) The concentration of dissolved iron at the surface of FeS will be assumed to be an equilibrium concentration with solution pH.

Bibliography

American Society of Agronomy; Soil Science Society of America, Methods of soil analysis, 1982, 2nd edition, Madison, WI

Abadzic, S.D.; Ryan, J.N., Particle release and permeability reduction in a natural zeolite (Clinoptilolite) and sand porous medium, Environmental Science & Technology, 2001, 35, 4502-4508

Arnold, W.A.; Roberts, A.L., Pathways and kinetics of chlorinated ethylene and chlorinated Acetylene reaction with Fe(0) particles, Environmental Science & Technology, 2000, 34, 1794-1805

AWWA; APHA; WEF, Standard methods for the examination of water and wastewater, American Public Health Association, New York, 19th edition, 1995

Bebie, J.; Schoonen, M.A.A.; Fuhrmann, M.; Strongin, D.R., Surface charge development on transition metal sulfides: an electrokinetic study, Geochemica et Cosmochimica Acta, 1998, 62, 633-642

Benning L.G.; Wilkin, R.T.; Barnes, H.L., Reaction pathways in the Fe-S system below 100°C, Chemical Geology, 2000, 167, 25-51

Bitea, C.; Walther, C.; Kim, J.I.; Geckeis, H.; Rabung, T.; Scherbaum, F.J.; Cacuci, D.G., Time-resolved observation of ZrO_2-colloid agglomeration, Colloids and Surfaces A, 2003, 215, 55-66

Blowes, D.W.; Ptacek, C.J.; Jambor, J.L., In-situ remediation of Cr(VI)-contaminated groundwater using permeable reactive walls: laboratory studies, Environmental Science and Technology, 1997, 31 (12), 3348 - 3357

Blowes, D.W.; Ptacek, C.J.; Benner, S.G.; McRae, C.W.T.; Bennett, T.A.; Puls, R.W., Treartment of inorganic contaminants using permeable reactive barriers, Journal of Contaminant Hydrology, 2000, 45, 123-137

Bunn, R.A.; Magelky, R.D.; Ryan, J.N.; Elimelech, M., Mobilization of natural colloids form an iron oxide-coated sand aquifer: Effect of pH and ionic strength, Environmental Science and Technology, 2002, 36, 314-322

Burner R.A., Thermodynamic stability of sedimentary iron sulfides, American Journal of Science, 1967, 265, 773-785

Butler, E.C.; Hayes. K.F., Effects of solution composition and pH on the reductive dechlorination of hexachloroethane by iron sulfide. Environmental Science and Technology, 1998, 32 (9), 1276-1284

Butler, E. C.; Hayes, K.F., Kinetics of the transformation of trichloroethylene and tetrachloroethylene by iron sulfide. Environmental Science and Technology, 1999, 33 (12), 2021-2027

Cantrell, K.J.; Kaplan, D.I., Zero-valent iron colloid emplacement in sand columns, Journal of Environmental Engineering, 1997, 123, 499-505

Cantrell, K.J.; Kaplan, D.I.; Gillmore, T.J., Injection of colloidal Fe0 particles in sand with shear-thinning fluids, Journal of Environmental Engineering, 1997, 123, 786-791

Choe, S.; Chang, Y.; Hwang, K.; Khim, J., Kinetics of reductive denitrification by nanoscale zero-valent iron, Chemosphere, 2000, 40, 1307-1311.

Chung, N.K., Chemical precipitation in H.M. Freeman, Standard handbook of harzardous waste treatment and disposal, McGraw-Hill, New York, 1989.

Coles, C.A.; Ramachandra Rao, S.; Yong, R.N., Lead and cadmium interactions with Mackinawite: Retention mechanisms and the role of pH, Environmental Science and Technology, 2000, 34 (6), 996-1000

Coulibaly, K.M.; Borden, R.C., Impact of edible oil injection on the permeability of aquifer sands, Journal of contaminant hydrology, 2004, 71, 219-237

Davison, W.; Philips, N.; Tabner B., Soluble iron sulfide species in natural waters: Reappraisal of their stoichiometry and stability constants, Aquatic Sciences, 1999, 61, 23-43

Day, S.R.; O'Hannesin, S.F., Marsden, L., Geotechnical techniques for the construction of reactive barriers, Journal of Hazardous Materials, 1999, B67, 285-297

Derjaguin, B.V.; Landau, L., Theory of the stability of strongly charged lyophobic sols and of the adhesion of strongly charged particles in solution of electrolytes, Acta Physicochimica (URSS), 1941, 14, 633

Elliott, D.W.; Zhang, W., Field assessment of nanoscale bimetallic particles for groundwater treatment, Environmental Science and Technology, 2001, 35, 4922-4926

Fitzpatrick, J.A. and Spielman, L.A., Filtration of aqueous latex suspension through beds of glass spheres, Journal of colloid and interface science, 1973, 43, 350-369

Friedlander, S.K., Theory of aerosol filtration, Industrial & Engineering Chemistry, 1958, 50(8), 1161-1164

Gallegos, T., Dissertation (Ph.D.), Sequestration of As(III) by synthetic mackinawite under anoxic conditions, University of Michigan, 2007

Gavaskar, A.R., Design and construction techniques for permeable reactive barriers, Journal of Hazardous Materials, 1999, 68, 41-71

Grolimund, D.; Elimelech, M.; Borkovec, M.; Barmettler, K.; Kretzschmar, R.; and Sticher, H., Transport of in situ mobilized colloidal particles in packed soil column, Environmental Science & Technology, 1998, 32, 3562-3569

Grolimund, D.; Borkovec, M., Long-term release kinetics of colloidal particles from natural porous media, Environmental Science & Technology, 1999, 33, 4054-4060

Grolimund, D.; Borkovec, M., Release of colloidal particles in natural porous media by monovalent and divalent cations, Journal of Contaminant Hydrology, 2006, 87, 155-175

Han, Y.S., Dissertation (Ph.D.), Iron sulfide-coated sand for remediation of arsenic (III) - contaminated anoxic groundwater, University of Michigan, 2009

Hansson, E.B., Odziemkowski, M.S.; Gillham, R.W., Formation of poorly crystalline iron monosulfides: Surface redox reactions on high purity iron, spectroelectrochemical studies, Corrosion Science, 2006, 48, 3767-3783

Hanus, L.H.; Sooklal, K.; Murphy, C.J.; Ploehn, H.J., Aggregation kinetics of dendrimer-stabilized CdS nanoclusters, Lanmuir, 2000, 16, 2621-2626

He, Y.T.; Wilson, J.T.; Wilkin R.T., Transformation of reactive minerals in a permeable reactive barrier (biowall) used to treat TCE in groundwater, Environmental Science and Technology, 2008, 42(17), 6690-6696

Henderson, A.D. and Demond, A.H., Long-term performance of zero-valent iron permeable reactive barriers: A critical review, Environmental Engineering Science, 2007, 24, 401-423

Henderson, A.D. and Demond, A.H., Unpublished data, Department of Civil and Environmental Engineering, University of Michigan.

Hunger, S; Benning, L.G.; Greigite: a true intermediate on the polysulfide pathway to pyrite, Geochemical Transactions, 2007, v. 8 :1, doi:10.1186/1467-4866-8-1

Hunter, R.J. Foundation of Colloid Science, 2nd Ed., Oxford, New York, 2001

Interstate Technology & Regulatory Council, Permeable Reactive Barriers Team, Permeable reactive barriers: Lessons learned/New directions, 2004

Ives, K.J. and Sholji, I., Research on Variables Affecting Filtration, Journal of the Sanitary Engineering Division, American Society of Civil Engineering, 1965, 91, SA4, 1

Iwasaki, T., Some Notes on Sand Filtration, Journal of American Water Works Association, 1937, 29, 1591

Joanny, J.F.; Leibler, L.; De Gennes, P.G., Effects of polymer solutions on colloid stability, Journal of Polymer Science: Polymer Physics Edition, 1979, 17(6) 1073-1084

Jeong, H.; Hayes, K., Impact of transition metals on reductive dechlorination rate of hexachlorothylene by Mackinawite. Environmental Science and Technology, 2003, 37 (20), 4650-4655

Kamolpornwijit, W.; Liang, L.; West, O.R.; Moline, G.R.; Sullivan, A.B., Preferential flow path development and its influence on long-term PRB performance: column study, Journal of Contaminant Hydrology, 2003, 66, 161-178

Kallay, N.; Biškup, B.; Tomič, M.; Matijevič, E., Particle adhesion and removal in model systems, X. The effect of electrolytes on particle detachment, Journal of colloid and interface sciences, 1986, 114(2), 357-362

Kallay, N.; Dojnović, Z.; Čop, A.; Surface potential at the hematite-water interface, Journal of Colloid and Interface Science, 2005, 286, 610-614

Khilar, K.C.; Fogler, H.S., Migration of fines in porous media, Dordrecht, Netherlands, Kluwer Academic Publishers, 1998, Chapter 3

Klausen, J.; Ranke, J.; Schwarzenbach, R.P., Influence of solution composition and column aging on reduction of nitroaromatic compounds by zero-valent iron, Chemosphere, 2001, 44, 511-517

Kouvo, O.; Long, J.V.P.; Vuorelainen, Y., A tetragonal iron sulfide, American Mineralogist, 1963, 48, 511-514

Kouznetsova, I.; Bayer, P.; Ebert, M.; Finkel, M., Modeling the long-term performance of zero-valent iron using a spatio-temporal approach for iron aging, Journal of Contaminant Hydrology, 2007, 90, 58-80

Kuhnen, F.; Barmettler, K.; Bhattacharjee, S.; Elimelech, M.; Kretzschmar, R., Transport of iron oxide colloids in packed quartz sand media: monolayer and multilayer deposition, Journal of Colloid and Interface Science, 2000, 231, 32-41

Kulkarni, R.; Sureshkumar, R.; Biswas, R., Hierarchical approach to model multilayer colloidal deposition in porous media, Environmental Science and Technology, 2005, 39, 6361-6370

Kyprianidou-Leodidou, T.; Althaus, H.J.; Wyser, Y.; Vetter, D.; Büchler, M., Caseri, W.; Suter, U.W., High refractive index materials of iron sulfides and poly(ethylene oxide), Materials Research Society, 1997, 12, 2198-2206

Lee, W.J.; Batchelor, B., Abiotic reductive dechlorination of chlorinated ethylenes by iron-bearing soil minerals. 1. pyrite and magnetite, Environmental Science and Technology, 2002, 36, 5147-5154

Li, X.; Zhang, W., Sequestration of metal cations with zerovalent iron nanoparticles – a study with high resolution X-ray photoelectron spectroscopy (HR-XPS), journal of physical chemistry, 2007, 111, 6939-6946.

Li, X.; Brown, D.G., Zhang, W., Stability of biosolids with nanoscale zero-valent iron (nZVI), Journal of Nanoparticle Research, 2007, 9, 233-243

Liang, L.Y.; Morgan J.J., Chemical aspects of iron oxide coagulation in water: Laboratory studies and implications for natural systems, Aquatic Sciences, 1990, 52(1), 1015-1621

Liang, L.Y.; Sullivan, A.B.; West. O.R.; Moline, G.R.; Kamolpornwijit, W., Predicting the precipitation of mineral phases in permeable reactive barriers, Environmental Engineering Science, 2003, 20, 635-653

Liang, L.Y.; Moline, G.R.; Kamolpornwijit, W.; West, O.R., Influence of hydrogeochemical processes on zero-valent iron reactive barrier performance: a field investigation, Journal of Contaminant Hydrology, 2005, 78, 291-312

Lin, M.Y.; Lindsay, H.M.; Weitz, D.A.; Ball, R.C.; Klein, R., Meakin, P., Universality in colloid aggregation, Nature, 1989, 339, 360-362

Liou, Y.H.; Lo, S.; Kuan, W.H.; Lin, C.; Weng, S.C., Effect of precursor concentration on the characteristics of nanoscale zerovalent iron and its reactivity of nitrate, Water Research, 2006, 40, 2485-2492

Litton, G.M.; Olson, T.M., Colloid deposition rates on silica bed media and artifacts related to collector surface preparation methods, Environmental Science and Technology, 1993, 27, 185-193

Liu, C.C.; Tseng, D.H.; Wang, C.Y., Effects of ferrous ions on the reductive dechlorination of trichloroethylene by zero-valent iron, Journal of Hazardous Materials, 2006, B136, 706-713

Liu, J.; Valsaraj, K.T.; Devai, I.; DeLaune, R.D., Immobilization of aqueous Hg(II) by mackinawite (FeS), Journal of Hazardous Materials, 2008, 157, 432-440

Liu, Y. and Lowry, G.V., Effect of particle age (Fe^0 content) and solution pH on NZVI reactivity: H_2 evolution and TCE dechlorination, Environmental Science and Technology, 2006, 40, 6085-6090

Livens, F.R.; Jones, M.J.; Hynes, A.J.; Charnock, J.M.; Mosselmans, F.W.; Hennig, C.; Steele, H.; Collison, D.; Vaughan, D.J.; Pattrick, R.A.D.; Reed, W.A.; Moyes, L.N, X-ray adsorption spectroscopy studies of reactions of technetium, uranium and neptunium with mackinawite, Journal of Environmental Radioactivity, 2004, 74, 211-219

Matheson, L.J.; Tratnyek, P.G., Reductive dechlorination of chlorinated methanes by iron iron metal, Environmental Science and Technology, 1994, 28, 2045-2053

Mattigod, S.V.; Fryxell G.E.; Alford, K.; Gilmore, T.; Parker, K.; Serne, J.; Engelhard, M., Functionalized TiO2 nanoparticles for use for in situ anion immobilization, Environmental Science and Technology, 2005, 39, 7306-7310

Mayer, K.U.; Blowes, D.W.; Frind, E.O., Reactive transport modeling of an in situ reactive barrier for the treatment of hexavalent chromium and trichloroethylene in groundwater, Water Resourses Research, 2001, 37, 3091-3103

Mylon, S.E.; Chen, K.L.; Elimelech, M., Influence of natural organic matter and ionic composition on the kinetics and structure of Hematite colloid aggregation: Implication to iron depletion in estuaries, Langmuir, 2004, 20, 9000-9006

Mullet, M.; Boursiquot S.; Ehrhardt, J.J., Removal of hexavalent chromium from solution by Mackinawite, tetragonal FeS, Colloids and Surfaces A: Physicochemical and Engineering Aspects, 2004, 224, 77-85

National Research Council, Alternatives for ground water cleanup, National Academy Press, Washington, D.C., 1994, 80-124

Noubactep, C.; Schoner, A.; Meinrath, G., Mechanism of uranium removal from the aqueous solution by elemental iron, Journal of Hazardous Materials, 2006, B132, 202-212

Ohfugi, H.; Rickard, D.; High resolution transmission electron microscopic study of synthetic nanocrystalline mackinawite, Earth and Planetary Science Letters, 2006, 241, 227-233

Patterson, R.R.; Fendorf, S., Reduction of hexavalent chromium by amorphous iron sulfide. Environmental Science and Technology. 1997, 31 (7) 2039-2044

Phenrat, T.; Saleh, N.; Sirk K.; Tilton, R.D.; Lowry, G.V., Aggregation and sedimentation of aqueous nanoscale zerovalent iron dispersions, Environmental Science and Technology, 2007, 41, 284-290

Philips, D.H.; Gu, B.; Watson, D.B.; Roh, Y.; Liang, L.; Lee, S.Y., Performance evaluation of a zerovalent iron reactive barrier: mineralogical characteristics, Environmental Sciences and Technology, 2000, 34, 4169-4176

Rickard, D.; Morse, J.W., Acid volatile sulfide (AVS), Marine Chemistry, 2005, 97, 141-197

Rickard, D., The solubility of FeS, Geochemica et Cosmochimica Acta, 2006, 70, 5779-5789

Rickard, D.; Luther, G.W., Chemistry of iron sulfides, Chemical Reviews, 2007, 107, 514-562

Ritter, K.; Odziemkowski, M.S.; Gillham, R.W., An in situ study of the role of surface films on granular iron in the permeable iron wall technology, Journal of Contaminant Hydrology, 2002, 55, 87-111

Roy, S.B.; Dzombak, D.A., Colloid release and transport processes in natural and model porous media, Colloids and Surfaces A: Physicochemical and Engineering Aspects, 1996, 107, 245-262

Ryan, J.N.; Elimelech, M., Review, Colloid mobilization and transport in groundwater, Colloid and Surfaces, A: Physicochemical and Engineering Aspect, 1996, 107, 1-56

Ryan, J.N.; Gschwend, P.M., Effects of ionic strength and flow rate on colloid release: relating kinetics to intersurface potential energy, Journal of Colloid and Interface Science, 1994, 164, 21-34

Saleh, N.; Sirk, K.; Liu, Y.; Phenrat, T.; Dufour, B.; Matyjaszewski, K.; Tilton, R.D.; Lowry, G.V., Surface modifications enhance nanoiron transport and NAPL targeting in saturated porous media, Environmental Engineering Science, 2007, 24, 45-57

Scherer, M.M.; Richter, S.; Valentine, R.L.; Alvares, P.J.J., Chemistry and microbiology of permeable reactive barrier for in situ groundwater cleanup, Critical reviews in Environmental Science and Technology, 2000, 30, 363-411

Schoonen, M.A.A.; Barnes, H.L.; Reaction forming pyrite and marcasite from solution: II. Via FeS precursors below 100^{o}C, Geochemica et Cosmochimica Acta, 1991, 55, 1505-1514

Schrick, B.; Hydutsky, B.W.; Blough, J.L.; Mallouk, T.F., Delivery vehicles for zerovalent metal nanoparticles in soil and groundwater, Chemistry of Materials, 2004, 16, 2187-2193

Sen, T.K.; Khilar, K.C., Review on subsurface colloids and colloid-associated contaminant transport in saturated porous media, Advances in Colloids and Interface Science, 2006, 119, 71-96

Shen, C.Y.; Li, B.G.; Huang, Y.F.; Jin, Y., Kinetics of coupled primary- and secondary-minimum deposition of colloids under unfavorable chemical conditions, Environmental Science and Technology, 2007, 41, 6976-6982

Smoluchowski, M., Drei Vortrage, Physik, Zeitschr, XVII, 1916, 557

Stumm, W; Morgan, J.J., Aquatic chemistry: chemical equilibria and rates on natural waters, New York, Wiley, 3rd edition, 1996

Suleimenov, O.M.; Seward, T.M., A spectrophotometric study of hydrogen sulphide ionisation in aqueous solution to 350^{o}C, Geochimica et Cosmochimica Acta, 1997, 61(24), 5187-5198

Taylor, P.; Rummery, T.E.; Owen, D.G., On the conversion of mackinawite to greigite, Journal of Inorganic and Nuclear Chemistry, 1979, 41, 595-596

Tufenkji, N. and Elimelech, M., Deviation from the classical colloid filtration theory in the presence of repulsive DLVO interactions, Langmuir, 2004, 20, 10818-10828

United States Environmental Protection Agency, 2002, Economic Analysis of the implementation of permeable reactive barriers for remediation of contaminated ground water, 2002

United States Environmental Protection Agency, Field applications of *in situ* remediation technologies: permeable reactive barriers, 2002

Vaughan, D.J.; Craig, J.R., Mineral Chemistry of Metal Sulfides, Cambridge, England, Cambridge University Press, 1978

Verwey, E.J.W.; Overbeek, J.T.G., Theory of the stability of lyophobic colloids, Elsevier, Amsterdam, 1948

Vikesland, P.J.; Klausen, J.; Zimmermann, H., Longevity of granular iron in groundwater treatment processes: changes in solute transport properties over time, Journal of Contaminant Hydrology, 2003, 64, 3-33

Virden J.W.; Berg, J.C., The use of photon correlation spectroscopy for estimating the rate constant for doublet formation in an aggregating colloidal dispersion, Journal of Colloid and Interface Science, 1992, 149, 528-535

Wang, S. Simulation of bioaugmentation involving exogenous bacteria injection, Water resources Research, 2002, 38, 1293

Ward, A.S., Filtration: Principles and Practices, Edited by Matteson, M.J. and Orr, C., New York, Marcel Dekker, INC, 1987, Chapter 2

Weber, Jr, W.J., Physicochemical Processes for Water Quality Control, John Wiley & Sons, Inc., 1972, Chapter 4. Filtration, 139-198

Weber, W. J. Jr.; DiGiano, F.A., Process Dynamics in Environmental Systems, Wiley, NY, 1996

Weerasooriya, R.; Dharmasena, B., Pyrite-assisted degradation of trichloroethane (TCE), Chemosphere, 2001, 42, 389-396

Widler, A.M.; Seward, T.M., The adsorption of gold(I) hydrosulphide complexes by iron sulphide surfaces, Geochimica et Cosmochimica Acta, 2002, 66, 383-402

Wilkin, R.T.; Barnes, H.L., Pyrite formation by reaction of iron monosulfides with dissolvied inorganic and organic sulfur species, Geochimica et Cosmochimica Acta, 1996, 60, 4167-4179

Wolthers, M.; van Der Gaast, S.J.; Rickard, D., The structure of dissordered makinawite, American Mineralogist, 2003, 88, 2007-2015

Wolthers, M.; Charlet, L.; van Der Linde, P.R.; Rickard, D.; van Der Weuden, C.H., Surface chemistry of disordered mackinawite (FeS), Geochimica et Cosmochimica Acta, 2005, 69, 3469-3481

Yao, K.M,; Habibian, M.T.; O'Melia, C.R., Water and waste water filtration: Concepts and applications, Environmental Science and Technology, 1971, 5, 1105-1112

Zeta-Meter, Inc, Staunton, VA 24402, USA, http://www.zeta-meter.com/5min.pdf

Zhang, W., Nanoscale iron particles for environmental remediation: an overview, Journal of nanoparticle Research, 2003, 5, 323-332

Zherenkova, L.V.; Mologin, D.A.; Khalatur, P.G.; Khokhlov, A.R., Interaction between small colloidal particles and polymer chains in a semidilute solution: Monte Carlo simulation, Colloid Polymer Science, 1998, 276, 753-768